Incremental Backstepping Control for Helicopters

Investigating the effect of dynamic inflow modelling on incremental backstepping controller performance

Wessel Pieter den Ouden

Delft University of Technology

TU Delft

Incremental Backstepping Control for Helicopters

Investigating the effect of dynamic inflow modelling on incremental backstepping controller performance

by

Wessel Pieter den Ouden

to obtain the degree of Master of Science
at the Delft University of Technology,
to be defended publicly on Friday August 26, 2022 at 02:30 PM.

Student number:	4205618	
Project duration:	September, 2019 – August, 2022	
Thesis committee:	Dr. M.D. Pavel,	TU Delft C&S, supervisor
	Dr. ir. E. van Kampen,	TU Delft C&S
	Dr. S.J. Hulshoff,	TU Delft Aerodynamics

Cover: Dutch Army MBB Bo-105 with special anniversery paint, by NIMH (Modified)

An electronic version of this thesis is available at `http://repository.tudelft.nl/`.

TU Delft

Preface

With this thesis an end has come to my life as a student in Delft. From the first day as a bachelor student until now I have had many fun and meaningful experiences, being part of an exiting community. It also presented some challenges along the way, with the Covid pandemic having a big effect on my graduation period.

For my thesis I wanted to apply my interest in control systems to a subject that I did not came across frequently during my studies. I have the feeling that helicopters are often overlooked during courses, while they are beautifully engineered machines. This resulted in a topic that combined control theory with modelling of aerodynamics and helicopter dynamics. Investigating the peculiarities of helicopters gave interesting insights.

First of all I would express my gratitude to my daily supervisor Marilena Pavel. She never stopped motivating me to push through the difficult Covid times, when losing motivation was never far away. I will remember her enthusiasm for and knowledge about helicopters, making our discussions during the meetings very interesting. Furthermore I want to mention all the nice students I have met during my studies and the graduation phase. They made studying much easier, providing distraction or help whenever needed.

Finally I would like to thank all my friends and family for supporting me throughout this journey. Most importantly my mother and girlfriend, who kept motivating me to the end and through the Covid lockdowns. This would not have been possible without them.

Wessel den Ouden
Delft, September 2022

Contents

List of Figures

List of Tables

Nomenclature

Acronyms

Acronym	Definition
BS	BackStepping
CFD	Computational Fluid Dynamics
CLF	Control Lyapunov Function
CP	Control Plane
DP	Disk Plane
HP	Hub Plane
IBS	Incremental BackStepping
INDI	Incremental Non-linear Dynamic Inversion
MAV	Micro Aerial Vehicle
NDI	Non-linear Dynamic Inversion
NFP	Non-Feathering Plane
PID	Proportional-Integral-Derivative
RPM	Rounds Per Minute
SP	Shaft Plane
TPP	Tip-Path Plane
VTOL	Vertical Take-Off and Landing

Symbols

Symbol	Description	Unit
a_1	Longitudinal disk tilt with respect to CP	rad
C_D	Drag coefficient	-
C_l^α	Lift curve slope	1/rad
C_L	Roll moment coefficient	-
C_M	Pitching moment coefficient	-
$[C_M]$	Damping matrix of multi-blade flap equations	-
C_T	Thrust coefficient	-
D	Frontal surface drag	N
$[D_M]$	Stiffness matrix of the multi-blade flap equations	-
g	Gravitational acceleration	m/s^2
h_{cg}	Height of the rotor hub above center of gravity	m
$[H_M]$	Forcing function matrix of the multi-blade flap equations	-
I_{xx}	Helicopter moment of inertia around x axis	kgm^2
I_{xz}	Helicopter moment of inertia around asymmetrical xz axis	kgm^2
I_{yy}	Helicopter moment of inertia around y axis	kgm^2
I_{zz}	Helicopter moment of inertia around z axis	kgm^2
K	Rotational acceleration per radian of disc tilt	rad/s^2
K_β	Flap hinge spring constant	Nm/rad
L	Lateral rolling moment	Nm
$[L]$	Inflow gain matrix	-
$\hat{L}_{aero}$	Keller roll moment coefficient	-

m	Helicopter mass	kg
M	Longitudinal pitching moment	Nm
$[M]$	Apparent mass matrix	-
$\hat{M}_{aero}$	Keller pitch moment coefficient	-
N	Yawing moment	Nm
N_b	Number of rotor blades	-
p	roll rate	rad/s
q	Pitch rate	rad/s
r	Yaw rate	rad/s
R	Rotor radius	m
s	Complex plane pole	-
t	Time	s
T	Thrust force, perpendicular to the DP	N
u	Body velocity in x direction	m/s
v	Body velocity in y direction	m/s
V	Airspeed	m/s
w	Body velocity in z direction	m/s
W	Helicopter weight	N
x	Longitudinal body axis, positive through nose	m
X	Force in x direction	N
y	Lateral body axis, positive right	m
Y	Force in y direction	N
z	Vertical body axis, positive down	m
Z	Force in z direction	N

α_{DP}	Angle of attack of the DP	rad
β	Individual blade flap angle, positive from SP to DP	rad
β_0	Coning angle, positive up	rad
β_{1c}	Longitudinal disk tilt coefficient, positive for forward tilt of the DP	rad
β_{1s}	Lateral disk tilt coefficient, positive for leftward tilt of the DP	rad
β_M	Multi-blade coordinate flap angle vector	rad
γ	Lock number	-
θ	Individual blade pitch angle	rad
θ	Fuselage pitch angle, positive nose-up	rad
θ_0	Collective pitch input	rad
θ_{1c}	Lateral cyclic pitch input, positive for left-roll	rad
θ_{1s}	Longitudinal cyclic pitch input, positive for pitch-up	rad
θ_{tw}	Blade linear twist angle	rad
λ_β	Non-dimensional flap frequency	-
λ_i	Total inflow ratio, positive downward in z direction	1/rad
λ_0	Mean inflow ratio	1/rad
λ_{1c}	Longitudinal inflow ratio gradient	1/rad
λ_{1s}	Lateral inflow ratio gradient	1/rad
μ	Advance ratio	1/rad
μ_x	Normalized longitudinal velocity of the rotor hub in SP	1/rad
μ_y	Normalized lateral velocity of the rotor hub in SP	1/rad
μ_z	Normalized vertical velocity of the rotor hub in SP	1/rad
ν	Induced velocity	m/s
ρ	Atmospheric density	kg/m^3
σ	Rotor solidity	-
τ_β	Flap time constant	s
τ_λ	Induced velocity time constant	s
τ_i	Keller induced velocity time constant	s
ϕ	Fuselage roll angle	rad
ψ	Fuselage yaw angle	rad

Ψ	Blade azimuth angle	rad
Ω	Rotor rotational speed	rad/s
$\dot{x}$	First derivative of variable with respect to time	-
$\ddot{x}$	Second derivative of variable with respect to time	-
x'	Derivative of variable with respect to azimuth angle	-
$\overline{x}$	Variable normalized by rotor speed	-
$\frac{\partial}{\partial x}$	Partial fraction with respect to variable	-

Part I

Paper

Investigating the Effect of Dynamic Inflow Modelling on Incremental Backstepping Controller Performance for Helicopters

W.P. den Ouden[1]
Delft University of Technology, 2629 HS Delft, The Netherlands

Due to their highly coupled and non-linear behavior, helicopters seem excellent subjects to apply non-linear control theory to. Handling qualities of helicopters are consistently rated lower than aircraft. Furthermore, the rotor is operating in its own wake, leading to complex aerodynamics. A Command Filtered Incremental Backstepping controller has been applied to a simulation model of an MBB Bo-105 hingeless rotorcraft. The model incorporates the Pitt-Peters inflow model to calculate the inflow variations of the main rotor. Incremental controllers rely on sensor measurements of state derivatives instead of model knowledge, making them robust to modelling errors. However, some states of the helicopter model, such as blade flap angles and rotor inflow, cannot be measured in real life. Because for the MBB Bo-105 the blades are rigidly attached to the rotor hub, the dynamics of the rotor couple with the body dynamics, speeding up the body motion. This results in a violation of the time-scale separation principle on which incremental controllers rely on. Therefore a process called residualization and synchronization is used to remove these states from the controller model and compensate for their dynamics in a synchronization filter. This process has already been performed for the flap angles. In this paper the inflow states are also residualized and added to the synchronization filter. Furthermore, the Pitt-Peters inflow model of the simulation model is updated with the Keller correction to better simulate off-axis response to control input. Modelling the off-axis response of helicopters is notoriously difficult and is often of the wrong sign compared to experimental data. Having a more precise helicopter model is key to perform piloted simulation or research to non-linear controllers. Although the updated inflow model did alter the inflow states, changes in the helicopter dynamics remained very limited. Furthermore, the application of residualization was successful but synchronizing the rotor inflow did not improve controller performance.

Nomenclature

α_{DP}	=	angle of attack of the disk plane
$\beta_0, \beta_{1c}, \beta_{1s}$	=	rotor disk tilt angles in multi-blade coordinates
γ	=	rotor Lock number
$\lambda_0, \lambda_{1s}, \lambda_{1c}$	=	inflow coefficients
λ_β	=	blade flapping frequency
μ	=	advance ratio
μ_x,μ_y,μ_z	=	non-dimensional hub velocities
Ω	=	rotor speed
ϕ, θ, ψ	=	helicopter attitude angles

[1]Graduate Student, Faculty of Aerospace Engineering, Control and Simulation Division, 2629 HS Delft, The Netherlands.

$\theta_0, \theta_{1s}, \theta_{1c}$	=	helicopter control inputs
θ_{tw}	=	blade twist angle
C_L	=	lateral moment coefficient
C_M	=	longitudinal moment coefficient
C_T	=	thrust coefficient
p, q, r	=	body rotational rates
R	=	rotor radius
u, v, w	=	boy velocities
x, y, z	=	helicopter position

I. Introduction

Helicopters and other rotorcraft are known to have certain advantages compared to conventional fixed-wing aircraft, mainly due to their hovering and VTOL capabilities. They are therefore used for a large variety of tasks that are impossible to perform by their fixed-wing counterpart. For instance, helicopters are well suited for search & rescue operations, transportation of people or cargo to remote locations where runways are not available, construction in mountainous terrain and several military applications. Most of these tasks utilize the high degree of maneuverability of a helicopter, it being able to perform vertical take-offs and landings, hover and fly sideways and backwards while maintaining a high degree of precision.

As with many systems these advantages come at a cost. It has been recognized for a long time that helicopters are notoriously difficult to control as a pilot, with Handling Quality ratings consistently lower than aircraft. The main reason for this are the cross-couplings in the control system and the non-linear dynamics of the helicopter. Unlike aircraft, the control surfaces do not directly affect the angular rates of the body, but rather influence the orientation of the thrust vector through tilting of the main rotor plane. Thus attitude control is done through a single actuation device, instead of the separated channels found in aircraft design. Cross-couplings between longitudinal and lateral modes originate from gyroscopic precession that is experienced by the main rotor subjected to control inputs and airspeed. The non-linear behavior of helicopters is due to complex aerodynamics surrounding the helicopter, especially near hovering flight, as it operates in its own wake. The wake of the rotor, composed of multiple vortices coming from each blade, interferes with the blade aerodynamics and the induced velocity generated by the rotor disk. Furthermore, a large portion of a generic helicopter flight task is done outside trimmed cruise flight, often at low altitude and in the vicinity of hazardous objects. This makes predictable helicopter response and helicopter stability very important.

With the introduction of digital fly-by-wire control systems in helicopters, it becomes possible to implement non-linear controllers[1]. In recent years the development and application of non-linear controllers show promising results in many research areas. Within the TU Delft Control & Simulation group, research has been performed on implementing these controller types to helicopter models. Especially their incremental versions of these non-linear methods have been studied, as they are successfully applied to micro aerial vehicles and aircraft [2]. Based on a generic helicopter model tailored to the specifications of an MBB Bo-105 hingeless helicopter [3], an Incremental Non-linear Dynamic Inversion (INDI) controller was implemented [4]. Later, application of an Incremental Backstepping controller (IBS) on an improved helicopter model proved to be successful [5]. The application of INDI to an Apache AH-64D model, the Apache FlyRT model provided by Boeing, proved to be more challenging [6].

The advantage of incremental controllers is that they hardly rely on accurate model knowledge, as their regular variants do, but rather on measurements of the state of the helicopter. This circumvents the costly determination of the helicopter dynamics model of the to be controlled system, which needs to be of high accuracy to ensure stability of the closed loop system. However, the sensory equipment of contemporary helicopters is unable to measure certain important states, making real life implementation of these controllers

impossible without proper adaptation. In particular the flap dynamics, the movement of individual blades under inertial and aerodynamics forces, needs to be accounted for. In [7] these adaptations were made concerning the flap dynamics, by residualizing the flap states in the controller model and compensate for their dynamics with a synchronization filter. The dynamics of the airflow around the main rotor however has not yet been investigated. As said, the non-linear behavior of the helicopter comes partly from the fact that it operates in its own wake. It is known that the inflow of the main rotor has an effect on the flapping of the blades. Accounting for the inflow dynamics in the controller design could have a positive effect on its performance. Besides the flapping of the blade it is also impossible to measure the inflow in real-time. Thus only residualizing the flap dynamics will not result in a solution that can be implemented in real life.

Aside from the possible influence of inflow dynamics on controller performance, also the inflow dynamics modelling itself needs to be addressed. The inflow model that is used in the works of Van der Goot and Arons, although widely applied, models the off-axis response incorrectly [8]. This is the lateral response of the helicopter to longitudinal control input and vice versa. In general, for certain conditions the estimated flow is of opposite sign compared to test data. It is known that inflow is a difficult phenomenon to model and many papers have been published concerning correct off-axis inflow modelling [9]. Implementing accurate inflow models might alter the pilots perception during piloted simulation and minimizes the gap between reality and modelling results, enabling better research to control system behavior.

II. Helicopter Simulation Model

The main helicopter simulation model that is used in this analysis is adopted from [7]. Relevant helicopter data for the MBB Bo-105 can be found in table 1 in the appendix. The state of the helicopter consists of the classical six body rotational and translational DoF's, augmented with three flap DoF's of the main rotor blades and four inflow DoF's of the main and tail rotor. This results in 22 states: $\boldsymbol{x} = [u\ v\ w\ x\ y\ z \mid p\ q\ r\ \phi\ \theta\ \psi \mid \beta_0\ \beta_{1s}\ \beta_{1c}\ \dot{\beta}_0\ \dot{\beta}_{1s}\ \dot{\beta}_{1c} \mid \lambda_0\ \lambda_{1s}\ \lambda_{1c}\ \lambda_{0,tr}]^{\mathrm{T}}$. Their derivatives are calculated using non-linear differential equations and the corresponding states are obtained with a time-marching integration scheme, in this case Runge-Kutta4. The states are then used for detailed force and calculations for the horizontal and vertical tail plane, fuselage, tail rotor and main rotor. Because the inflow dynamics, flap dynamics and body dynamics are the most important parts of the helicopter model, they are treated in section II.A, section II.B and section II.C respectively. For a complete description of the helicopter model, the reader is referred to [7] or [10]. Along with the descriptions of some important dynamics of the helicopter, section II.D gives an overview of the command filtered incremental backstepping controller.

A. Flap dynamics

The flap dynamics are an important part of the total helicopter dynamics, as it is the cause for rotations of the disk plane and therefore attitude changes of the helicopter. Using a Coleman transformation, the individual flap angles are converted in multi-blade coordinates that describe the orientation of the rotor disk as a whole [11]. This results in four parameters for a four-bladed helicopter such as the Bo-105. The coning angle β_0 represents the upward collective flapping off all blades. The longitudinal disk tilt angle β_{1c} represents the forward tilting of the rotor cone. The lateral disk tilt angle β_{1s} represents the leftward tilting of the rotor. The last angle is the differential coning β_{0d}, representing the blades opposite to each other having the same but with a flipped sine as the other blade pair. This mode is reactionless, as it is not producing any net force or moment on the rotor hub. It is therefore neglected in any further calculations.

The differential equation that is used to calculate the derivative of the three parameters is given in eq. (1). Based on the required accuracy of the simulation and the type of helicopter, one can consider to set the second derivative and/or the first derivative to zero. This means only the steady state disk tilt angles are calculated, which is allowed for for trim calculations or articulated rotors for which the body modes and flap

modes are widely separated in time and frequency. Including the first and second derivative of the MBC's adds the regressing and progressing flap modes respectively to the simulated dynamics. The regressing flap mode is a low frequency wobble of the rotor plane. When simulating hingeless rotorcraft it is often the case that the regressing flap mode couples with the body modes. This changes the response of the helicopter to control inputs and is why this mode must be included when simulating hingeless or bearingless rotorcraft. The progressing flap mode however is of higher frequency and is unlikely to couple with any of the body modes [12].

$$\ddot{\beta}_M = -\Omega \mathrm{C}_M \dot{\beta}_M - \Omega^2 \mathrm{D}_M \beta_M + \Omega^2 \mathrm{H}_M \quad , \quad \beta_M = \begin{bmatrix} \beta_0 \\ \beta_{1c} \\ \beta_{1s} \end{bmatrix} \tag{1}$$

The damping matrix C_M, stiffness matrix D_M and forcing function matrices H_M that are present in eq. (1) are shown in eq. (2) [10].

$$\begin{aligned}
\mathrm{C}_M &= \frac{\gamma}{8} \begin{bmatrix} 1 & 0 & \frac{2}{3}\mu \\ 0 & 1 & \frac{16}{\gamma} \\ \frac{4}{3}\mu & -\frac{16}{\gamma} & 1 \end{bmatrix} \\
\mathrm{D}_M &= \frac{\gamma}{8} \begin{bmatrix} \frac{8\lambda_\beta^2}{\gamma} & 0 & 0 \\ \frac{4}{3}\mu & \frac{8\left(\lambda_\beta^2 - 1\right)}{\gamma} & 1 + \frac{\mu^2}{2} \\ 0 & \frac{\mu^2}{2} - 1 & \frac{8\left(\lambda_\beta^2 - 1\right)}{\gamma} \end{bmatrix} \\
\mathrm{H}_M &= \frac{\gamma}{8} \begin{bmatrix} \theta_0 \left(1 + \mu^2\right) + 4\theta_{tw} \left(\frac{1}{5} + \frac{\mu^2}{6}\right) + \frac{4}{3}\mu\theta_{1s} + \frac{4}{3}\left(\mu_z - \lambda_0\right) + \frac{2}{3}\mu\left(\bar{p} - \lambda_{1s}\right) \\ \frac{16}{\gamma}\bar{p} + \theta_{1c}\left(1 + \frac{\mu^2}{2}\right) + \left(\bar{q} - \lambda_{1c}\right) \\ -\frac{16}{\gamma}\bar{q} + \frac{8}{3}\mu\theta_0 + 2\mu\theta_{tw} + \theta_{1s}\left(1 + \frac{3}{2}\mu^2\right) + 2\mu\left(\mu_z - \lambda_0\right) + \left(\bar{p} - \lambda_{1s}\right) \end{bmatrix}
\end{aligned} \tag{2}$$

The matrices clearly show that there exists multiple couplings between the equations. Also in the forcing functions angular rates and control inputs appear in multiple rows. Moreover, the coefficients of the harmonic inflow appear in the forcing matrix H_M. This shows that the flap dynamics are influenced by the inflow dynamics and can lead to coupling of the dynamics.

B. Inflow dynamics

Already in 1974 it was found that incorporating force and moment coefficients of the helicopter in a dynamic inflow model had significant effects on the transient response [13]. A landmark in the development of dynamic inflow modeling is the paper by Pitt and Peters [14]. In this paper the authors present a relatively simple inflow model in closed form governed by 3 parameters which can be added to the helicopter dynamics as a state-space system. The parameters are inflow coefficients that describe the uniform, fore to aft and side to side inflow variation. The model is based on Kinner pressure distributions, which can give pressure discontinuities across a circular disk. The benefit of the proposed model is that the formulation is in closed

form, something previous research was not able to obtain. Until this day, the majority of developed dynamic inflow models use the Pitt-Peters model as a starting point, showing the importance of the findings presented in the paper. It is implemented in both the flight simulation tool FLIGHTLAB [15] as well as the U.S. Army's Rotorcraft Comprehensive Analysis System [16]. The matrix equation is shown in eq. (3) [14]. This model is also incorporated in the current helicopter simulation model.

$$\begin{bmatrix} & & \\ & M & \\ & & \end{bmatrix} \begin{bmatrix} \dot{\lambda}_0 \\ \dot{\lambda}_{1s} \\ \dot{\lambda}_{1c} \end{bmatrix} + V \begin{bmatrix} & & \\ & L & \\ & & \end{bmatrix}^{-1} \begin{bmatrix} \lambda_0 \\ \lambda_{1s} \\ \lambda_{1c} \end{bmatrix} = \begin{bmatrix} C_T \\ C_L \\ C_M \end{bmatrix} \tag{3}$$

with apparent mass and gain matrix:

$$M = \begin{bmatrix} \frac{128}{75\pi} & 0 & 0 \\ 0 & \frac{-16}{45\pi} & 0 \\ 0 & 0 & \frac{-16}{45\pi} \end{bmatrix}, L = \begin{bmatrix} \frac{1}{2} & 0 & \frac{15\pi}{64}\sqrt{\frac{1-sin(\alpha_{DP})}{1-sin(\alpha_{DP})}} \\ 0 & \frac{-4}{1+sin(\alpha_{DP})} & 0 \\ \frac{15\pi}{64}\sqrt{\frac{1-sin(\alpha_{DP})}{1-sin(\alpha_{DP})}} & 0 & \frac{-4sin(\alpha_{DP})}{1+sin(\alpha_{DP})} \end{bmatrix}$$

with mass flow parameter:

$$V = \frac{\mu^2 + (\lambda_0 - \mu_z)(2\lambda_0 - \mu_z)}{\sqrt{\mu^2 + (\lambda_0 - \mu_z)^2}}$$

The largest difference in helicopter dynamics due to the inflow is present during the hovering flight phase [17]. When hovering, the only other movement that is influencing the angle of attack of the blade is coming from the rotational velocity of the rotor. As forward airspeed builds up, the wake gets skewed backwards, making the distance between the previous vortex and the blade greater. This diminishes its ability to produce induced velocity locally at the blade and increases the influence of the incoming free flow.

C. Body dynamics

Besides the derivatives of the inflow and flap states, also the derivatives of the body states have to be calculated. This is done with the equations of motion of the helicopter. First the total force and moment acting on the body in the body reference frame is determined by adding the contributions of each subsystem in eqs. (4) and (5).

$$F_{tot} = F_{mr} + F_{tr} + F_{ht} + F_{vt} + F_{fus} \tag{4}$$

$$M_{tot} = M_{mr} + M_{tr} + M_{ht} + M_{vt} + M_{fus} \tag{5}$$

The total force and moment vectors are used in the translational and rotational dynamic equations. Note that there will be some uncertainty in the magnitude of the components of these vectors, as they are obtained from differential equations that inevitable have modelling errors. Thus they will never exactly match the moments and forces in real life. The translational and rotational motion dynamics are given in eq. (6) and eq. (7) [18].

$$\begin{bmatrix} \dot{u} \\ \dot{v} \\ \dot{w} \end{bmatrix} = m^{-1} F_{tot} + \begin{bmatrix} -sin(\theta) \\ sin(\phi)cos(\theta) \\ cos(\phi)sin(\theta) \end{bmatrix} g - \begin{bmatrix} qw - rv \\ ru - pw \\ pv - qu \end{bmatrix} \tag{6}$$

$$\begin{bmatrix} \dot{p} \\ \dot{q} \\ \dot{r} \end{bmatrix} = \begin{bmatrix} I_{xx} & 0 & -I_{xz} \\ 0 & I_{yy} & 0 \\ -I_{xz} & 0 & Izz \end{bmatrix}^{-1} \left(M_{tot} - \begin{bmatrix} p \\ q \\ r \end{bmatrix} \times \begin{bmatrix} I_{xx} & 0 & -I_{xz} \\ 0 & I_{yy} & 0 \\ -I_{xz} & 0 & Izz \end{bmatrix} \begin{bmatrix} p \\ q \\ r \end{bmatrix} \right) \tag{7}$$

Contrary to the the dynamic relations, the kinematic relations are exact. Because of the physical relation of the body frame and the NED frame through the three Euler angles of the body, this conversion will not introduce new uncertainties. The translational and rotational motion kinematics are given in eq. (8) and eq. (9) [18]. Note that for the translational kinematic relation the cosine and sine symbols are replaced by c and s respectively for easier readability.

$$\begin{bmatrix} \dot{x} \\ \dot{y} \\ \dot{z} \end{bmatrix} = \begin{bmatrix} c(\psi)c(\phi) & c(\psi)s(\theta)s(\phi) - s(\psi)c(\phi) & c(\psi)s(\theta)c(\phi) + s(\psi)s(\phi) \\ s(\psi)c(\theta) & s(\psi)s(\theta)s(\phi) + c(\psi)c(\phi) & s(\psi)s(\theta)c(\phi) - c(\psi)s(\phi) \\ -s(\theta) & c(\theta)c(\phi) & c(\theta)c(\phi) \end{bmatrix} \begin{bmatrix} u \\ v \\ w \end{bmatrix} \tag{8}$$

$$\begin{bmatrix} \dot{\phi} \\ \dot{\theta} \\ \dot{\psi} \end{bmatrix} = \begin{bmatrix} 1 & sin(\phi)sin(\theta)cos(\theta)^{-1} & cos(\phi)sin(\theta)cos(\theta)^{-1} \\ 0 & cos(\phi) & -sin(\phi) \\ 0 & sin(\phi)cos(\theta)^{-1} & cos(\phi)cos(\theta)^{-1} \end{bmatrix} \begin{bmatrix} p \\ q \\ r \end{bmatrix} \tag{9}$$

D. Command Filtered Incremental Backstepping

Besides the popular incremental non-linear dynamic inversion control technique that is often applied to aircraft and drones [19–22], other incremental control methods exist. One of them is Incremental Backstepping (IBS), first described in [23]. It uses the stability characteristics of Control Lyapunov Functions (CLF) to guarantee stability. Applications of the IBS control structure can also be found in literature [2, 24, 25]. Like all incremental methods, it starts with applying a Taylor series expansion on the dynamic model description.

$$\dot{x} = f(x) + g(x, u) \tag{10}$$

$$\dot{x} = f(x_0) + g(x_0, u_0) + \frac{\partial}{\partial x}\Big[f(x) + g(x, u)\Big]_{x_0, u_0} (x - x_0) + \frac{\partial}{\partial u}\Big[f(x) + g(x, u)\Big]_{x_0, u_0} (u - u_0) + O\left((x - x_0)^2, (u - u_0)^2\right) \tag{11}$$

$$\dot{x} = \dot{x}_0 + F(x_0, u_0)\Delta x + G(x_0, u_0)\Delta u + O\left((x - x_0)^2, (u - u_0)^2\right) \tag{12}$$

where $\dot{x}_0$ is the current state derivative, $f(x)$ is the system dependent dynamics, $g(x)$ is the control dependent dynamics, $F(x_0, u_0)$ is the linearized system dependent dynamics derivative, $G(x_0, u_0)$ is the linearized control dependent dynamics derivative, Δx is the state increment and Δu is the control increment. Based on a number of assumptions, it is possible to simplify this equation. First of all the system sample rate should be high enough, meaning that the sensors and controller operate at a sufficiently high frequency. Furthermore the actuators are assumed to react instantly to command signals. At last, it is assumed that the changes in the states are slow compared to the changes in control input. This is called time scale separation. By assuming time scale separation, the system term $F(x_0, u_0)\Delta x$ is assumed to be small compared to the control term

$G(x_0, u_0)\Delta u$ and can be neglected. Therefore the system coefficients in F do not need to be estimated and only control effectiveness G remains. At the moment this assumption is violated, as the flap states have significant influence on the angular acceleration derivatives due to the hingeless configuration of the MBB Bo-105. This is the reason that residualization and synchronization will be applied in a later stage[7].

Resulting eq. (13) is a simplified description of the system which, assuming that all the controlled states can be measured and the sampling rate is sufficiently high, can be used to construct the incremental backstepping controller that controls the system using increments of control inputs.

$$\Delta \dot{x} = G(x_0, u_0)\Delta u \tag{13}$$

Simulation models also consists of kinematic relations to calculate translational velocities and rotational attitude. Since these relations are exactly known, there is no need to apply incremental control for these parts of the model as there is no change of model mismatch. This allows for application of conventional NDI or BS. Therefore the focus is on the incremental control laws that govern the dynamic relations.

Defining error state z as the difference between the current state and the reference state, one can assure stability and tracking if the derivative of a chosen CLF is negative definite. For this example CLF $V = \frac{1}{2}x^2$ is used.

$$z = x - x_{ref} \tag{14}$$
$$\dot{z} = \dot{x} - \dot{x}_{ref} \tag{15}$$
$$V = \tfrac{1}{2}z^2 \tag{16}$$
$$\dot{V} = z\dot{z} \tag{17}$$
$$\dot{V} = z\left(\dot{x} - \dot{x}_{ref}\right) \tag{18}$$
$$\dot{V} = z\left(\dot{x}_0 + G(x_0, u_0)\Delta u - \dot{x}_{ref}\right) \tag{19}$$

Which is negative definite if:

$$\Delta u = G(x_0, u_0)^{-1}\left(-\dot{x}_0 + \dot{x}_{ref} - Cz\right), C > 0 \tag{20}$$

The final control IBS law is shown in eq. (20). When choosing gain C>0 the use of a CLF assures stability and tracking, given that the time scale separation principle and sampling frequency assumptions hold. Although incremental controllers are commonly applied to dynamic systems in literature, only recently time delay margins and robustness tolerances against parameter uncertainties were explicitly quantified. Until this point sampling rates were always assumed sufficiently high and no systematic theory existed to calculate maximum parameter mismatch. It was found that control effectiveness mismatch could reach up to 50% of its true value when actuator dynamics were not included in the model [26]. Adding actuator dynamics even increased the robustness of the controller controller against model errors.

A special type of IBS that is applied in the current helicopter simulation model is Command Filtered Incremental Backstepping (CFIBS). Until now this explanation assumed that eq. (10) corresponded to the dynamics system description with a direct relation to the control input. If eq. (20) was based on a dynamic model with more than one layer to step through, the control law would also contain a $\dot{\alpha}$ term. This is the derivative of the intermediate control law α_i in the previous layer. This happens when for instance also kinematic relations are taken into account. The control law based on k steps through the system of lower triangular form would result in eq. (21).

$$\Delta u = G_k(x_0, u_0)^{-1}\left(-\dot{x}_0 + \dot{x}_{ref} - C_k z_k + \dot{\alpha}_{(k-1)}\right), C > 0 \tag{21}$$

Since the intermediate control law of the previous step is also containing their predecessors, the final control law would require the analytical time derivatives of each of the control laws which quickly become

prohibitively difficult to calculate. A solution to this problem is to apply a command filter on the intermediate control laws before passing them to the next control law as a reference. By using a command filter, the derivative of the signal is known and do not need to be derived. Furthermore, the intermediate reference signals can be tweaked in order to obtain favourable dynamics. The error states can be redefined as:

$$z = x_i - x_{i,ref} \tag{22}$$

$$\bar{z}_i = z_i - \chi_i \tag{23}$$

Note that in this case a bar over the variable does not mean that it is normalized by the rotor speed. $\bar{z}_i$ is the compensated error state, which is used in the Control Lyapunov Function to obtain the intermediate and final control laws as is done in eq. (20). χ_i is a compensation term for using the command filters, defined as:

$$\dot{\chi}_i = -C_i\chi_i + G_i\left(x_{(i+1),ref} - x^0_{(i+1),ref}\right) \tag{24}$$

The last two terms in this equation are the output signal of the command filter and the input signal of the command filter. The input signal to the command filter is given in eq. (25), while the command filter itself is shown in eq. (26).

$$x^0_{(i+1),ref} = \alpha_i - \chi_{(i+1)} \tag{25}$$

$$\begin{bmatrix} \dot{x}_{i,ref} \\ \ddot{x}_{i,ref} \end{bmatrix} = \begin{bmatrix} \dot{x}_{i,ref} \\ 2\zeta\omega_n\left(\mathrm{S}_{rate}\left\{\frac{\omega_n^2}{2\zeta\omega_n}\left[S_{mag}\left(x^0_{i,ref}\right) - x_{i,ref}\right]\right\} - \dot{x}_{i,ref}\right) \end{bmatrix} \tag{26}$$

With the parameters S_{mag} and S_{rate} magnitude and rate limits can be imposed on the intermediate reference signals. Moreover, bandwidth and damping limitations can be set by choosing the appropriate natural frequency ω_n and damping term ζ. It is important to state that these limits will be applied to the commanded states of the system in the controller, not the actual states.

The intermediate control function and final control law can then be found by eq. (27), knowing that $\alpha_k = \Delta u + u_0 = \Delta u + G_i(x_0, u_0)^{-1}\dot{x}_0$ when time scale separation is applied.

$$\begin{aligned} \alpha_i &= G_i(x_0, u_0)^{-1}\left(\dot{x}_{ref} - C_i z_i - G_{(i-1)}\bar{z}_{(i-1)}\right) \\ \Delta u &= G_k(x_0, u_0)^{-1}\left(-\dot{x}_0 + \dot{x}_{ref} - C_k z_k - G_{(k-1)}\bar{z}_{(k-1)}\right) \end{aligned} \tag{27}$$

III. Methodology

In this section the methodology of the adaptations are presented that are applied to the helicopter simulation model. section III.A treats the updated inflow model and shows the additional steps taken before the inflow model could be implemented in the simulation model. In section III.B the process of residualizing the flap angle and inflow states is discussed and why this step is necessary. section III.C explains the synchronization process.

A. Update of the inflow model

After the Pitt-Peters model was published, continuous efforts have been made to improve the fit of the inflow model with experimental data. Although the Pitt-Peters model predicts helicopter response in the direction of the control input well, the off-axis response is predicted poorly [27]. In some cases the off-axis response is even of opposite sign as compared with experimental data. Based on the Pitt-Peters model, multiple publications

have been published proposing solutions to improve the fit between the predicted off-axis response of inflow models and test data. It was shown that including wake distortion effects due to rotor shaft translation and rotor disk rotation the off-axis response has the correct sign and shows a better fit to test data [28–31]. This improved model is given in eq. (28) [17].

$$\begin{aligned} \tau_i v'_c + v_c &= -K_L \hat{M}_{aero} + K_T \mu_x + K_R \left(\bar{q} - \beta'_{1c}\right) \\ \tau_i v'_s + v_s &= -K_L \hat{L}_{aero} + K_T \mu_y + K_R \left(\bar{p} - \beta'_{1s}\right) \end{aligned} \tag{28}$$

where v is the non-dimensional inflow ratio, τ_i is the inflow time constant, $\hat{M}_{aero}$ and $\hat{L}_{aero}$ are the pitch and rol moment, K_L, K_T and K_R are the gains for moments, wake skew and wake rotation respectively. Before the inflow model correction described by eq. (28) from [17] can be implemented in the simulation model, it has to be converted to a form that is easier to implement in the current set up of the inflow calculations. As a basis the Pitt-Peters inflow model that is currently implemented is used. This is possible since it is known that when K_R is set to zero the two models are equal [29]. The new inflow model including the proposed correction for the off-axis response is shown in eq. (29), with the matrices unchanged from their original description given in eq. (3).

$$\begin{bmatrix} \dot{\lambda}_0 \\ \dot{\lambda}_{1s} \\ \dot{\lambda}_{1c} \end{bmatrix} = M^{-1} \left(\begin{bmatrix} C_T \\ C_L \\ C_M \end{bmatrix} - VL^{-1} \begin{bmatrix} \lambda_0 \\ \lambda_{1s} \\ \lambda_{1c} \end{bmatrix} + VL^{-1} K_R \begin{bmatrix} 0 \\ \bar{p} - \frac{\dot{\beta}_{1s}}{R} \\ \bar{q} - \frac{\dot{\beta}_{1c}}{R} \end{bmatrix} \right) \tag{29}$$

Before the rotational rates and flap velocities can be used in the model, they have to be transformed to another reference frame. Namely, the inflow model is defined in the disk plane-wind reference frame, which is the disk plane axis system rotated by the side slip angle. This causes the velocity vector to only have forward and downward components. Both the angular rates and the flap velocities are defined in the hub plane. Therefore two transformations are needed, the first from the hub plane to the disk plane and the second to the disk plane-wind frame.

The value for K_R is set to 3.0, as this is the recommended value based on curve fitting to experimental data [17]. However, as is also suggested, the identified value differs depending on the identification method of the parameter [30]. Values for K_R are ranging from 0.75 to 3.5 in literature.

B. Residualization of flap and inflow states

The residualization procedure in its original form is to separate slow and fast states in a state space system and thereby simplifying the system [32]. The fast states are assumed to be constantly at steady state compared to the slow states, and their dynamics have therefore no effect on the slow states. This principle is similar to that of only using steady state flap angles for articulated helicopters, as the response of body states and flap states are widely separated in time.

In this instance the procedure is implemented to remove states from the controller model that cannot be measured, as the incremental control law relies on measurements of the helicopter state. This entails the flap angle states and the inflow states. These states can have significant effect on the helicopter dynamics. This means that the time delay that is introduced by the residualized states in the actuation process of the actuator disk is also lost. These dynamics have to be accounted for in the synchronization filter.

Residualization is performed by setting the derivatives of the flap and inflow states equal to zero and fold their dynamics into the remaining states. This will transfer the control dependency of the flap and inflow states to the remaining states, such that the time scale separation principle is less likely to be violated. The

residualized state vector will become $\boldsymbol{x}_{res} = [u\ v\ w\ x\ y\ z \mid p\ q\ r\ \phi\ \theta\ \psi]^{\mathrm{T}}$. The residualization procedure is given in eqs. (30) to (34), with the flap angle vector and inflow vector represented by β and λ respectively. The final residualized system is given in eq. (35).

$$\ddot{\beta} = F_{\dot{\beta},x_{res}} x_{res} + F_{\dot{\beta},\beta}\beta + F_{\dot{\beta},\dot{\beta}}\dot{\beta} + G_{\dot{\beta}} u \tag{30}$$

$$\dot{\lambda} = F_{\lambda,x_{res}} x_{res} + F_{\lambda,\lambda}\lambda + G_{\lambda} u \tag{31}$$

Setting all derivatives to zero and rearranging the terms:

$$\beta = -F^{-1}_{\dot{\beta},\beta} F_{\dot{\beta},x_{res}} x_{res} - F^{-1}_{\dot{\beta},\beta} G_{\dot{\beta}} u \tag{32}$$

$$\lambda = -F^{-1}_{\lambda,\lambda} F_{\lambda,x_{res}} x_{res} - F^{-1}_{\lambda,\lambda} G_{\lambda} u \tag{33}$$

These equations can then be inserted into the residualized dynamics:

$$\dot{x}_{res} = F_{x_{res},x_{res}} x_{res} + F_{x_{res},\beta}\beta + F_{x_{res},\lambda}\lambda + G_{x_{res}} u \tag{34}$$

The final residualized system then becomes:

$$\begin{aligned} \dot{x}_{res} = &\underbrace{\left(F_{x_{res},x_{res}} - F_{x_{res},\beta} F^{-1}_{\dot{\beta},\beta} F_{\dot{\beta},x_{res}} - F_{x_{res},\lambda} F^{-1}_{\lambda,\lambda} F_{\lambda,x_{res}}\right)}_{F_R} x_{res} + \\ &\underbrace{\left(G_{x_{res}} - F_{x_{res},\beta} F^{-1}_{\dot{\beta},\beta} G_{\dot{\beta}} - F_{x_{res},\lambda} F^{-1}_{\lambda,\lambda} G_{\lambda}\right)}_{G_R} u \end{aligned} \tag{35}$$

C. Synchronization of the input signal

Now the state space system for the controller model is residualized, the control dependency of the remaining states in G_R is high enough to apply an incremental control law. However, there is now a large difference between the controller model and the actual model describing the helicopter dynamics. Namely the latter model includes dynamics and time delays from flap dynamics and inflow dynamics while the former does not. This means that the controller model expects the helicopter to react much faster than is happening in real life. Furthermore, sensors, filters and actuator dynamics also have an influence on the control deflection feedback and state measurement feedback. When not accounting for these time differences, instabilities and divergent behavior can occur. Therefore a synchronization filter is implemented for the flap dynamics in the current helicopter simulation model [5]. This filter delays the feedback measurement of the control input to mimic the delay that the control input otherwise had due to the flap dynamics, inflow dynamics and other uncontrolled signal manipulations. A downside of this synchronization filter is that some system dynamics coefficients have to be estimated, as it needs to map the expected effect of the controller input by the controller to the real effect of the rotorcraft including the time delay. However, this is just a portion of the total amount of system dynamics coefficients in $f(x)$ that would have been estimated if a non-incremental controller was used. As the inflow dynamics also plays a role in the response of a helicopter, it should be investigated whether they also need to be residualized and included in the synchronization filter. A similar case was investigated with respect to the lead-lag dynamics of the rotor system by [33], but it was concluded that this was not necessary for this specific part of the helicopter dynamics.

The time delay that is removed during the residualization process can be synchronized using eq. (36). The filter is placed in the feedback path of the actuator deflection measurement, converting the measured actuator

deflections to synchronized actuator deflections. As in residualization procedure, β and λ are the flap and inflow vector. θ represents the control vector, while ω represents the angular rates. The sensor dynamics can be accounted for by placing the model of the sensors also on the actuator feedback path. This will cause the possible delay of the sensors to by applied to both the state estimation signal as the actuator feedback, thereby cancelling out any effect of the sensors. The synchronized control input θ_{sync} can now be used to calculate the new control output of the controller by adding it to the incremental control output Δu of the controller.

$$\begin{bmatrix} \dot{\beta}_{sync} \\ \dot{\lambda}_{sync} \\ \theta_{sync} \end{bmatrix} = \begin{bmatrix} F_{\beta,\beta} \\ 0 \\ G_R^{-1} F_{\omega,\beta} \end{bmatrix} \beta_{sync} + \begin{bmatrix} 0 \\ F_{\lambda,\lambda} \\ G_R^{-1} F_{\omega,\lambda} \end{bmatrix} \lambda_{sync} + \begin{bmatrix} G_\beta \\ G_\lambda \\ G_R^{-1} G_\omega \end{bmatrix} \theta_{meas} \tag{36}$$

IV. Results & Discussion

The results of the applied changes in the inflow model and the residualized controller model in combination with the extended synchronization filter are discussed in two parts. The effects of changing the inflow model from a Pitt-Peters model to the Keller model is discussed in section IV.A. The analysis is based on pole-zero locations, simulations of the free response to control input without any interference of the control system and a tracking task of rotational rate reference signals. The outcomes of adapting the residualized dynamic model and synchronization for accounting for inflow dynamics is given in section IV.B. All simulations performed in this chapter are initiated from hovering conditions.

A. Applying Keller inflow model

To see if the modified inflow dynamics have influence on the helicopter dynamics as a whole, one can look at the complex plane representation of the linearized systems. With this method one can see if the inflow modes cause the body modes or flap modes to change position with respect to the nominal model. Figure 1 shows the complex plane representation of the nominal model and a zoomed-in figure for the poles near the origin. Note that only the positive side of the imaginary axis is displayed, as the locations of oscillatory poles is mirrored across the real axis.

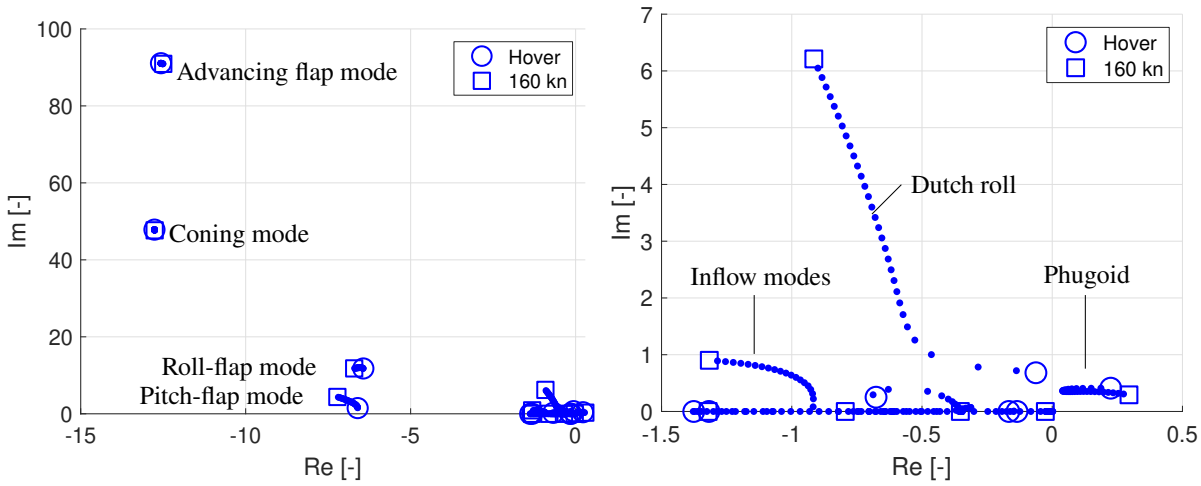

(a) Nominal model. **(b) Nominal model, zoomed-in around origin.**

Figure 1. Complex plane representation of linearized nominal helicopter model.

In order to compare both models, the complex plane representation of the linearized helicopter model with the Keller inflow model is given in fig. 2.

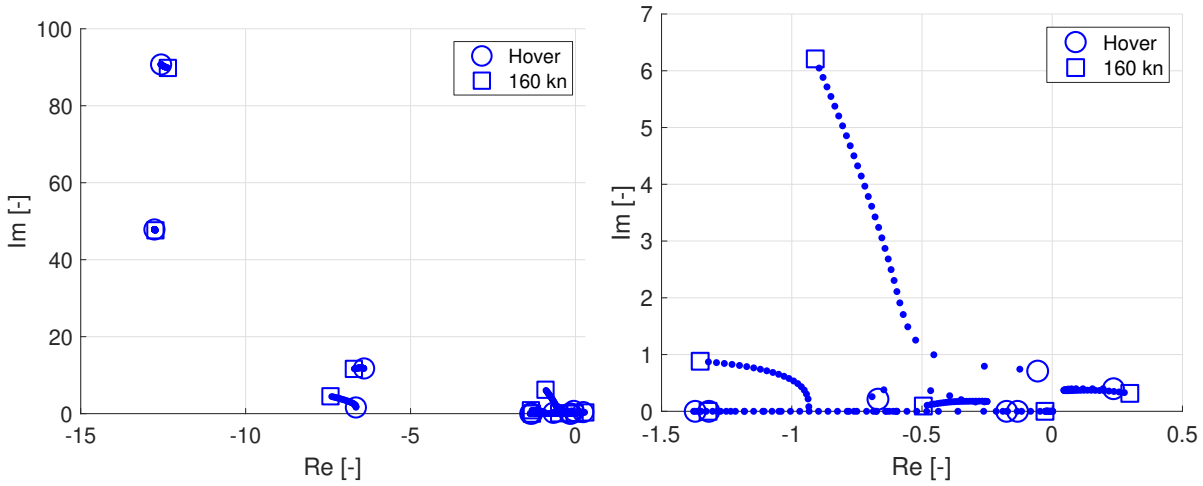

(a) Modified model with K_R=3. **(b) Modified model with K_R=3,zoomed-in around origin.**

Figure 2. Complex plane representation of linearized helicopter model with Keller correction.

Comparing the complex plane representations fig. 1 (a) and fig. 2 (a), one can conclude that they look very similar. For both hover and forward flight no shifting of the poles is visible due to the change in inflow dynamics. In fig. 1 (a) some typical modes are identified. Two of the three flap modes, namely the advancing flap mode and the coning mode, are located at the same position as if the flap dynamics would be treated separately. This is to be expected since they are of relatively high frequency compared to the body modes. Leaving out the second derivative of the flap angles in eq. (2) of a helicopter simulation, the origin of this high frequency mode, is therefore justifiable in most cases. The regressing flap mode, normally on the same vertical axis as the other two modes but much closer to the real axis, has coupled with the pitch subsidence and roll subsidence. If only the body states would be treated, these would be non-oscillatory modes in case of the MBB Bo-105. This shows that for the MBB Bo-105 there is coupling between the regressing flap mode and the body modes, speeding up the body motion.

The poles close to the origin are visualized in fig. 1 and fig. 2. Also in this view the location of the poles have not changed significantly. One can identify the Dutch roll and phugoid modes in the figure, with the heave and spiral subsidence remaining on the real axis near the origin. The only observable difference are two non-oscillatory poles close to coordinate -0.5. As the flight speed increases they move from the real axis and become lightly oscillatory. However, no major coupling with other modes can be seen in this view. All three inflow modes start on the real axis, with one mode becoming oscillatory as flight speed increases.

Another way to see the possible influence of the changed inflow model is by looking at the free response of the helicopter model subjected to a step in control input without interference of the controller. The four inflow states of the helicopter model are presented in fig. 3 together with the angular rated of the helicopter. These are the responses to a doublet consisting of a negative step input of 1 second on the longitudinal cyclic of -3 degrees at 1 seconds follow by an opposite command at 2 seconds. For the remainder of simulation time and for the other control inputs there is no action. The simulation is performed from a hovering initial position.

From Figure (a) and (c) there are small differences visible during the time that longitudinal control input is given. This also translates into slightly different angular rates. However, between the nominal and modified model there should be a notably different reaction in the off-axis angular rates. Because longitudinal cyclic is applied in this example, there should be a difference between the roll rate of the nominal and modified

simulation. The simulation is performed for hover, as in this initial state the Keller correction is most effective. Simulations at other airspeeds were also performed but did not give other results.

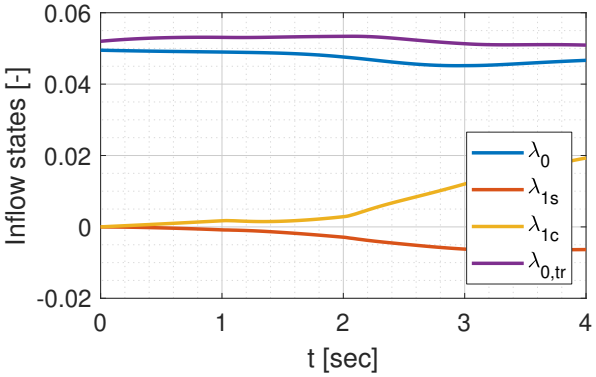

(a) Inflow parameters for the nominal model.

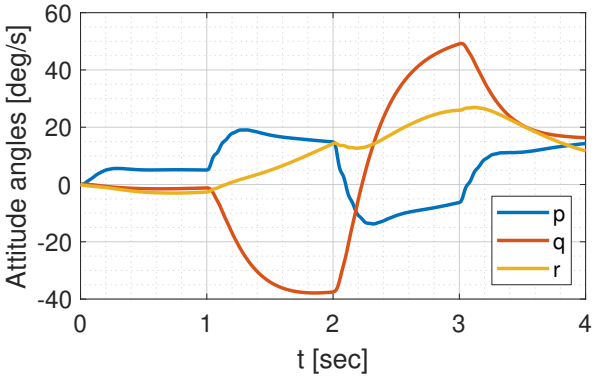

(b) Angular rates for the nominal model.

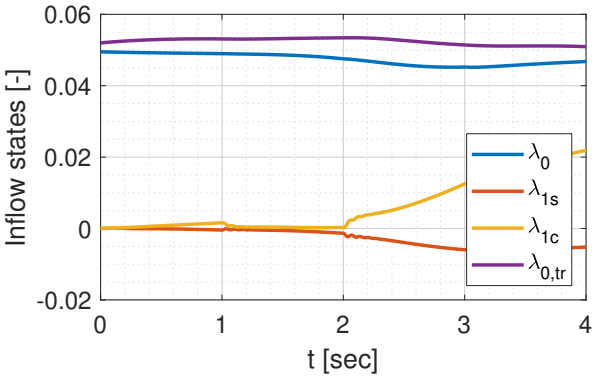

(c) Inflow parameters for the modified model.

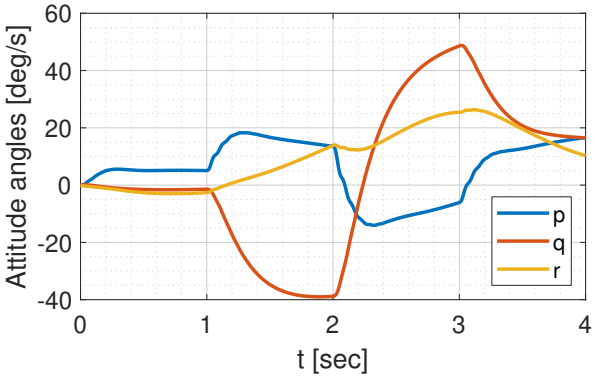

(d) Angular rates for the modified model.

Figure 3. Free helicopter response to step input in longitudinal cyclic in hover.

Finally, it is investigated whether the control inputs generated by the CFIBS controller have been altered by the change inflow dynamics. To this end a simulation has been performed in which the controller has to track a doublet in the pitch axis and roll axis. The results can be seen in fig. 4, which shows the calculated control inputs by the controller, the angular rates of the helicopter together with the reference signals and lastly the resulting inflow coefficients. In this experiment the residualization and synchronization procedure has only been performed for the flap states. Note that in fig. 4 (c) and (d) besides the reference input there is also a commanded input. This is the signal that the CFIBS is trying to track and is calculated based on the reference signal itself and the response requirements set in the ADS-33E-PRF handling qualities requirements [34].

As with the other experiments, no large difference is visible between the nominal and modified model. The harmonic inflow coefficients show a sharper change after the doublets are initiated, but the overall effect is insignificant. The largest effect during this simulation should be visible in the control inputs generated by the control system. If a change in off-axis coupling would be present, the lateral control input would change when a longitudinal doublet is performed because the controller tries to keep the other angular rates at zero. This also applied to the longitudinal control input when a roll doublet is performed. But just as for the other simulations in this section, the change inflow model hardly causes any difference in the tracked parameters.

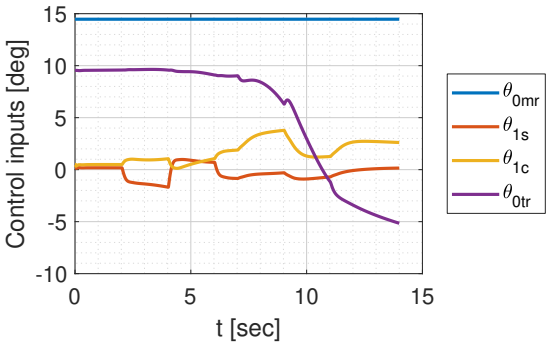

(a) Control inputs for the nominal model.

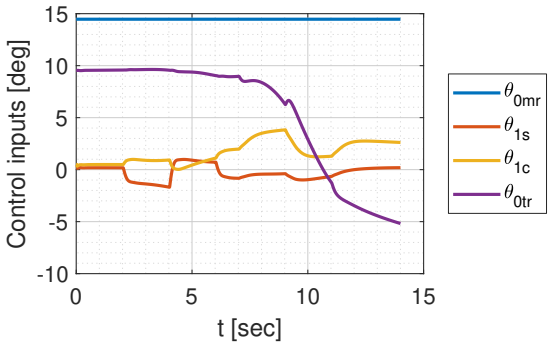

(b) Control inputs for the modified model.

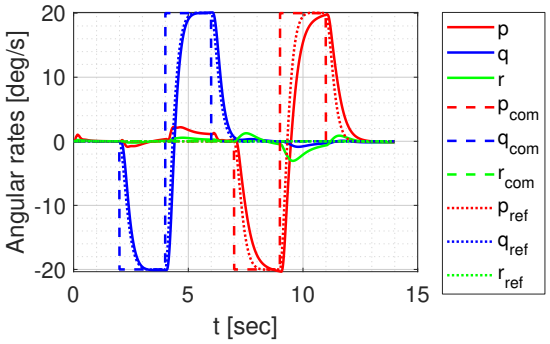

(c) Angular rates for the nominal model.

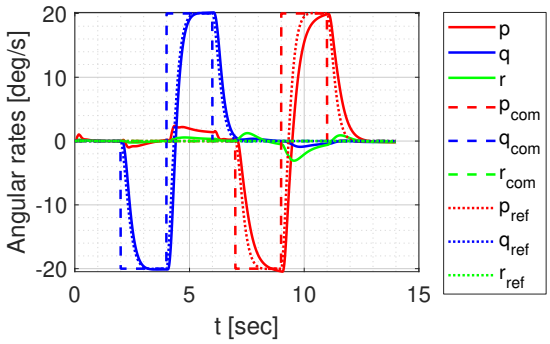

(d) Angular rates for the modified model.

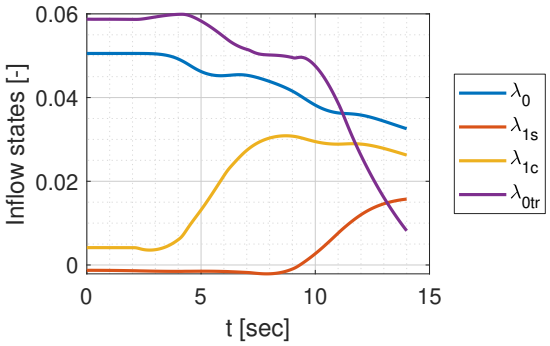

(e) Inflow parameters for the nominal model.

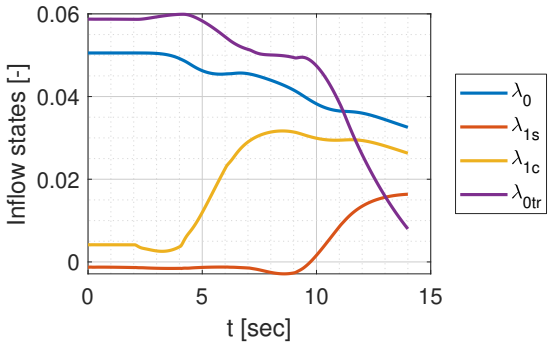

(f) Inflow parameters for the modified model.

Figure 4. Helicopter response to angular rate doublets using CFIBS in hover.

It can be concluded from the investigations above that the implementation of the Keller correction in the inflow model did not give any major difference in the helicopter characteristics. It is unclear why this is the case, as simulation experiments from [17] do show differences in the response of the helicopter and changes in the off-axis correction. The simulations shown here are only for hover, as this should be the condition in which the largest effect is visible, but are also carried out for a range of airspeeds. These showed no other behavior than the simulations discussed above. The modified model is implemented correctly and the mathematical model is checked against multiple other sources [35, 36]. Increasing the value of K_R multiple factors only increases the coupling between the harmonic inflow coefficients and the angular rates in the same axis, but the off-axis couplings remain the unchanged. There is some ambiguity between the references

whether some parameters are divided by Ω or not, but multiplying K_R by Ω gives unrealistic results and in turn do not change the off-axis coupling. Dividing K_R by Ω has no use, as the effect of the correction goes to zero as K_R approaches zero.

B. Inflow residualization and synchronization

Besides the investigation into the effect of modifying the inflow model, efforts have also been made to analyze the effect of including the inflow dynamics in the residualization and synchronization procedure. These can be seen as separate parts; for the analysis of these procedures it does not matter whether the original inflow model or the modified inflow model is used in the helicopter model.

Currently only the flap angles are residualized from the controller model. This is a logical choice as the flap angle states cannot be measured and are the most important states relating to controlling the helicopter. Controlling a helicopter while being unable to account for the time delays that the flap dynamics introduce is impossible. However, the inflow states are currently not residualized. An incremental control law based on such a model is not possible in real life as it is impossible to measure the inflow states. Therefore they either have to be removed from the controller model, leaving a model with a lower fidelity, or they have to be residualized and accounted for in the synchronization filter. Removing the inflow states from the controller model seems unwanted, since the rotor inflow has an effect on the flap dynamics according to the literature mentioned in section II.B and section III.A. Therefore this step is not merely to account for time scale separation, but also from an implementation point-of-view.

To analyze if residualizing and synchronizing the inflow dynamics is beneficial for controller performance, the synchronization filter of eq. (36) is added to the flap synchronization in the helicopter model. Furthermore, the system and control dependency matrices are adapted so both inflow states and flap dynamics are residualized. The updated model is compared to the original model by means of their tracking performance of attitude angle reference signals. As with other simulations in this chapter, the simulations are initiated in hover condition, as this is the situation wherein the inflow states are supposed to have the most influence on the helicopter dynamics. Figure 5 shows a comparison for a pitch and roll attitude tracking task with and without additional inflow residualization and synchronization using the CFIBS controller.

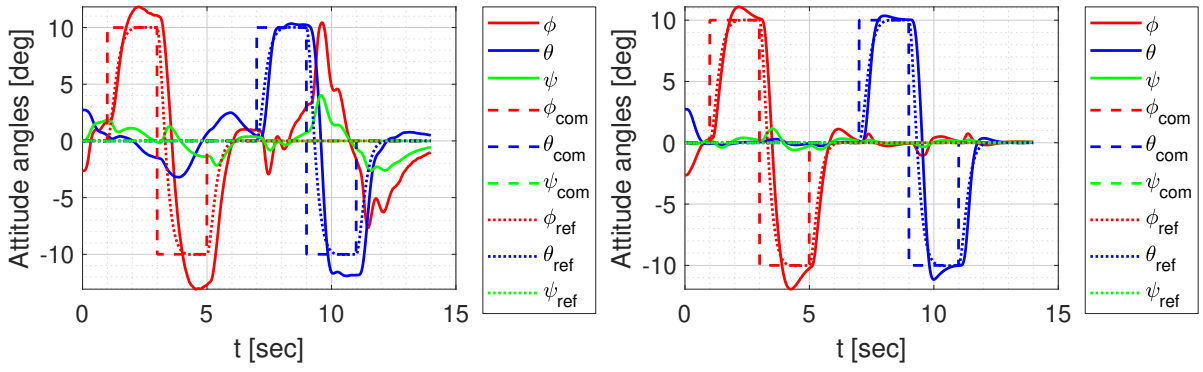

(a) Flap and inflow synchronization. **(b) Only flap synchronization.**

Figure 5. Tracking of attitude reference signals with CFIBS controller in hover.

It can be seen that the tracking performance with only flap synchronization is better than the adapted version of the controller. The tracking performance of the respective attitude angles to which a doublet reference signal is given is still somewhat satisfactory. However, large deviations in the other attitude angles are visible. The controller is unable to keep them close to their reference signal. The doublet tracking shows both overshoot of the reference value and time delay, with roll angle tracking worse than pitch angle tracking. This

is unexpected, since the moment of inertia of the helicopter around the roll axis is less than around the pitch axis.

The comparison between inflow synchronization of the nominal model and the model with the off-axis correction can be seen in fig. 6. It can be concluded that lack of tracking performance is not due to the added correction itself, but rather due to inflow synchronization as a whole. Moreover, the tracking performance keeps degrading for higher reference angles. If the reference signals reach above 30 degrees for this series of doublets, the simulation model will diverge in attitude control due to reaching actuator magnitude limits.

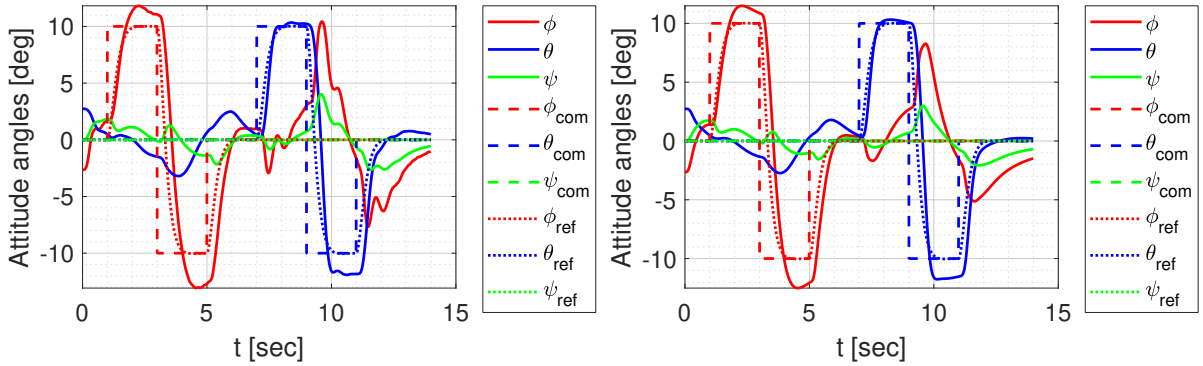

(a) Model with added inflow correction. **(b) Nominal model.**

Figure 6. Flap and inflow synchronization with CFIBS controller in hover.

The tracking task is also performed with an INDI controller to see whether the lack of tracking performance is specific to the CFIBS controller. Figure 7 (a) shows the tracking task for both flap and inflow synchronization, while subfigure (b) only employs flap synchronization. From subfigure (a) it can be concluded that INDI controller performance is also inadequate when using flap and inflow synchronization. This shows that the poor performance is not due to a specific control algorithm, but rather the application of residualization and synchronization of the inflow dynamics. Comparing the tracking performance with the CFIBS controller in fig. 5 one can see that both controllers have problems tracking the signal. The INDI controller does a slightly better job in mitigating the unwanted cross-couplings, but on the other end has more overshoot in the roll angle doublet.

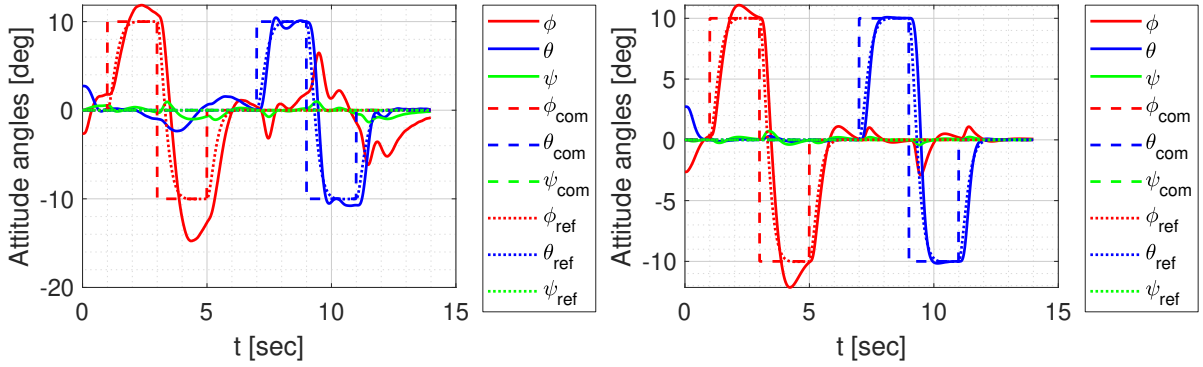

(a) Flap and inflow synchronization. **(b) Only flap synchronization.**

Figure 7. Tracking of attitude reference signals with INDI controller in hover.

V. Conclusion

This paper considers the investigation into the improvement of the off-axis response of an MBB Bo-105 hingeless helicopter due to the improvement of the current Pitt-peters inflow model. It was found in literature that the Keller inflow model improves the off-axis response of the helicopter simulation model due to a change in inflow dynamics. Furthermore, an analysis has been performed on the inclusion of inflow dynamics in the controller model of incremental controllers. Adding the inflow dynamics to the residualization and synchronization of the controller model could increase its performance and make the controller more suited for application in real life, since it is currently impossible to measure the inflow of the rotor.

After applying the Keller inflow model in the helicopter model it was found that the improved model did not have the desired outcome. The off-axis response did not change and the overall effect on the inflow states was very minor. This resulted in no changes in the overall helicopter dynamics, as was proved by analysis of the complex plane representation of the linearized helicopter dynamics and the execution of several angular rate tracking tasks.

The inclusion of the inflow states in the synchronization filter and the residualized system description also did not have the wanted effect. Tracking performance of the command filtered incremental backstepping controller degraded significantly, not being able to track attitude reference signal doublets above 30 degrees magnitude for the tested reference signals. Especially the attitude angles that were supposed to stay at zero showed significant coupling, compared to the simulation with only flap synchronization. However, the inflow residualization and synchronization is necessary because the inflow states cannot be measured in real life. The results did not change whether the simulation was performed with the improved Keller inflow model or the original Pitt-Peters inflow model. The tracking task was also performed with and incremental non-linear dynamic inversion controller, but this did not result in better tracking performance. From this it can be concluded that the degradation of controller performance is due to the process of residualization and synchronization, not from a specific incremental control methodology.

References

[1] Stiles, R. L., Mayo, J., Freisner, L. A., Landis, K. H., and Kothmann, B. D., “"Impossible to Resist" The Development of Rotorcraft Fly-By-Wire Technology,” *Annual Forum Proceedings - AHS International*, 2004, pp. 1–18.

[2] Keijzer, T., Looye, G., Chu, Q. P., and Van Kampen, E., “Flight Testing of Incremental Backstepping Based Control Laws with Angular Accelerometer Feedback,” *AIAA Scitech 2019 Forum*, 2019, pp. 1–25. doi: 10.2514/6.2019-0129.

[3] Pavel, M. D., “On the Necessary Degrees of Freedom for Helicopter and Wind Turbine Low-Frequency Mode Modeling,” Ph.D. Thesis, Delft University of Technology, 2001.

[4] Simplício, P., Pavel, M. D., Van Kampen, E., and Chu, Q. P., “An Acceleration Measurements-Based Approach for Helicopter Nonlinear Flight Control using Incremental Nonlinear Dynamic Inversion,” *Control Engineering Practice*, Vol. 21, No. 8, 2013, pp. 1065–1077. doi: 10.1016/j.conengprac.2013.03.009.

[5] Chu, Q. P., Pavel, M. D., and Van der Goot, R. R., “Incremental Adaptive Backstepping Flight Control for Rigid Rotor Helicopters,” *American Institute of Aeronautics and Astronautics*, 2017, pp. 1–33.

[6] Pavel, M. D., Shanthakumaran, P., Stroosma, O., Chu, Q. P., Wolfe, M., and Cazemier, H., “Development of Advanced Flight Control Laws for the AH-64 Apache Helicopter - Sketches from the Work of TU Delft-Boeing Project in SIMONA Simulator,” *Annual Forum Proceedings - AHS International*, Vol. 3, 2016, pp. 1778–1792.

[7] Van der Goot, R. R., “Helicopter Control using Incremental Adaptive Backstepping,” Master thesis, Delft University of Technology, 2017.

[8] Keller, J. D., and Curtiss, H. C., “Modeling the Induced Velocity of a Maneuvering Helicopter,” *Annual Forum Proceedings - American Helicopter Society*, Vol. 1, 1996, pp. 841–851.

[9] Peters, D. A., “How Dynamic Inflow Survives in the Competitive World of Rotorcraft Aerodynamics,” *Journal of the American Helicopter Society*, Vol. 54, No. 1, 2009, pp. 1–15. doi: 10.4050/JAHS.54.011001.

[10] Padfield, G. D., *Helicopter Flight Dynamics : The Theory and Application of Flying Qualities and Simulation*

Modelling, John Wiley & Sons, Incorporated, 2007.

[11] Hohenemser, K. H., and Yin, S., "Some Applications of the Method of Multiblade Coordinates," *Journal of the American Helicopter Society*, Vol. 17, No. 3, 1972, pp. 3–12. doi: 10.4050/JAHS.17.3.3.

[12] Johnson, W., *Helicopter Theory*, Dover Publications, New York, 1994.

[13] Peters, D. A., "Hingeless Rotor Frequency Response with Unsteady Inflow," *AHS/NASA-Ames Specialists' Meeting on Rotorcraft Dynamics*, 1974, pp. 1–12.

[14] Pitt, D. M., and Peters, D. A., "Theoretical Prediction of Dynamic-Inflow Derivatives," *Sixth European Rotorcraft and Powered Lift Aircraft Forum*, 1980, p. 19.

[15] Du Val, R. W., and He, C. J., "Validation of the FLIGHTLAB virtual engineering toolset," *Aeronautical Journal*, Vol. 122, No. 1250, 2018, pp. 519–555. doi: 10.1017/aer.2018.12.

[16] Saberi, H., Hasbun, M., Hong, J., Yeo, H., and Ormiston, R. A., "Overview of RCAS Capabilities, Validations, and Rotorcraft Applications," *Proceedings of the American Helicopter Society 71st Annual Forum*, 2015, p. 328.

[17] Keller, J. D., and Curtiss, H. C., "A Critical Examination of the Methods to Improve the Off-Axis Response Prediction of Helicopters," *Annual Forum Proceedings - AHS International*, 1998, pp. 1134–1147.

[18] Bramwell, A. R. S., Done, G., and Balmford, D., *Bramwell's Helicopter Dynamics*, second edi ed., Butterworth Heinemann, 2001.

[19] Sieberling, S., Chu, Q. P., and Mulder, J. A., "Robust Flight Control using Incremental Nonlinear Dynamic Inversion and Angular Acceleration Prediction," *Journal of Guidance, Control, and Dynamics*, Vol. 33, No. 6, 2010, pp. 1732–1742. doi: 10.2514/1.49978.

[20] Smeur, E. J. J., Chu, Q. P., and De Croon, G. C. H. E., "Adaptive Incremental Nonlinear Dynamic Inversion for Attitude Control of Micro Air Vehicles," *Journal of Guidance, Control, and Dynamics*, Vol. 39, No. 3, 2016, pp. 450–461. doi: 10.2514/1.G001490.

[21] Van 't Veld, R. C., Van Kampen, E., and Chu, Q. P., "Stability and Robustness Analysis and Improvements for Incremental Nonlinear Dynamic Inversion Control," *AIAA Guidance, Navigation, and Control Conference, 2018*, 2018, pp. 1–17. doi: 10.2514/6.2018-1127.

[22] Campolucci, P., "Model and Actuator Based Trajectory Tracking for Incremental Nonlinear Dynamic Inversion Controllers," Master thesis, Delft Univerity of Technology, 2021.

[23] Acquatella, P. J., Van Kampen, E., and Chu, Q. P., "Incremental backstepping for robust nonlinear flight control," *2nd CEAS Conference on Guidance, Navigation, and Control*, 2013, pp. 1444–1463.

[24] Koschorke, J., "Advanced Flight Control Design and Evaluation," Master thesis, Delft University of Technology, 2012.

[25] Acquatella, P. J., "Robust nonlinear attitude control of aerospace vehicles: An incremental nonlinear control approach," Ph.D. Thesis, Delft University of Technology, 2020.

[26] Huang, J., Zhang, Y., Pool, D. M., Stroosma, O., and Chu, Q. P., "Time-Delay Margin and Robustness of Incremental Nonlinear Dynamic Inversion Control," *Journal of Guidance, Control, and Dynamics*, Vol. 45, No. 2, 2022, pp. 394–404. doi: 10.2514/1.G006024.

[27] Su, A., Yoo, K. M., and Peters, D. A., "Extension and Validation of an Unsteady Wake Model for Rotors," *Journal of Aircraft*, Vol. 29, No. 3, 1992, pp. 374–383. doi: 10.2514/3.46172.

[28] Rosen, A., and Isser, A., "A New Model of Rotor Dynamics During Pitch and Roll of a Hovering Helicopter," *Journal of the American Helicopter Society*, Vol. 40, No. 3, 1995, pp. 17–28. doi: 10.4050/JAHS.40.17.

[29] Keller, J. D., "An Investigation of Helicopter Dynamic Coupling Using an Analytical Model," *Journal of the American Helicopter Society*, Vol. 41, 1996, pp. 322–330. doi: 10.4050/JAHS.41.322.

[30] Arnold, U. T. P., Keller, J. D., Curtiss, H. C., and Reichert, G., "The Effect of Inflow Models on the Predicted Response of Helicopters," *Journal of the American Helicopter Society*, Vol. 43, No. 1, 1998, pp. 25–36. doi: 10.4050/JAHS.43.25.

[31] Basset, P., and Tchen-Fo, F., "Study of the Rotor Wake Distortion Effects on the Helicopter Pitch-Roll Cross-Coupling," *24th European Rotorcraft Forum*, 1998, p. 13.

[32] Skogestad, S., and Postlethwaite, I., *Multivariable Feedback Control - Analysis and Design*, second edi ed., John Wiley & Sons, 2001. doi: 10.11406/rinketsu.20.1191.

[33] Arons, M. D. C., "Effect of Lead-Lag Dynamics on Command Filtered Incremental Adaptive Backstepping Hingeless Rotorcraft," Master thesis, Delft University of Technology, 2020.

[34] Baskett, B. J., "ADS-33E-PRF: Aeronautical Design Standard, Performance Specification and Handling Qualities

Re- quirements for Military Rotorcraft," , US Army Aviation and Missile Command, 2000.

[35] Barocela, E., Peters, D. A., Krothapalli, K. R., and Prasad, J. V. R., "The Effect of Wake Distortion on Rotor Inflow Gradients and Off-Axis Coupling," *22nd Atmospheric Flight Mechanics Conference*, 1997, pp. 272–282. doi: 10.2514/6.1997-3579.

[36] Zhao, J., "Dynamic Wake Distortion Model for Helicopter Maneuvering Flight," Ph.D. Thesis, Georgia Institute of Technology, 2005.

Appendix

Table 1. MBB Bo-105 helicopter parameters.

Parameter	Value	Unit	Description
Ω	44.4	rad/s	Rotor rotational speed
R	4.91	m	Rotor radius
N	4	-	Number of rotor blades
c_e	0.27	m	Equivalent blade chord
C_{l_a}	6.113	rad^{-1}	Blade lift curve slope
θ_{tw}	-8.0	deg	Linear blade twist
I_β	231.7	kg*m^2	Blade MoI about flapping hinge
K_β	113330	Nm/rad	Center-spring rotor stiffness
γ_s	0.0524	rad	Rotor shaft tilt angle
h_{cg}	0.94468	m	Height of main hub above center of gravity
F_0	1.3	-	Fuselage parasite drag area
m	2200	kg	Helicopter mass
I_{xx}	1433	kg*m^2	MoI about roll-axis
I_{yy}	497	kg*m^2	MoI about pitch-axis
I_{zz}	4099	kg*m^2	MoI about yaw-axis
I_{xz}	660	kg*m^2	MoI about nonsymmetry-axis
$\theta_{1s_{max}}$	11.0	deg	Maximum longitudinal control input
$\theta_{1s_{min}}$	-6.0	deg	Minimum longitudinal control input
$\theta_{1s_{rate}}$	28.8	deg/s	Maximum longitudinal control input rate
$\theta_{1c_{max}}$	4.2	deg	Maximum lateral control input
$\theta_{1c_{min}}$	5.7	deg	Minimum lateral control input
$\theta_{1c_{rate}}$	16.0	deg/s	Maximum lateral control input rate
$\theta_{0_{max}}$	20.0	deg	Maximum collective control input
$\theta_{0_{min}}$	-0.2	deg	Minimum collective control input
$\theta_{0_{rate}}$	16.0	deg/s	Maximum collective control input rate
γ	5.087	rad^{-1}	Rotor Lock number
λ_β	1.12	-	Normalized flapping frequency

Part II

Thesis work

1 Introduction

Helicopters and other rotorcraft are known to have certain advantages compared to conventional fixed-wing aircraft, mainly due to their hovering and VTOL capabilities. They are therefore used for a large variety of tasks that are impossible to perform by their fixed-wing counterpart. For instance, helicopters are well suited for search & rescue operations, transportation of people or cargo to remote locations where runways are not available, construction in mountainous terrain and several military applications. Most of these tasks utilize the high degree of maneuverability of a helicopter, it being able to perform vertical take-offs and landings, hover and fly sideways and backwards while maintaining a high degree of precision.

As with many systems these advantages come at a cost. It has been recognized for a long time that helicopters are notoriously difficult to control as a pilot, with Handling Quality ratings consistently lower than aircraft. The main reason for this are the cross-couplings in the control system and the non-linear dynamics of the helicopter. Unlike aircraft, the control surfaces do not directly affect the angular rates of the body, but rather influence the orientation of the thrust vector through tilting of the main rotor plane. Thus attitude control is done through a single actuation device, instead of the separated channels found in aircraft design. In this light Micro Aerial Vehicles (MAVs) also differ from conventional helicopters as they perform attitude control by distributing power over the available rotors, instead of combining all these functions in one rotor system. Cross-couplings between longitudinal and lateral modes originate from gyroscopic precession that is experienced by the main rotor subjected to control inputs and airspeed. The non-linear behavior of helicopters is due to complex aerodynamics surrounding the helicopter, especially near hovering flight, as it operates in its own wake. The wake of the rotor, composed of multiple vortices coming from each blade, interferes with the blade aerodynamics and the induced velocity generated by the rotor disk. All these effects have influence on the thrust vector, which is used to control the attitude of the helicopter. Furthermore, a large portion of a generic helicopter flight task is done outside trimmed cruise flight, often at low altitude and in the vicinity of hazardous objects. This makes predictable helicopter response and helicopter stability very important.

1.1. Problem definition

A solution to alleviate the workload of helicopter pilots and to deal with the non-linearities and instabilities of a rotorcraft is the implementation of advanced digital flight control systems in helicopters. In order to incorporate full authority digital flight control systems, the rotorcraft has to be controlled through fly-by-wire technology. Other advantages of such systems compared to hydraulic or mechanical control systems are the reduction of cost and weight. In older helicopter types the support of pilots is limited to mechanical mixing systems that compensate control inputs of the pilots by a fixed ratio. This only marginally improves helicopter handling. As the helicopter industry is much smaller than the aircraft industry, and therefore has lower funding, the introduction of fly-by-wire systems took place in a much later stage than for aircraft. Full authority digital flight control systems in military helicopters were introduced the NH-90 and V22 Osprey around 2004 (Stiles et al. 2004). The introduction of fly-by-wire systems in commercial helicopters started in 2015 with the Bell 525.

In recent years the development and application of non-linear controllers show promising results in

many research areas. Within the TU Delft Control & Simulation group, research has been performed on implementing these controller types to helicopter models. Especially their incremental versions of these non-linear methods have been studied, as they are successfully applied to micro aerial vehicles and aircraft (Keijzer et al. 2019). Based on a generic helicopter model tailored to the specifications of an MBB Bo-105 hingeless helicopter, developed by Pavel (2001), Simplício et al. (2013) implemented an Incremental Non-linear Dynamic Inversion (INDI) controller. Later, Chu, Pavel, and Van der Goot (2017) successfully applied an Incremental Backstepping controller (IBS) on an improved helicopter model. The application of INDI by Pavel, Shanthakumaran, Stroosma, et al. (2016) to an Apache AH-64D model, the Apache FlyRT model provided by Boeing, proved to be more challenging.

The advantage of incremental controllers is that they hardly rely on accurate model knowledge, as their regular variants do, but rather on measurements of the state of the helicopter. This circumvents the costly determination of the helicopter dynamics model of the to be controlled system, which needs to be of high accuracy to ensure stability of the closed loop system. However, the sensory equipment of contemporary helicopters is unable to measure certain important states, making real life implementation of these controllers impossible without proper adaptation. In particular the flap dynamics, the movement of individual blades under inertial and aerodynamics forces, needs to be accounted for. Van der Goot (2017) made these adaptations concerning the flap dynamics, by residualizing the flap states in the controller model and compensate for their dynamics with a synchronization filter. Arons (2020) looked at the influence of lead-lag dynamics, but showed that the IBS controller is robust to uncertainties in lead-lag dynamics. The dynamics of the airflow around the main rotor however has not yet been investigated. As said, the non-linear behavior of the helicopter comes partly from the fact that it operates in its own wake. It is known that the inflow of the main rotor has an effect on the flapping of the blades. Accounting for the inflow dynamics in the controller design could have a positive effect on its performance. Besides the effect on the flapping of the blades it is also impossible to measure the inflow in real-time. Thus only residualizing the flap dynamics will not result in a control solution that can be implemented in reality.

Aside from the possible influence of inflow dynamics on controller performance, also the inflow dynamics modelling itself needs to be addressed. The inflow model that is used in the works of Van der Goot and Arons, although widely applied, models the off-axis response incorrectly (Keller and Curtiss 1996). This is the lateral response of the helicopter to longitudinal control input and vice versa. In general, for certain conditions the estimated flow is of opposite sign compared to test data. It is known that inflow is a difficult phenomenon to model and many papers have been published concerning correct off-axis inflow modelling (Peters 2009). Implementing accurate inflow models might alter the pilots perception during piloted simulation and minimizes the gap between reality and modelling results, enabling better research to control system behavior.

1.2. Approach

To summarize the challenges that were touched upon in the previous section, a set of research questions and sub questions have been set. The simulation model that will form the basis of the investigations is the model developed by Van der Goot (2017). This model consist of a helicopter model, specified to model a MBB Bo-105 hingeless helicopter and a controller. The helicopter model comprises of body, flap and inflow states along with actuator dynamics and sensors. The control related part of the model consists of an IBS, INDI and PID controller together with relevant estimators and signal filters. This also includes the residualization and synchronization of the flap angles.

- **RQ-1** How can the dynamic inflow model be improved to get better correlation between the off-axis response from the simulation and test data?
  - **SRQ-1.1** Which improved inflow models can be found in literature that are applicable to real-time simulation and controller design?
  - **SRQ-1.2** Does the inflow response change after implementing the best candidate?
  - **SRQ-1.2** Is a difference in helicopter dynamics visible after changing the inflow model?
- **RQ-2** Can correcting for inflow dynamics in the controller design give better controller performance?
  - **SRQ-2.1** Does residualizing the inflow dynamics have a positive effect on the control effectiveness of the controller?

- **SRQ-2.2** Can one see a contribution of the inflow dynamics in the synchronization filter?
- **SRQ-2.3** Is the tracking performance of the controller improved, based on handling quality criteria?

Summarizing the research questions in one statement, the main research objective of this thesis is:

to analyze the influence of inflow dynamics on the dynamics of a hingeless helicopter and to investigate the effect of accounting for inflow dynamics in controller design, by adapting the inflow model to correctly model the off-axis response and to add the inflow states to the synchronization filter.

1.3. Thesis outline

This thesis is structured as follows. Chapter 2 provides an overview of the governing equations that describe helicopter motion. It also highlights some important parameters that influence helicopter motion substantially. In Chapter 3 background knowledge about inflow modelling is presented and the different inflow modelling methods are discussed. The model that is used for implementation is chosen based on applicability to the current helicopter model and the feasibility to apply it to real-time simulation and control. Chapter 4 discusses non-linear control theory, with the focus on INDI and IBS. Furthermore, it treats the adoptions that are necessary to apply these controllers to a helicopter model. Finally, in Chapter 5 a number of case studies are presented to show the influence of incorporating flap dynamics and inflow dynamics into the controller design and helicopter dynamics. The cases start with simplified models showing the importance of including flap or inflow dynamics in the controller. The last case will show the result of the modified inflow model en controller augmentation on the full rotor, inflow and body dynamics helicopter model.

2

Helicopter Dynamics

The main helicopter simulation model that is used in this analysis is adopted from Van der Goot (2017). The model closely follows the helicopter dynamics description that can be found in Padfield (2007). All relevant helicopter data for the MBB Bo-105 can be found in Appendix A. The state of the helicopter consists of the classical six body rotational and translational DoF's, augmented with three flap DoF's of the main rotor blades and four inflow DoF's of the main and tail rotor. This results in 22 states: $\boldsymbol{x} = [u\ v\ w\ x\ y\ z \mid p\ q\ r\ \phi\ \theta\ \psi \mid \beta_0\ \beta_{1c}\ \beta_{1s}\ \dot{\beta}_0\ \dot{\beta}_{1c}\ \dot{\beta}_{1s} \mid \lambda_0\ \lambda_{1c}\ \lambda_{1s}\ \lambda_{0,tr}]^\mathsf{T}$. Their derivatives are calculated using non-linear differential equations and the corresponding states are obtained with a time-marching integration scheme, in this case Runge-Kutta4. The states are then used for detailed force and calculations for the horizontal and vertical tail plane, fuselage, tail rotor and main rotor. The focus in the model is on the main rotor, as it the most complicated subsystem to describe and is the actuation system that controls the helicopter. In this regard the flap angle, the angle that a blade makes perpendicular to the plane of rotation, can be seen as a very important variable. Finally, the forces and moments are used in the equations of motion to determine the new attitude, angular velocity, position and translational velocity of the helicopter body.

Because the body dynamics and flap dynamics are the most important parts of the simulation model, they are treated in Section 2.3 and Section 2.4. For a complete description of the helicopter model, the reader is referred to the report of Van der Goot (2017) or the book of Padfield (2007). Since the inflow dynamics are further investigated and altered in this report, they are treated separately in Chapter 3. Section 2.1 describes the mechanics of the rotor system and the control system that controls the pitch angle of the rotor blades. In Section 2.2 a general overview is given of the reference frames that are used in the helicopter model.

2.1. Helicopter rotor system

Looking from a control point of view, the most interesting mechanical part of a helicopter is the rotor hub. This is where the rotor blades are actuated and where all the forces and moments generated by the rotor are transferred to the fuselage. All the blades of the rotor are attached to the rotor via a combination of hinges, as can be seen in Figure 2.1. Of all the 3 possible rotations of the blade, flapping, lagging and feathering, only the feathering angle can be controlled by the pilot or control system. The other 2 angles are the result of the dynamics of the rotor. The hinges were first introduced by Juan de la Cierva in 1922 during the early development of helicopters, to compensate for the dissymmetry of lift during non-hovering flight. When a helicopter takes off vertically and hovers, the rotating blades experience the same apparent velocity vector at every azimuth during a full rotation. This velocity vector is the result of the angular velocity of the blade and the induced velocity it produces. However, when the helicopter starts to move in a certain direction a difference in lift between two sides of the rotor plane builds up. The rotor blades on the retreating side will experience a lower air velocity since a part of the angular velocity of the rotating blade is cancelled by the airspeed of the helicopter. On the advancing side the opposite happens. Here the airspeed of the helicopter is added to the angular velocity of the blade. When the flight speed is high enough this can even cause stall at the retreating side of the rotor or local transsonic behavior at the advancing side of the rotor. Due to this difference in velocity the

advancing side will generate more lift than the retreating side, resulting in the helicopter pitching over. To overcome this problem flapping hinges were installed. This allowed the blades on the advancing side, in case of forward flight speed, to flap up and the blades on the retreating side to flap down in harmonic fashion.

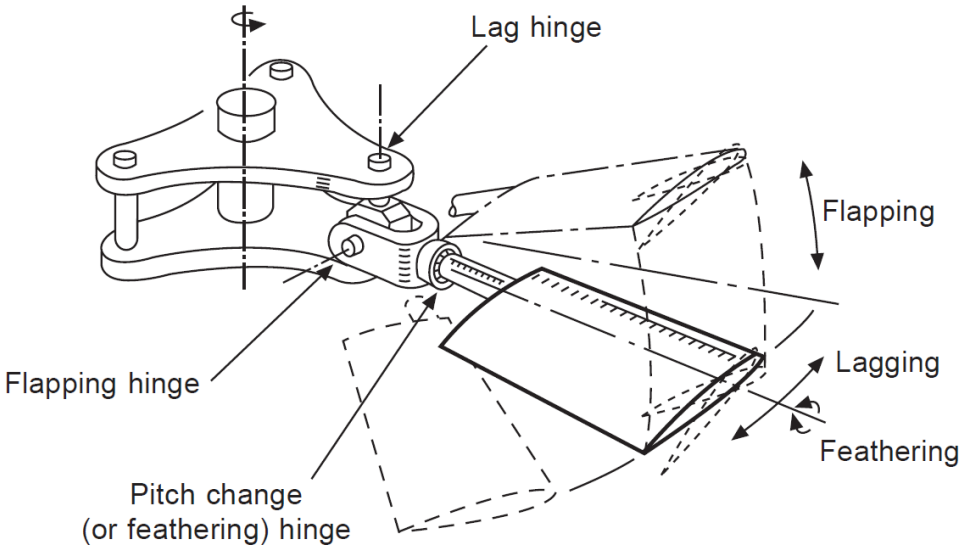

Figure 2.1: Typical hinge arrangement on a rotor hub (Bramwell, Done, and Balmford 2001).

Based on the number of hinges applied in the design of a helicopter, they can be classified in three categories: articulated, hingeless or bearingless rotors. Articulated rotors have hinges on all three axis, as shown in Figure 2.1, allowing the blade to move in every direction. This means that the blades can hardly transfer any moment to the rotor hub, making attitude changes solely possible by changing the orientation of the thrust vector. Thus causing the helicopter to respond relatively slow to control inputs. However, the use of hinges was the first logical and technological possible way to solve the dissymmetry of lift. Alternatively, later bearingless rotor designs have no hinges at all. They rely on structural bending of the blades and an elastomeric root to absorb the lead-lag and flap motion and facilitate blade pitching. A hingeless rotor combines the previous concepts, having only a hinge for blade pitch while relying on structural flexibility around the flap and lead-lag axis.

Because the bearingless and hingeless configurations are rigidly attached to the rotor hub, they can transfer much greater moments to it. This results in faster response to control inputs and therefore faster body motion. This is a key difference with articulated systems. For articulated systems the rotor dynamics and the body dynamics are well separated in time. A fast rotor response is followed by a slow body response, meaning that the rotor states can be treated as being constantly at steady state. This greatly simplifies controller design, as will be discussed in Chapter 4, as the influence of body dynamics on incremental control laws can be neglected and control dependency is high. With the increased flapping stiffness of hingeless rotorcraft the rotor dynamics speeds up the body motion, resulting in significant coupling between the body and flapping modes. In most cases, time-scale separation between body dynamics and flap dynamics cannot be assumed.

As mentioned the attitude of the helicopter is controlled by altering the pitch angles of the individual blades of the main rotor. The pilot or control system has 3 controls at its disposal for the main rotor: collective, longitudinal and lateral cyclic. The inputs of these controls are combined and result in a certain orientation of the swashplate. This is an apparatus that changes control inputs from the non-rotating fuselage to the rotating rotor system. The swashplate mechanism is visualized in Figure 2.2. Because the rotor blades are linked to the top part of the swashplate, the pitch angle of every blade changes constantly to be in line with the swashplate. This causes the pitch angle at a certain azimuth to stay constant. The orientation of the swashplate can be seen as a visualization of how the control system wants the plane of rotation of the blades to be oriented.

The collective is used to alter the pitch angle at every azimuth in the same way and mainly influences the thrust of the rotor. This is done by raising or lowering the swashplate entirely. The cyclic is used to rotate the helicopter in the longitudinal or lateral plane. For instance, when applying forward longitudinal

cyclic the swashplate will tilt forward. This will cause a positive pitch angle on the left and a negative pitch angle on the right, due to the pitch links being connected to the swashplate with a 90 degree lead to correct for gyroscopic precession. The plane that is trailed out by the tip of the blades is now tilted forward and the helicopter will start rotating.

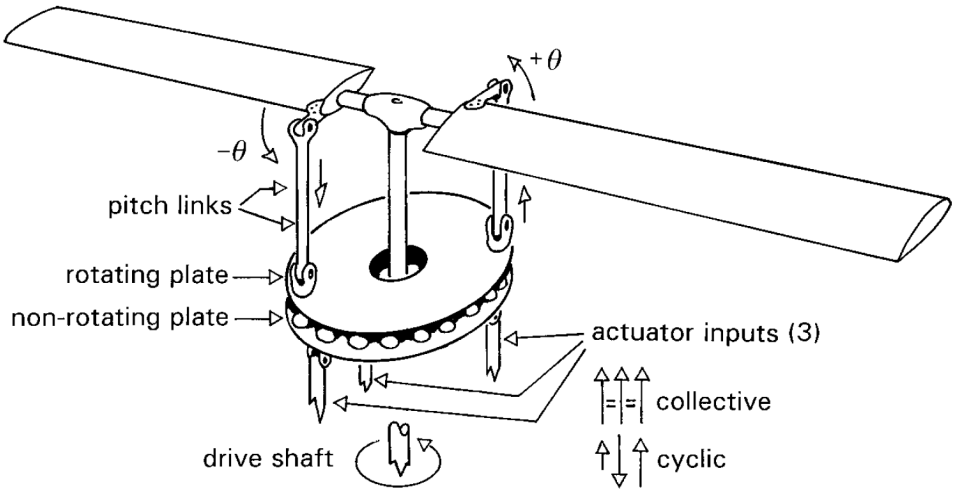

Figure 2.2: Swash plate system (Padfield 2007).

Besides the main rotor controls, their is also a tail rotor collective and engine throttle. The tail rotor collective has the same functionality as the main rotor collective and is operated by footpedals. It is used to control the yaw angle of the helicopter and is decoupled from the other system. As no cyclic inputs are used and the rotor is usually small, the flap dynamics are negligible and do not need to be accounted for. The engine throttle is often automated, as helicopter rotors are designed to work at a fixed RPM. As for example the collective is raised, the RPM of the rotor will drop because it will experience more drag due to the increased pitch angle of the blades. This is countered by increasing the throttle of the engine.

2.2. Reference systems and rotor planes

The body related variables, forces and moments follow the standard right-handed body axis system. A generic representation is given in Figure 2.3. Position coordinates are given in the North-East-Down reference frame, using the Euler attitude angles to convert the body velocities. The local reference system of the rotor proves to be more complicated. Due to the complexity of the rotor system different reference planes are used to calculate various parameters, with each plane offering simplifications for the equations at hand. The three most important reference planes can be seen in Figure 2.4. The figure shows a left side view of the planes, with the front of the helicopter on the left. All reference planes have their origin where the rotor hub meet the axis of rotation. The shaft plane (SP) or hub plane (HP) lies tangential to the body x and y axis and perpendicular to the z axis, corrected for the tilt angle and offset of the rotor hub. This plane is used to transfer variables, forces and moments to the body frame. The control plane (CP) is a fictive plane containing the swashplate. This plane sees no cyclic feathering of the rotor blades and is tilted compared to the shaft plane by the control input angles. The disk plane (DP) or tip-path plane (TPP) is made from the plane that the tips of the rotor blade make. Perpendicular to this plane is the thrust vector, while the angle with the shaft plane determines the flap angle of the blades. From the side view presented in Figure 2.4 one can see that if the disk plane coincides with the control plane, which can happen under specific circumstances, the cyclic pitch input that is given by the swashplate is equal to the flap angle of the blade 90 degrees later. This shows again the peculiarities of the control system. The difference between these planes is caused by the dynamics of the rotor, such as its response to angular rates.

For some calculations, the reference frames are rotated such that the sideslip angle is zero and there is no lateral airspeed in that frame. This is done for the inflow dynamics modelling, with its motion defined in the disk plane, and the flap dynamics modelling, with its motion defined in the shaft plane. In this way the inflow and flap models can directly be applied as found in literature. Orthonormal

transformation matrices are used that rotate the reference systems with the sideslip angle calculated from the body velocities.

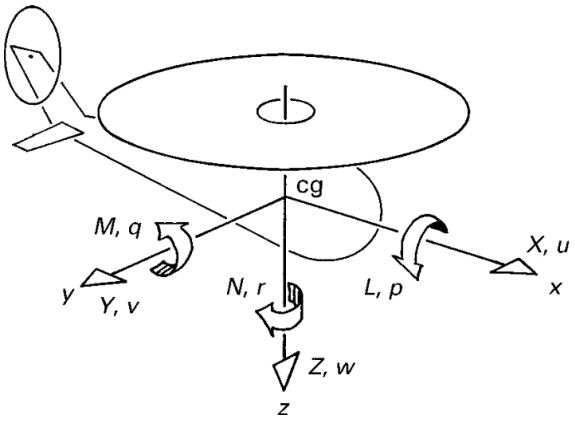

Figure 2.3: Illustration of the body reference system.

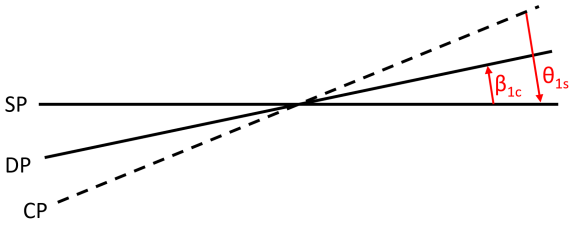

Figure 2.4: Reference planes of the rotor system.

To describe the pitch and flap angle of a blade during one revolution, one can make use of harmonic functions. The pitch angle of a blade is determined by equation Equation (2.1), with the coefficient being equal to the collective and cyclic control inputs. Equation (2.2) describes the flap angle of a blade at any azimuth. The coefficients in this equation are coming from the multi-blade coordinate coefficients treated in Section 2.3. Contrary to older descriptions found in literature, this equation has positive signs in front of the coefficients. Care should be taken when comparing the different flap angle formulations and their definition in relation with control related research, as they can be defined from other planes than the shaft plane. In Appendix B it is shown via a simplified example why this is important.

In a similar fashion, the induced velocity distribution across the disk plane can be constructed, in which $\bar{r_b}$ is the relative radial position on the rotor disk. The other are coming from the inflow model that will be discussed in Chapter 3.

$$\theta = \theta_0 + \theta_{1c}cos(\Psi) + \theta_{1s}sin(\Psi) \tag{2.1}$$

$$\beta = \beta_0 + \beta_{1c}cos(\Psi) + \beta_{1s}sin(\Psi) \tag{2.2}$$

$$\lambda_i = \lambda_0 + \bar{r_b}\left(\lambda_{1c}cos(\Psi) + \lambda_{1s}sin(\Psi)\right) \tag{2.3}$$

2.3. Main rotor flap dynamics

The flap dynamics are an important part of the total helicopter dynamics, as it is the cause for rotations of the disk plane and therefore attitude changes of the helicopter. In this regard, the flap angle of each individual blade is converted to flap angles that describe the rotor cone as a whole. This is done using a Coleman transformation and results in the so called multi-blade coordinates (Hohenemser and Yin 1972). For a four-bladed helicopter such as the Bo-105, the four individual flap angles are transformed into four parameters describing the orientation of the rotor cone. The coning angle β_0 represents the upward collective flapping off all blades. The longitudinal disk tilt angle β_{1c} represents the forward tilting of the rotor cone. The lateral disk tilt angle β_{1s} represents the leftward tilting of the rotor. A schematic representation of the parameters can be seen in Figure 2.5, bearing in mind that the disk plane is formed by the plane which contains the tip of each rotor.
The last angle is the differential coning β_{0d}, representing the blades opposite to each other having the same but with a flipped sine as the other blade pair. This mode is reactionless, as it is not producing any net force or moment on the rotor hub. It is therefore neglected in any further calculations.

The differential equation that is used to calculate the derivative of the three parameters is given in Equation (2.4). Based on the required accuracy of the simulation and the type of helicopter, one can consider to set the second derivative and/or the first derivative to zero. This means only the steady state disk tilt angles are calculated, which is allowed for for trim calculations or articulated rotors for which the body modes and flap modes are widely separated in time and frequency.

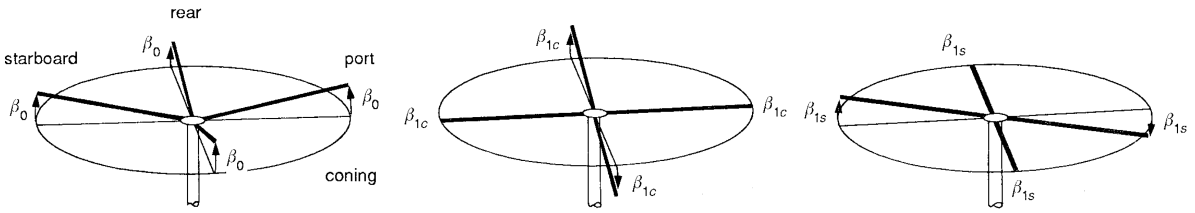

Figure 2.5: Rotor disk angles in multi-blade coordinates (Padfield 2007).

Including the first and second derivative of the MBC's adds the regressing and progressing flap modes respectively to the simulated dynamics. The regressing flap mode is a low frequency wobble of the rotor plane. When simulating hingeless rotorcraft it is often the case that the regressing flap mode couples with the body modes. This changes the response of the helicopter to control inputs and is why this mode must be included when simulating hingeless or bearingless rotorcraft. The progressing flap mode however is of higher frequency and is unlikely to couple with any of the body modes (Johnson 1994).

$$\ddot{\beta}_M = -\Omega \mathsf{C}_M \dot{\beta}_M - \Omega^2 \mathsf{D}_M \beta_M + \Omega^2 \mathsf{H}_M \quad , \quad \beta_M = \begin{bmatrix} \beta_0 \\ \beta_{1c} \\ \beta_{1s} \end{bmatrix} \tag{2.4}$$

The damping matrix C_M, stiffness matrix D_M and forcing function matrices H_M that are present in Equation (2.4) are shown in Equation (2.5) (Padfield 2007).

$$\begin{aligned}
\mathsf{C}_M &= \frac{\gamma}{8} \begin{bmatrix} 1 & 0 & \frac{2}{3}\mu \\ 0 & 1 & \frac{16}{\gamma} \\ \frac{4}{3}\mu & -\frac{16}{\gamma} & 1 \end{bmatrix} \\
\mathsf{D}_M &= \frac{\gamma}{8} \begin{bmatrix} \frac{8\lambda_\beta^2}{\gamma} & 0 & 0 \\ \frac{4}{3}\mu & \frac{8\left(\lambda_\beta^2 - 1\right)}{\gamma} & 1 + \frac{\mu^2}{2} \\ 0 & \frac{\mu^2}{2} - 1 & \frac{8\left(\lambda_\beta^2 - 1\right)}{\gamma} \end{bmatrix} \\
\mathsf{H}_M &= \frac{\gamma}{8} \begin{bmatrix} \theta_0 \left(1 + \mu^2\right) + 4\theta_{tw} \left(\frac{1}{5} + \frac{\mu^2}{6}\right) + \frac{4}{3}\mu\theta_{1s} + \frac{4}{3}\left(\mu_z - \lambda_0\right) + \frac{2}{3}\mu\left(\bar{p} - \lambda_{1s}\right) \\ \frac{16}{\gamma}\bar{p} + \theta_{1c}\left(1 + \frac{\mu^2}{2}\right) + \left(\bar{q} - \lambda_{1c}\right) \\ -\frac{16}{\gamma}\bar{q} + \frac{8}{3}\mu\theta_0 + 2\mu\theta_{tw} + \theta_{1s}\left(1 + \frac{3}{2}\mu^2\right) + 2\mu\left(\mu_z - \lambda_0\right) + \left(\bar{p} - \lambda_{1s}\right) \end{bmatrix}
\end{aligned} \tag{2.5}$$

The matrices clearly show that there exists multiple couplings between the equations. Also in the forcing functions angular rates and control inputs appear in multiple rows. Moreover, the coefficients of the harmonic inflow appear in the forcing matrix H_M. This shows that the flap dynamics are influenced by the inflow dynamics and can lead to coupling of the dynamics.

Due to the lateral and longitudinal flap angle of the rotor disk the orientation of the thrust vector changes, initiating angular accelerations of the body. Furthermore, for hingeless and bearingless rotors the flap angle of the individual blades cause bending moments at the rotor hub. This is captured in Equations (2.6) and (2.7) by means of the K_β term. For typical hingeless rotorcraft such as the MBB Bo-105, this term is around five times as large as the thrust component. Therefore these helicopters are able to produce much larger rotor moments (Padfield 2007)

$$M_{mr} = -\left(Th_{cg} + \frac{N_b}{2} K_\beta\right) \beta_{1c} \tag{2.6}$$

$$L_{mr} = -\left(Th_{cg} + \frac{N_b}{2} K_\beta\right) \beta_{1s} \tag{2.7}$$

2.4. Body dynamics

Besides the derivatives of the inflow and flap states, also the derivatives of the body states have to be calculated. This is done with the equations of motion of the helicopter. First the total force and moment acting on the body in the body reference frame is determined by adding the contributions of each subsystem in Equations (2.8) and (2.9). In the present simulation model these subsystems are the main rotor, tail rotor, horizontal tail plane, vertical tail plane and fuselage.

$$F_{tot} = F_{mr} + F_{tr} + F_{ht} + F_{vt} + F_{fus} \tag{2.8}$$

$$M_{tot} = M_{mr} + M_{tr} + M_{ht} + M_{vt} + M_{fus} \tag{2.9}$$

The total force and moment vectors are used in the translational and rotational dynamic equations. Note that there will be some uncertainty in the magnitude of the components of these vectors, as they are obtained from differential equations that inevitable have modelling errors. Thus they will never exactly match the moments and forces in real life. The translational motion dynamics are given in Equation (2.10), while the rotational motion dynamics are given in Equation (2.11).

$$\begin{bmatrix} \dot{u} \\ v \\ w \end{bmatrix} = m^{-1} F_{tot} + \begin{bmatrix} -sin(\theta) \\ sin(\phi)cos(\theta) \\ cos(\phi)sin(\theta) \end{bmatrix} g - \begin{bmatrix} qw - rv \\ ru - pw \\ pv - qu \end{bmatrix} \tag{2.10}$$

$$\begin{bmatrix} \dot{p} \\ q \\ r \end{bmatrix} = \begin{bmatrix} I_{xx} & 0 & -I_{xz} \\ 0 & I_{yy} & 0 \\ -I_{xz} & 0 & Izz \end{bmatrix}^{-1} \left(M_{tot} - \begin{bmatrix} p \\ q \\ r \end{bmatrix} \times \begin{bmatrix} I_{xx} & 0 & -I_{xz} \\ 0 & I_{yy} & 0 \\ -I_{xz} & 0 & Izz \end{bmatrix} \begin{bmatrix} p \\ q \\ r \end{bmatrix} \right) \tag{2.11}$$

Contrary to the the dynamic relations, the kinematic relations are exact. Because of the physical relation of the body frame and the NED frame through the three Euler angles of the body, this conversion will not introduce new uncertainties. The translational motion kinematics are given in Equation (2.12), while the rotational motion kinematics are given in Equation (2.13). Note that for the translational kinematic relation the cosine and sine symbols are replaced by c and s respectively for easier readability.

$$\begin{bmatrix} \dot{x} \\ y \\ z \end{bmatrix} = \begin{bmatrix} c(\psi)c(\phi) & c(\psi)s(\theta)s(\phi) - s(\psi)c(\phi) & c(\psi)s(\theta)c(\phi) + s(\psi)s(\phi) \\ s(\psi)c(\theta) & s(\psi)s(\theta)s(\phi) + c(\psi)c(\phi) & s(\psi)s(\theta)c(\phi) - c(\psi)s(\phi) \\ -s(\theta) & c(\theta)c(\phi) & c(\theta)c(\phi) \end{bmatrix} \begin{bmatrix} u \\ v \\ w \end{bmatrix} \tag{2.12}$$

$$\begin{bmatrix} \dot{\phi} \\ \theta \\ \psi \end{bmatrix} = \begin{bmatrix} 1 & sin(\phi)sin(\theta)cos(\theta)^{-1} & cos(\phi)sin(\theta)cos(\theta)^{-1} \\ 0 & cos(\phi) & -sin(\phi) \\ 0 & sin(\phi)cos(\theta)^{-1} & cos(\phi)cos(\theta)^{-1} \end{bmatrix} \begin{bmatrix} p \\ q \\ r \end{bmatrix} \tag{2.13}$$

3

Inflow Modelling

The modelling of induced velocity, or inflow, generated by the rotor and its influence on helicopter dynamics has been the subject of ongoing research. As highlighted in Chapter 2 it forms a part of rotorcraft dynamics and should be well understood in order to perform piloted simulation or control related research. To this end, several approaches to model the induced velocity have been developed. The difference between the approaches is that they differ in complexity and therefore their applicability to certain problems. This chapter gives an overview of these induced velocity modelling methods and zooms in on the method that is most applicable for real-time simulation and controller design, namely dynamic inflow modeling. In Section 3.1 the different approaches are elaborated upon, with dynamic inflow modelling as main focus. Section 3.2 discusses the effect of accurately modelling dynamic inflow on helicopter dynamics.

3.1. Methods to model induced velocity

The rotor inflow is the name given to the flow field induced by the rotor at the rotor disc, thus contributing to the local blade incidence and dynamic pressure. In general, the induced flow at the rotor consists of components due to the shed vorticity from all the blades, extending into the far wake of the aircraft. To take account of these effects fully, a complex vortex wake, distorted by itself and the aircraft motion would need to be modelled. The rotor induced velocity does not only have an effect on the rotorcraft dynamics, but also on blade aerolasticity, structural loading, vibrations and performance calculations. These different purposes require different levels of modelling accuracy. Inflow modelling is predominantly done with four methods: free wake and prescribed wake models, computational fluid dynamics and finite-state dynamic inflow modelling. Each method and their applicability to real-time applications is described below.

3.1.1. Computational fluid dynamics

For modelling the dynamics of a fluid around an object, generally Computational Fluid Dynamics (CFD) achieves the highest accuracy. It has gained a lot of ground in the last decade due to the increasing availability of computational power. CFD programs numerically approximate the Navier-Stokes equations or, when the viscosity of the flow is ignored, the Euler equations in a grid around the object (Zawawi et al. 2018). It has many applications in the automotive, aerospace, maritime and wind energy sectors.

Although CFD can produce the most accurate rotor wake modelling, the computational cost to run such a solver is the major drawback. This is especially true for real-time simulation and control applications where computation times are very limited. Efforts have been made to simplify the simulated model and thereby reducing the computational effort. Barakos et al. (2020) performed CFD simulations of rotor flow based on unsteady actuator disk theory instead of fully resolved blades. The results captured well the main vortical structures around the rotor disk in comparison to the fully resolved cases. This was also attempted by Leza (2015) and Filippone and Mikkelsen (2009), who coupled a blade element method for computing the loads to a CFD simulations with an actuator disk approach.

The above methods reduce the computational workload and therefore increase the ability to be

run at a higher frequency. Bottai et al. (2018) successfully coupled CFD calculations for the main and tail rotor using actuator disk models with a multi-degree-of-freedom dynamic model of a helicopter. Applying such methods to real-time simulation however is still in an early phase. A trade-off between the accuracy and completeness of the CFD calculations and the frequency at which a simulation can be performed is remains necessary. This is unwanted if one wants to perform piloted simulation or use it online for control purposes. Furthermore, CFD solvers use artificial viscosity in their calculation to maintain numerical stability. This tends to decay concentrated vorticity, thereby losing the most powerful source of induced flow - the vortex wake produced by the spinning rotor blades (Peters 2009). To overcome this dissipation over time sometimes CFD calculations are coupled with free wake or prescribed wake methods, which are described in the next subsection. CFD calculations are then responsible for the velocity field near the rotor blades, whereas the mid and far field characteristics are modeled with a free wake or prescribed wake model (Komerath and Smith 2009).

3.1.2. Free wake and prescribed wake

Other approaches to model the induced velocity distribution over the rotor disk and its aerodynamic influence on the rest of the helicopter are the prescribed wake and free wake models. Contrary to CFD they do not numerically approximate the flow, but use Biot-Savart law to evaluate the induced velocity at a certain point at a particular distance from vortex segments with a certain strength and length (Van Hoydonck, Haverdings, and Pavel 2009).

Prescribed wake models describe the geometry of the wake based on certain parameters that are extracted from experimental studies. Examples of these parameters are wake contraction, viscosity and wake skew. The wake vorticity is then carried downstream by sheets of filaments along this predetermined path. Empirical relations from experimental data are necessary for their application. Therefore their use is restricted to similar geometries and flight conditions as the ones used to gather the experimental data.

The free wake models, as their name suggest, let the wake geometry deform under its own influence. Thus all the vorticity is located on a continuous truncated cylinder. The result is a more accurate representation of the wake. This comes with the cost of more computational power, as the velocity of a point is influenced by all other vorticity carrying elements (Martini 2019). Furthermore, it does not need experimental data to be used in simulation. But because of the many converge parameters they are not robust, sometimes even unstable, at low speeds and in hover (Wilke 2019).

As with the CFD models in the previous section, efforts have been made to modify prescribed and free wake methods to remove their drawbacks for real-time applications. For instance, Rand and Khromov (2018) successfully extracted a linearized state-space dynamic inflow model from a free wake based model. Gennaretti et al. (2017) developed a procedure to obtain a finite state dynamic wake model from interpreting harmonic perturbations of rotor kinematics with a generic high fidelity aerodynamic solver. This allows to still capture aerodynamic phenomena such as blade vortex interaction, while reducing computational workload.

3.1.3. Dynamic inflow modelling

Although the aforementioned methods produce more accurate representations of the induced velocity distribution around the rotor, dynamic inflow modelling still remains the most popular method for real-time simulation. It has the advantage of being computationally efficient, is relatively easy to incorporate due to its state-space like structure and is not depending on the time history of the state of the system (Hidalgo 2014). As already mentioned, the additional effects that are modelled by the previous methods are often to be introduced into the system by capturing them in a dynamic inflow model. This shows the popularity and applicability of the dynamic wake models.

Dynamic inflow models exist in various degrees of complexity. Depending on the goal of the calculations, additional states in the model increase the completeness of the outcome. For preliminary trim calculations, simple one degree of freedom descriptions suffices. For piloted simulation a more elaborate model is needed, which can model changes of the inflow distribution across the rotor disk more realistically. For research on structural loading one might opt for a model that takes into account higher order variations both radially and azimuthally.

The most basic model that calculates the induced velocity is referred to as actuator disk theory, a mathematical artifact effectively representing a rotor with infinite number of blades, able to accelerate the air through the permeable disc and to support a pressure jump across it (Bramwell, Done, and

Balmford 2001). A simplified representation of the (induced) air flow in forward flight can be seen in Figure 3.1. In this figure V is the velocity of the helicopter, α the angle of attack of the disk plane, T the thrust produced by the rotor and v_i the induced velocity produced by the rotor. By relating the change in kinetic energy of the flow to the work done by the actuator disk through the rate of change of momentum, one can prove that the induced velocity effect in the far wake is twice the induced velocity at the rotor.

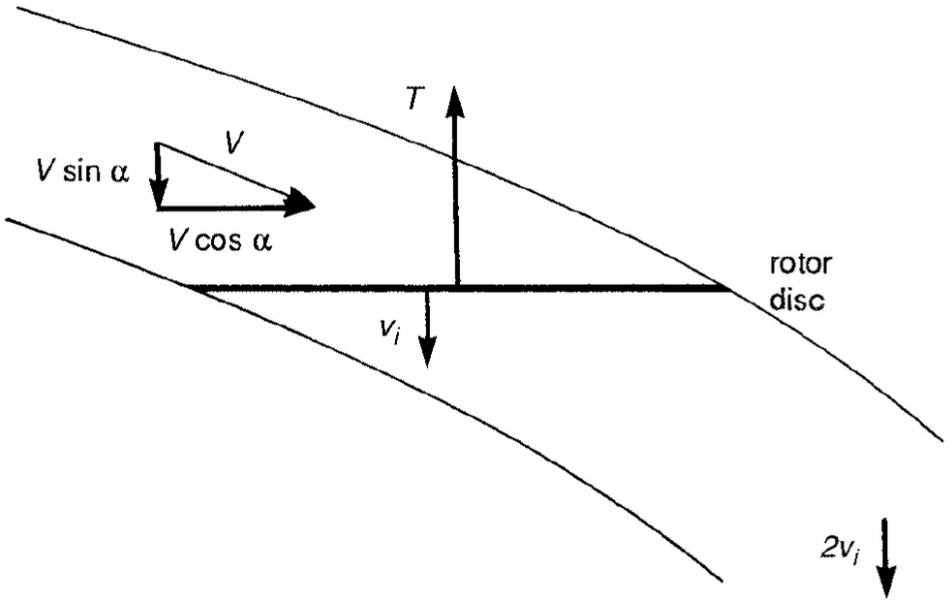

Figure 3.1: Airflow through a rotor in forward flight (Padfield 2007).

Using this principle it is possible to combine the expression for mass flow rate through the rotor and the fact that the thrust is equal to the mass flow rate times the induced velocity in the wake. This results in the Glauert formula for forward flight, given by Equation (3.1).

$$v_i = \frac{T}{2\rho\pi R\sqrt{\left(V\,cos(\alpha_{DP})\right)^2 + \left(V\,sin(\alpha_{DP}) + v_i\right)^2}} \tag{3.1}$$

By non-dimensionalizing the velocities and using the thrust coefficient instead of the thrust, one can use the Glauert formula together with the thrust coefficient obtained from blade element theory to get a derivative of the induced velocity. This method is shown in Equation (3.2). To account for inflow dynamics, a quasi-steady inflow model is created by means of a time constant τ_{λ_i} (Van Aalst and Pavel 2002). To initialize this system one can use the induced velocity at hover as a first estimate if a trim procedure of the rotorcraft model is not available.

$$\begin{aligned} C_T^{gl} &= 2\lambda_i\sqrt{\mu\,cos(\alpha_{DP})^2 + \left(\mu\,sin(\alpha_{DP}) + \lambda_i\right)^2} \\ C_T^{elem} &= \frac{\sigma C_l^\alpha}{2}\left[\left(\frac{1}{3} + \frac{\mu^2}{2}\right)\theta_0 + \frac{\mu}{2}\theta_{1s} + \left(\frac{\mu_z - \lambda_i}{2}\right) + \left(\frac{1+\mu^2}{4}\right)\theta_{tw}\right] \\ \tau_{\lambda_i}\dot{\lambda}_i &= C_T^{elem} - C_T^{gl} \end{aligned} \tag{3.2}$$

The assumption of uniform inflow is appropriate for a preliminary analysis of helicopter performance, but insufficient for accurate simulation. In maneuvering or forward flight conditions, the constant inflow leads to overestimated or underestimated blade lift. In fact, in forward flight the inflow is conveyed to the aft region of the rotor. This leads to a reduction of the angle of attack and the subsequent overestimation of the blade lift in the aft region of the rotor disc. Therefore a more realistic model is needed when applying inflow modelling in piloted simulation or control related research.

Already in 1974, Peters (1974) found that incorporating force and moment coefficients of the helicopter in a dynamic inflow model had significant effects on the transient response. A landmark in the

development of dynamic inflow modeling is the paper of Pitt and Peters (1980). In this paper the authors present a relatively simple inflow model in closed form governed by 3 parameters which can be added to the helicopter dynamics as a state-space system. The parameters are inflow coefficients that describe the uniform, fore to aft and side to side inflow variation. The model is based on Kinner pressure distributions, which can give pressure discontinuities across a circular disk. With a matrix equation containing an apparent mass and gain matrix, the inflow parameters are related to the aerodynamic coefficients. The benefit of the proposed model is that the formulation is in closed form, something previous researches were not able to obtain. Until this day, the majority of developed dynamic inflow models use the Pitt-Peters model as a starting point, showing the importance of the findings presented in the paper. The matrix equation is shown in Equation (3.3) (Pitt and Peters 1980).

$$\begin{bmatrix} \\ M \\ \\ \end{bmatrix} \begin{bmatrix} \dot{\lambda}_0 \\ \dot{\lambda}_{1s} \\ \dot{\lambda}_{1c} \end{bmatrix} + V \begin{bmatrix} \\ L \\ \\ \end{bmatrix}^{-1} \begin{bmatrix} \lambda_0 \\ \lambda_{1s} \\ \lambda_{1c} \end{bmatrix} = \begin{bmatrix} C_T \\ C_L \\ C_M \end{bmatrix} \tag{3.3}$$

with apparent mass and gain matrix:

$$M = \begin{bmatrix} \frac{128}{75\pi} & 0 & 0 \\ 0 & \frac{-16}{45\pi} & 0 \\ 0 & 0 & \frac{-16}{45\pi} \end{bmatrix}, L = \begin{bmatrix} \frac{1}{2} & 0 & \frac{15\pi}{64}\sqrt{\frac{1-sin(\alpha_{DP})}{1-sin(\alpha_{DP})}} \\ 0 & \frac{-4}{1+sin(\alpha_{DP})} & 0 \\ \frac{15\pi}{64}\sqrt{\frac{1-sin(\alpha_{DP})}{1-sin(\alpha_{DP})}} & 0 & \frac{-4sin(\alpha_{DP})}{1+sin(\alpha_{DP})} \end{bmatrix}$$

with mass flow parameter:

$$V = \frac{\mu^2 + (\lambda_0 - \mu_z)(2\lambda_0 - \mu_z)}{\sqrt{\mu^2 + (\lambda_0 - \mu_z)^2}}$$

In the following years Peters tried to improve the dynamic inflow model to better capture the non-uniformities in the modeled flow and thereby increase the correlation with measurement data. This updated model, first published in (Peters, Boyd, and He 1989) and in closed form in (Peters and He 1991; Peters and He 1995), is still relevant as new research on it is done to this date (Ho and Yeo 2021). It is implemented in both the flight simulation tool FLIGHTLAB (Du Val and He 2018) as well as the U.S. Army's Rotorcraft Comprehensive Analysis System (Saberi et al. 2015). The model can be configured to use an arbitrary number of harmonics and radial distributions of the inflow, increasing its modelling accuracy at every step. When truncating the system to three states, one ends up with the original Pitt-Peters model as described by Equation (3.3). For piloted simulation purposes, a three degree of freedom state-space system for the inflow dynamics is sufficient to obtain high enough fidelity (Pitt and Peters 1980; Güner 2016).

Although the Pitt-Peters and Peters-He models predict helicopter response in the direction of the control input well, the off-axis response is still poorly predicted (Su, Yoo, and Peters 1992). In some cases the off-axis response is even of opposite sign as compared with experimental data. Based on the Peters-He model, multiple publications have been published proposing solutions to improve the fit between the predicted off-axis response of inflow models and test data. Rosen and Isser (1995), Keller (1996), Keller and Curtiss (1996) and Basset and Tchen-Fo (1998) show that by including wake distortion effects due to rotor shaft translation and shaft rotation, the off-axis response has the correct sign and shows a better fit to test data. Arnold et al. (1998) further extend this inflow model by adding the effect of the rotor disk plane motion. The model is given in Equation (3.4) based on a Peters-He model truncated to 3 states, as increasing the number of harmonics or radial distributions does not give better off-axis results (Keller 1996). Again, better agreement with test data is presented, as compared to the old Pitt-Peters and Peters-He models Arnold et al. (1998). This model is commonly referred to the Keller inflow model or extended momentum theory.

$$\begin{aligned}\tau_i \lambda'_{1s} + \lambda_{1s} &= -K_L \hat{L}_{aero} + K_T \mu_y + K_R \left(\bar{p} - \beta'_{1s}\right) \\ \tau_i \lambda'_{1c} + \lambda_{1c} &= -K_L \hat{M}_{aero} + K_T \mu_x + K_R \left(\bar{q} - \beta'_{1c}\right)\end{aligned} \tag{3.4}$$

Note that when K_R is set to zero, Equation (3.3) and Equation (3.4) are similar. The term with K_T is due to the translation of the wake, also called wake skew. The term with K_R is from the curvature of the wake due to angular rate of the disk plane in which the equations are derived. The angular rate of the disk plane is determined by adding the angular rate of the shaft plane, q and p, to the angular rate of the disk plane relative to the shaft plane, β_{1c} and β_{1c}. The effect of wake spacing is incorporated in the mass flow parameter of the original model. As an example, imagine the helicopter to have a steady positive pitch rate. This will cause the vortices in the aft region of the rotor disk to be closer together. This in turn will cause the induced velocity to increase, which is reflected in the increase of λ_{1c} by the new term. The values of K_T and K_R are around 0.6-0.8 and 1.5-3.2 respectively, depending on which validation routine and benchmark helicopter model is used (Arnold et al. 1998).

In a later stage, Zhao, Prasad, and Peters (2004) modelled the dynamics of these wake distortion effects by means of a set of first order equations. Furthermore, the authors incorporated the wake distortion parameters in the gain matrix L instead of adding them as a forcing term. This alleviated divergence problems near hover that were observed with the quasi-steady models and qualitatively captured the correct off-axis response with an ideal K_R equal to 1. However, for better correlation with flight test data this has to be increased to 3.8. This was attributed to unmodelled on-axis response, unsteady aerodynamic effects or fuselage interference with the inflow.

To illustrate the differences between the Pitt-Peters and Keller inflow model, Figure 3.2 includes comparisons of simulations with both inflow models to experimental data. The experimental data is taken from an experiment with a UH-60 helicopter, reacting to a lateral cyclic stick displacement of 0.7 inches at 1 second. The simulations were performed with a non-linear model with body, flap and inflow degrees of freedom.

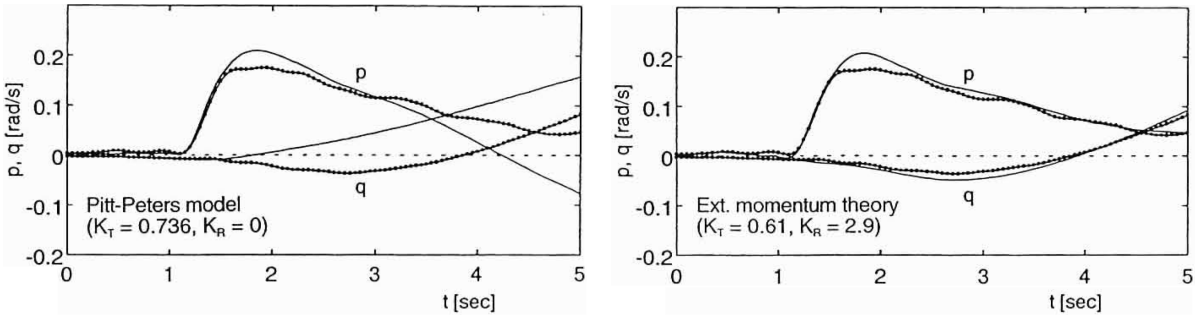

(a) Simulation with Pitt-Peters inflow model.

(b) Simulation with Keller inflow model.

Figure 3.2: Effect of inflow model on correlation between a non-linear flight dynamics model and experimental data of a UH-60 in hover (Arnold et al. 1998).

The comparisons show that for the on-axis roll rate response both models react in a similar fashion, especially within two seconds of the step input. However, there is a large difference in the off-axis between the models. Whereas the simulation with the Keller inflow model approximates the roll response well, the simulation with the Pitt-Peters model shows an initial response that is of opposite sign compared to the experimental data. This shows that the application of the Keller model causes substantial changes in the helicopter behavior.

Besides the developments described above, adaptions were also made to the model based on other principles than directly incorporating wake distortion. When using the Peters-He model to analyze the induced power of rotors, discrepancies were found between the measured and predicted induced power (Garcia-Duffy 2009; Peters, Hsieh, and Garcia-Duffy 2009). After investigation it was found that this was due to the so-called ”swirl” velocity in the wake. This is a component of the induced velocity which is in the plane of motion of the rotor. It can also be described as a yawing motion of the wake. Makinen and Peters (2005) already found that the kinetic energy lost to the swirl velocity could be corrected for in the model by a simple adaption of the apparent mass matrix of the Peter-He model for propellers with large swirl velocity. Huang, Peters, and Prasad (2015) blended the Peters-He model and Duffy

model to obtain accurate velocity field both on and off the disk, including swirl velocity. However this model is not in closed-form and is therefore not convenient to incorporate in real-time applications. The latest new approach of capturing the correct off-axis response is done by Lu et al. (2021). They present and augmented formulation for the fore-to-aft and side-to-side inflow ratio of the Pitt-Peters model, by adding four correction factors linked to pitch rate, roll rate, heave velocity and sway velocity. The gains for these correction factors are then found by fitting the model to flight test data. The model captures the response of the rotorcraft very well. The major downside of this method that the extracted gains can only be used for a helicopter model on which the flight test data was obtained with. This makes it a less flexible approach than the other methods discussed earlier.

3.2. Effects of dynamic inflow modelling on helicopter dynamics

From the previous section it is clear that a change in the induced velocity model is changing the dynamics of a rotorcraft. Until now the focus was mainly on providing improvements for the off-axis response of helicopter models. In short, this is done by incorporating wake distortion parameters such as wake skew and wake curvature in the dynamic inflow model. The general influence of the induced velocity created by the rotor on helicopter dynamics have not been discussed so far.

The aerodynamic loading of a rotor blade is determined by its angle of attack to the oncoming airflow. The loads on the blade cause it to flap, which in turn influence the rotational rates of the body. The angle of attack is consists mainly of three contributions, namely the commanded pitch blade pitch angle through the controls, the velocity of the blade flapping and the induced velocity. Note that the velocity of the blade also consists of the body velocities and the rotor rotational speed. The interdependency of these parameters is captured in Figure 3.3.

The largest difference in helicopter dynamics due to the inflow is present during the hovering flight phase (Keller and Curtiss 1998). When hovering, the only other movement that is influencing the angle of attack of the blade is coming from the rotational velocity of the rotor. As forward airspeed builds up, the wake gets skewed backwards, making the distance between the previous vortex and the blade greater. This diminishes its ability to produce induced velocity locally at the blade and increases the influence of the incoming free flow.

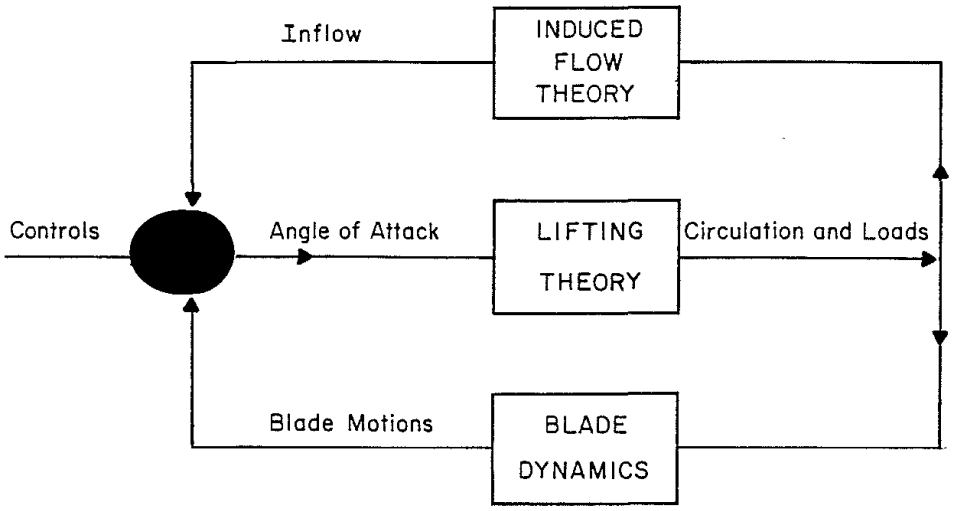

Figure 3.3: Block diagram of coupled rotor and inflow dynamics (Pitt and Peters 1980).

Carpenter and Fridovich (1953) noted in their research that the induced velocity did not change instantaneously to a rapid change in blade pitch, having a time constant around 1 second depending on the rate of change. Initial overshoot in the response of the thrust coefficient and flap angle are caused by the coupling between rotor disc-tit dynamics and inflow dynamics. The effects are modelled by introducing an apparent additional mass. This means it takes time to accelerate the flow, delaying the reduction in angle of attack by the downward induced velocity of the air. This causes the spike in thrust coefficient, as a higher angle of attack in the transient phase causes more thrust.

Furthermore, it has been show that dynamic inflow produces significant changes in the modes of

motion of helicopters (Curtiss 1986). The time constants associated with the inflow dynamics can be of the same order as the low frequency flap dynamics. Therefore it seems that if flap dynamics are be included in a helicopter model inflow dynamics should be included as well. This causes the inflow dynamics to have an effect on the body dynamics through altering the flap dynamics. It was found that increased coupling was present between the lower flap and body roll mode. This resulted in a change in transient roll response to a cyclic step input. This was also found by Sissingh (1951) and Keller and Curtiss (1998). The change of roll or pitch response is predominantly due to the change in damping of those motions. In the case of a rolling motion, roll damping of a helicopter comes from the tilt of the disk plane that develops in response to a roll rate. The thrust vector always opposes the roll motion, thus giving a roll damping. Because the thrust changes distribution across the rotor disk it influences the inflow and therefore decreases the aerodynamic effectiveness of the blades and increases the damping (Peters 2009).

4

Non-linear Control Methods

Controlling a helicopter can be very demanding for a pilot because of all the cross couplings in its dynamics. A control system can relieve the work load of the pilot by removing these cross couplings and improve handling qualities. Furthermore, advanced control systems can execute certain flight phases automatically, as can be seen in the aircraft sector. The reason that these system have not widely been applied to helicopters is the lack of fly-by-wire systems. In the past helicopter controls were very basic mechanical systems and cross-couplings were canceled by mechanically mixing the pilot control inputs. With the introduction of fly-by-wire control systems (Stiles et al. 2004), digital control algorithms can be used which are more capable of providing stable and predictable control of the helicopter. Because rotorcraft are known for their non-linear dynamics, controllers based on non-linear control theory are a good candidate to be applied. However, conventional non-linear control methods heavily rely on the availability of accurate model knowledge. This can be problematic, as for many system an accurate model is not available and has to be estimated during flight. Incremental control theory solves for this sensitivity to modelling errors by relying on sensors instead. In general this will improve the robustness of the controller.

This chapter discusses the general theory behind incremental non-linear control methods based on Non-linear Dynamic Inversion (NDI) and Backstepping (BS). This is done in Section 4.1. The addition of adding command filters to the incremental backstepping procedure is described in Section 4.1.3, as it is implemented in the simulation model of Van der Goot (2017). Finally, Section 4.2 emphasizes the necessary adoptions to incorporate these aforementioned controllers in a helicopter dynamics model.

4.1. Incremental control methods

The non-linear controllers described above all have a drawback. They rely on the availability of accurate models of the controlled vehicle. If the model is inaccurate or the dynamic characteristics of the controlled element change, for instance due to a failure, the controller may become unstable. Simulation models of rotorcraft have various states which cannot be measured, which is problematic as feedback linearization requires full state feedback. Furthermore, conventional dynamic inversion requires the system model to be affine in control and minimum phase (Horn 2019). Non-minimum phase systems have zeros in the right half plane of the complex plane which become, after inversion, unstable poles. These can become a problem if present in the closed loop system.

A special type of non-linear controllers that circumvent this issue are incremental controllers. Instead of relying on system dynamics modeling, incremental controllers rely on sensor measurements of the controlled states. Therefore they are not sensitive to modeling errors, something which is often the case for non-linear systems such as helicopters. The first step when applying incremental controllers to a system is to create an incremental system description. This is done by applying a Taylor series expansion on the dynamics that need to be controlled. This process is shown in Equation (4.1) to Equation (4.3) for a general time-invariant system, where x, u, f, g are the state vector, input vector, system dependent dynamics and control dependent dynamics respectively. Note that due to this linearization, this system description is only valid for a small region around x_0.

$$\dot{x} = f(x) + g(x,u) \tag{4.1}$$

$$\dot{x} = f(x_0) + g(x_0,u_0) + \frac{\partial}{\partial x}\Big[f(x)+g(x,u)\Big]_{x_0,u_0}(x-x_0) + \frac{\partial}{\partial u}\Big[f(x)+g(x,u)\Big]_{x_0,u_0}(u-u_0) + \mathcal{O}\left((x-x_0)^2,(u-u_0)^2\right) \tag{4.2}$$

$$\dot{x} = \dot{x}_0 + F(x_0,u_0)\Delta x + G(x_0,u_0)\Delta u + \mathcal{O}\left((x-x_0)^2,(u-u_0)^2\right) \tag{4.3}$$

Based on a number of assumptions, it is possible to simplify this equation. First of all the system sample rate should be high enough, meaning that the sensors and controller operate at a sufficiently high frequency. Furthermore the actuators are assumed to react instantly to command signals. At last, it is assumed that the changes in the states are slow compared to the changes in control input. This is called time scale separation. By assuming time scale separation, the system term $F(x_0,u_0)\Delta x$ is assumed to be small compared to the control term $G(x_0,u_0)\Delta u$ and can be neglected. Therefore the system coefficients in F do not need to be estimated and only control effectiveness G remains. Resulting Equation (4.4) is a simplified description of the system which, assuming that all the controlled states can be measured and the sampling rate is sufficiently high, can be used to construct an incremental controller that controls the system using increments of control input.

$$\Delta\dot{x} = G(x_0,u_0)\Delta u \tag{4.4}$$

Simulation models also consists of kinematic relations to calculate translational velocities and rotational attitude. Since these relations are exactly known, there is no need to apply incremental control for these parts of the model as there is no change of model mismatch. This allows for application of conventional NDI or BS. Therefore the focus is on the incremental control laws that govern the dynamic relations.

4.1.1. Incremental Non-linear Dynamic Inversion

With the system description given in Equation (4.4) one can implement several control algorithms. The first algorithm discussed here is INDI. Example applications of INDI control structure to rotorcraft are shown in (Simplício et al. 2013), (Van der Goot 2017), (Pavel, Shanthakumaran, Chu, et al. 2020). The INDI control law is constructed by inverting the system description of Equation (4.4). Thereafter, the state derivative variable $\dot{x}$ is replaced by virtual control input v. The final control law is shown in Equation (4.7). Thus, the control input u will be such that the difference between the current state derivative $\dot{x}_0$ and the desired state derivative $\dot{x}$ tends to zero. This means that the outer loop system, the system that determines virtual control v, will experience linear behavior of the inner loop system. v can be governed by a PID controller that minimizes the error between a reference signal and a certain state, for instance pitch attitude or rate. A downside of INDI is that stability cannot be guaranteed and the PID controller still needs tuning.

$$\Delta u = G(x_0,u_0)^{-1}\Delta\dot{x} \tag{4.5}$$

$$\Delta u = G(x_0,u_0)^{-1}(\dot{x}-\dot{x}_0) \tag{4.6}$$

$$\Delta u = G(x_0,u_0)^{-1}(v-\dot{x}_0) \tag{4.7}$$

4.1.2. Incremental Backstepping

Another promising and more recent control algorithm is IBS. It uses the stability characteristics of Control Lyapunov Functions (CLF) to guarantee stability. Applications of the IBS control structure is given in (Koschorke 2012), (Keijzer et al. 2019) and (Acquatella 2020). It departs from the same system description given in Equation (4.4). Defining error state z as the difference between the current state and the reference state, one can assure stability and tracking if the derivative of a chosen CLF is negative definite. For this example CLF $V = \frac{1}{2}x^2$ is used.

$$z = x - x_{ref} \tag{4.8}$$

$$\dot{z} = \dot{x} - \dot{x}_{ref} \tag{4.9}$$

$$V = \tfrac{1}{2}z^2 \tag{4.10}$$

$$\dot{V} = z\dot{z} \tag{4.11}$$

$$\dot{V} = z\left(\dot{x} - \dot{x}_{ref}\right) \tag{4.12}$$

$$\dot{V} = z\left(\dot{x}_0 + G(x_0, u_0)\Delta u - \dot{x}_{ref}\right) \tag{4.13}$$

Which is negative definite if:

$$\Delta u = G(x_0, u_0)^{-1}\left(-\dot{x}_0 + \dot{x}_{ref} - Cz\right), C > 0 \tag{4.14}$$

The final control law is shown in Equation (4.14). When choosing gain C>0 the use of a CLF assures stability and tracking, given that the time scale separation principle and sampling frequency assumptions hold. Other than the INDI controller, no additional PID controller is necessary.

Note that in some cases the INDI and IBS control laws can become equal. When no outer loop dynamics are considered, Equation (4.7) equals Equation (4.14) if the P(ID) controller that drives v is designed as $v = K_p(x_{ref} - x) + \dot{x}_{ref}$, where K_p is a proportional gain larger than zero and equal to C from the IBS law. This results in the same controller dynamics for both methods.

Although INDI and IBS controllers are commonly applied to dynamic systems in literature, only recently time delay margins and robustness tolerances against parameter uncertainties were explicitly quantified (Huang, Zhang, et al. 2022). Until this point sampling rates were always assumed sufficiently high and no systematic theory existed to calculate maximum parameter mismatch. It was found that control effectiveness mismatch could reach up to 50% of its true value when actuator dynamics were not included in the model. Adding actuator dynamics even significantly increased the robustness of the INDI controller against model errors. It was also found that underestimation of the control effectiveness lead to better tracking performance than perfect estimation.

4.1.3. Command Filtered Incremental Backstepping

A special type of IBS that is applied in the simulation model of Van der Goot (2017) is CFIBS. If Equation (4.14) was based on a dynamic model with more than one layer to step through, the control law would also contain a $\dot{\alpha}$ term. This is the derivative of the intermediate control law α_i in the previous layer. The control law based on k steps through the system of lower triangular form would result in Equation (4.15).

$$\Delta u = G_k(x_0, u_0)^{-1}\left(-\dot{x}_0 + \dot{x}_{ref} - C_k z_k + \dot{\alpha}_{(k-1)}\right), C > 0 \tag{4.15}$$

Since the intermediate control law of the previous step is also containing their predecessors, the final control law would require the analytical time derivatives of each of the control laws which quickly become prohibitively difficult to calculate. A solution to this problem is to apply a command filter on the intermediate control laws before passing them to the next control law as a reference. By using a command filter, the derivative of the signal is known and do not need to be derived. Furthermore, the intermediate reference signals can be tweaked in order to obtain favourable dynamics. The error states in Section 4.1.2 can be redefined as:

$$z = x_i - x_{i,ref} \tag{4.16}$$

$$\bar{z}_i = z_i - \chi_i \tag{4.17}$$

Note that in this case a bar over a variable does not mean that it is normalized by the rotor speed. $\bar{z}_i$ is the compensated error state, which is used in the Control Lyapunov function to obtain the intermediate and final control laws as is done in the previous subsection. χ_i is a compensation term for using the command filters, defined as:

$$\dot{\chi}_i = -C_i\chi_i + G_i\left(x_{(i+1),ref} - x^0_{(i+1),ref}\right) \tag{4.18}$$

The last two terms in this equation are the output signal of the command filter and the input signal of the command filter. The input signal to the command filter is given in Equation (4.19), while the command filter itself is shown in Equation (4.20).

$$x^0_{(i+1),ref} = \alpha_i - \chi_{(i+1)} \tag{4.19}$$

$$\begin{bmatrix} \dot{x}_{i,ref} \\ \ddot{x}_{i,ref} \end{bmatrix} = \begin{bmatrix} \dot{x}_{i,ref} \\ 2\zeta\omega_n \left(\mathsf{S}_{rate} \left\{ \frac{\omega_n^2}{2\zeta\omega_n} \left[S_{mag} \left(x^0_{i,ref} \right) - x_{i,ref} \right] \right\} - \dot{x}_{i,ref} \right) \end{bmatrix} \tag{4.20}$$

With the parameters S_{mag} and S_{rate} magnitude and rate limits can be imposed on the intermediate reference signals. Moreover, bandwidth and damping limitations can be set by choosing the appropriate natural frequency ω_n and damping term ζ. It is important to state that these limits will be applied to the commanded states of the system in the controller, not the actual states.

The intermediate control function and final control law can then be found by Equation (4.21), knowing that $\alpha_k = \Delta u + G_i(x_0, u_0)^{-1}\dot{x}_0$ when time scale separation is applied.

$$\begin{aligned} \alpha_i &= G_i(x_0, u_0)^{-1} \left(\dot{x}_{ref} - C_i z_i - G_{(i-1)} \bar{z}_{(i-1)} \right) \\ \Delta u &= G_k(x_0, u_0)^{-1} \left(-\dot{x}_0 + \dot{x}_{ref} - C_k z_k - G_{(k-1)} \bar{z}_{(k-1)} \right) \end{aligned} \tag{4.21}$$

4.2. Adaptions to successful application

When applying an incremental controller, one relies on sensor measurements instead of a mathematical model to obtain the state of the system. Thus this is also the case when these controllers are applied to helicopters. In principle this is a big advantage, since estimation errors in the mathematical model are excluded. However, a rotorcraft has a lot of states that cannot be measured. Two of these states are flap angles and inflow velocities. Moreover, these quantities have a large effect on the overall helicopter dynamics. In particular the flap dynamics is the main contributor to angular acceleration for hingeless rotorcraft like the MBB Bo-105, as was discussed in Section 2.3. This is because the control inputs indirectly influences the angular accelerations through the flap angles of the rotor disk. Since the system dependent dynamics are neglected while assuming time scale separation and the direct control effectiveness of the control input on pitch acceleration is negligible, the controller will be unable to control the helicopter. Effectively the time-scale separation assumption is violated because the flap states have significant influence on the accelerations. Therefore the controller model on which the control law is based has to be adapted to increase control dependency of the angular accelerations. Furthermore it was assumed that the actuators and sensors operate at a sufficiently high frequency. While this true for the majority of sensors, actuator delays and dynamics can often not be neglected. Furthermore filters are use to obtain certain states, so the filters induce some form of delay as well. It is known that incremental controllers have relatively small stability robustness margin when subjected to time delays and unmodelled dynamics that influence the feedback path (Kumtepe, Pollack, and Van Kampen 2022).

Two solutions to these issues will be treated in this section. They can be best explained based on a generic controller-helicopter combination as can be seen in Figure 4.1. The first part of the solution is to apply residualization of the unmeasurable states in the model that is used in the controller block. This is explained in Section 4.2.1. The second part of the solution is to synchronize the control output of the controller model with the actual control deflection of the relevant actuation system. Furthermore, this process can also account for any other delay, such as sensor or filter delays. The application of the synchronization filter is given in Section 4.2.2.

4.2.1. Residualization of flap and inflow states

The residualization procedure in its original form is to separate slow and fast states in a state space system and thereby simplifying the system (Skogestad and Postlethwaite 2001). The fast states are assumed to be constantly at steady state compared to the slow states, and their dynamics have therefore no effect on the slow states. This principle is similar to that of only using steady state flap angles for articulated helicopters, as the response of body states and flap states are widely separated in time.

In this instance the procedure is implemented to remove states from the controller model that cannot be measured. They cannot be used in the incremental control law as it relies on measurements of the helicopter state. However, also states that have significant effect on the helicopter dynamics, such as the flap angle, are residualized. This means that the time delay that is introduced by the flap dynamics

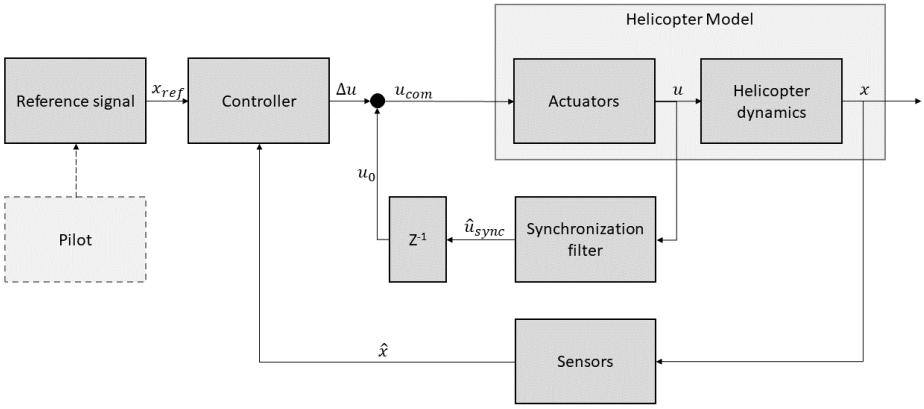

Figure 4.1: Generic system visualization.

in the actuation process of the actuator disk is also lost. This delay has to be accounted for in the synchronization filter.

Residualization is performed by setting the derivatives of the flap and inflow states equal to zero and fold their dynamics into the remaining states. This will transfer the control dependency of the flap and inflow states to the remaining states, such that the time scale separation principle is less likely to be violated. The residualized state vector will become $\boldsymbol{x}_{res} = [u\ v\ w\ x\ y\ z \mid p\ q\ r\ \phi\ \theta\ \psi]$. The residualization procedure is given in Equations (4.22) to (4.26), with the flap angle vector and inflow vector represented by β and λ respectively. The final residualized system is given in Equation (4.27).

$$\ddot{\beta} = F_{\dot{\beta},x_{res}} x_{res} + F_{\dot{\beta},\beta}\beta + F_{\dot{\beta},\dot{\beta}}\dot{\beta} + G_{\dot{\beta}}u \tag{4.22}$$

$$\dot{\lambda} = F_{\lambda,x_{res}} x_{res} + F_{\lambda,\lambda}\lambda + G_{\lambda}u \tag{4.23}$$

Setting all derivatives to zero and rearranging the terms:

$$\beta = -F^{-1}_{\dot{\beta},\beta} F_{\dot{\beta},x_{res}} x_{res} - F^{-1}_{\dot{\beta},\beta} G_{\dot{\beta}} u \tag{4.24}$$

$$\lambda = -F^{-1}_{\lambda,\lambda} F_{\lambda,x_{res}} x_{res} - F^{-1}_{\lambda,\lambda} G_{\lambda} u \tag{4.25}$$

These equations can then be inserted into the residualized dynamics:

$$\dot{x}_{res} = F_{x_{res},x_{res}} x_{res} + F_{x_{res},\beta}\beta + F_{x_{res},\lambda}\lambda + G_{x_{res}}u \tag{4.26}$$

The final residualized system then becomes:

$$\begin{aligned}\dot{x}_{res} = &\underbrace{\left(F_{x_{res},x_{res}} - F_{x_{res},\beta}F^{-1}_{\dot{\beta},\beta}F_{\dot{\beta},x_{res}} - F_{x_{res},\lambda}F^{-1}_{\lambda,\lambda}F_{\lambda,x_{res}}\right)}_{F_R} x_{res} + \\ &\underbrace{\left(G_{x_{res}} - F_{x_{res},\beta}F^{-1}_{\dot{\beta},\beta}G_{\dot{\beta}} - F_{x_{res},\lambda}F^{-1}_{\lambda,\lambda}G_{\lambda}\right)}_{G_R} u\end{aligned} \tag{4.27}$$

4.2.2. Synchronization of input signal

Now the state space system for the controller model is residualized, the control dependency of the remaining states in G_R is high enough to apply an incremental control law. However, there is now a large difference between the controller model and the actual model describing the helicopter dynamics. Namely the latter model includes dynamics and time delays from flap dynamics and inflow dynamics. This means that the controller model expects the helicopter to react much faster than is happening

in real life. Furthermore, sensors, filters and actuator dynamics also have an influence on the control deflection feedback and state measurement feedback. When not accounting for these time differences, instabilities and divergent behavior can occur. Therefore Arons (2020) and Van der Goot (2017) introduced a so called synchronization filter. This filter delays the feedback measurement of the control input to mimic the delay that the control input otherwise had due to the flap dynamics, inflow dynamics and other uncontrolled signal manipulations. A downside of this synchronization filter is that some system dynamics coefficients have to be estimated, as it needs to map the expected effect of the controller input by the controller to the real effect of the rotorcraft including the time delay. However, this is just a portion of the total amount of system dynamics coefficients in $f(x)$ that would have been estimated if a non-incremental controller was used. As the inflow dynamics also plays an important role in the response of a helicopter, it should be investigated whether they also need to be residualized and included in the synchronization filter. A similar case was investigated with respect to the lead-lag dynamics of the rotor system by Arons (2020), but it was concluded that this was not necessary for this specific part of the helicopter dynamics.

The time delay that is removed during the residualization process can be synchronized using Equation (4.28). The filter is placed in the feedback path of the actuator deflection measurement, converting the measured actuator deflections to synchronized actuator deflections. As in residualization procedure, β and λ are the flap and inflow vector. θ represents the control vector, while ω represents the angular rates. The sensor dynamics can be accounted for by placing the model of the sensors also on the actuator feedback path. Thus in Figure 4.1 the sensor block is also placed inside the synchronization block. This will cause the possible delay of the sensors to by applied to both the state estimation signal as the actuator feedback, thereby cancelling out any effect of the sensors. The synchronized control input θ_{sync} can now be used to calculate the new control output of the controller by adding it to the incremental control output Δu of the controller.

$$\begin{bmatrix} \dot{\beta}_{sync} \\ \dot{\lambda}_{sync} \\ \theta_{sync} \end{bmatrix} = \begin{bmatrix} F_{\beta,\beta} \\ 0 \\ G_R^{-1} F_{\omega,\beta} \end{bmatrix} \beta_{sync} + \begin{bmatrix} 0 \\ F_{\lambda,\lambda} \\ G_R^{-1} F_{\omega,\lambda} \end{bmatrix} \lambda_{sync} + \begin{bmatrix} G_\beta \\ G_\lambda \\ G_R^{-1} G_\omega \end{bmatrix} \theta_{meas} \tag{4.28}$$

5

Case Studies

In this chapter the challenges of helicopter flight control and the relevant helicopter dynamics are discussed based on different case studies. The consecutive cases are increasing in complexity, making them come closer to reality at every step. The first three cases use a longitudinal helicopter model with second order flap dynamics and quasi-steady inflow dynamics to perform the underlying helicopter simulations. This model is similar to the controller model used in Section 5.3, except for the extra derivative in the flap dynamics. The first case, described in Section 5.1, shows the resulting helicopter dynamics when no flap dynamics is assumed in the controller model. Section 5.2 explains the application of applying simplified flap dynamics in the controller model, based on a time constant. This is an essential step if one wants to construct a controller that is able to control a helicopter in a stable manner. The helicopter model on which the controller is based greatly influences its complexity and ability to control and/or stabilize the actual helicopter. When the discrepancy between the controller model and the helicopter is too large, unwanted oscillations can make the helicopter unstable and diverge. In Section 5.3 inflow and forward velocity is introduced in the controller model, together with first order flap dynamics. All the sections up to this point work with the assumption that only the longitudinal plane is studied. Furthermore, they work with simplified IBS controllers instead of the more complex CFIBS method that is used in Section 5.4. As mentioned in Section 4.1.2, by choosing the appropriate PID controller in the INDI controller, the final IBS and INDI control laws can become equal. Therefore only results based on an implemented IBS control law will be discussed in the first 3 simplified cases. Finally, in Section 5.4 the model from Van der Goot (2017) is investigated. In this section the adaptions proposed in Chapter 3 and Chapter 4 are applied and their influence is analyzed. All simulations performed in this chapter are initiated from hovering conditions. As discussed in Chapter 3 the influence of inflow is the most pronounced in this condition.

5.1. 1 DoF model - Pitch rate only

The simplest form to describe helicopter motion, is the pitch acceleration equation in the longitudinal plane of motion. Additionally, hover condition, no flap dynamics or collective controls are assumed. In this way a further simplification can be made by replacing the thrust needed to hover by the weight of the helicopter. This reduces the helicopter model to Equations (5.1) to (5.3).

$$\dot{q} = -\frac{K}{I_{yy}} \left(\beta_{1c}\right) \tag{5.1}$$

with:

$$K = W h_{cg} + \frac{N_b}{2} K_\beta \tag{5.2}$$

$$\beta_{1c} = \frac{16}{\gamma} \frac{q}{\Omega} - \theta_{1s} \tag{5.3}$$

resulting in:

$$\dot{q} = -K\left(\frac{16}{\gamma}\frac{q}{\Omega} - \theta_{1s}\right) \tag{5.4}$$

Looking at the pole of this motion described by Equation (5.4), $s = -\frac{16}{\gamma}\frac{K}{\Omega}$, this motion is always stable and non-oscillatory. Following the steps presented in Section 4.1.2, the resulting IBS controller for this system will be:

$$\theta_{1s} = \theta_{1s,0} + G_q^{-1}\left(-\dot{q}_0 + \dot{q}_{ref} - c_q z_q\right) \tag{5.5}$$

with:

$$z_q = q - q_{ref} \tag{5.6}$$
$$G_q = K \tag{5.7}$$

Equation (5.4) shows a direct relation between the control input θ_{1s} and the pitch acceleration q. This suggests that there is no delay between applying cyclic control input and producing pitch acceleration. While this might be true if the actual helicopter can be precisely described by Equation (5.4), resulting in the asymptotic tracking seen in Figure 5.1, if the controller is applied to higher order models with more dynamics the controller fails to deliver adequate performance. This is shown in Figure 5.2. The latter case is more realistic, as the rotor system acts as an actuator and introduces delays in the system. Furthermore, the actuation of the blades itself takes some time as well. Therefore, if no time scale separation can be applied due to coupling of the rotor and body modes, Equation (5.4) is not an accurate representation of the helicopter dynamics. In this and subsequent figures, $\Delta\theta_{1s}$ is the control input increment that is calculated by the IBS control law.

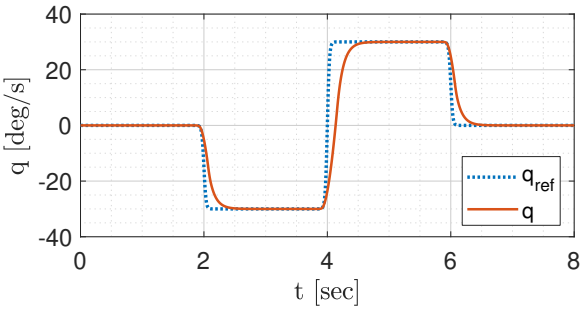

(a) Pitch rate.

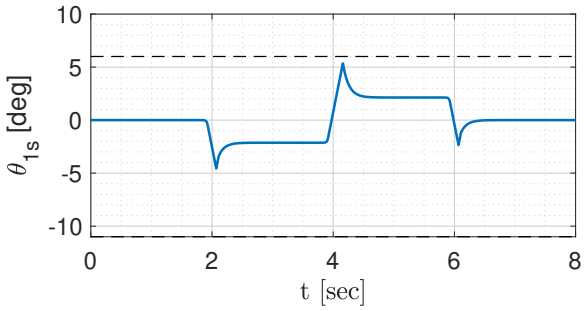

(b) Control input.

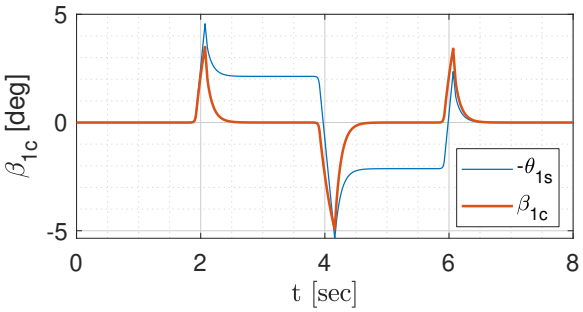

(c) Longitudinal flap angle.

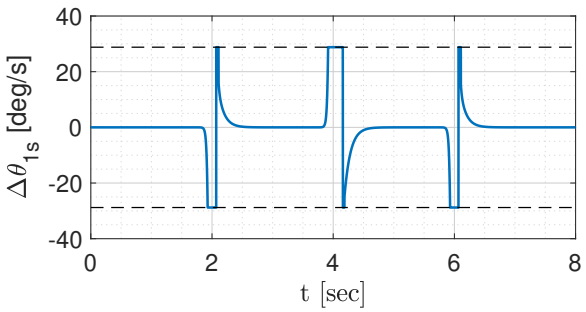

(d) Control input increment.

Figure 5.1: Tracking task with steady state IBS controller and steady state dynamics.

The reason for this oscillatory behavior is that in the helicopter model there is delay between the input of cyclic control and the desired pitch acceleration, due to the flap dynamics. Other dynamics, such as actuator dynamics and inflow dynamics, do also contribute but are not considered for this example.

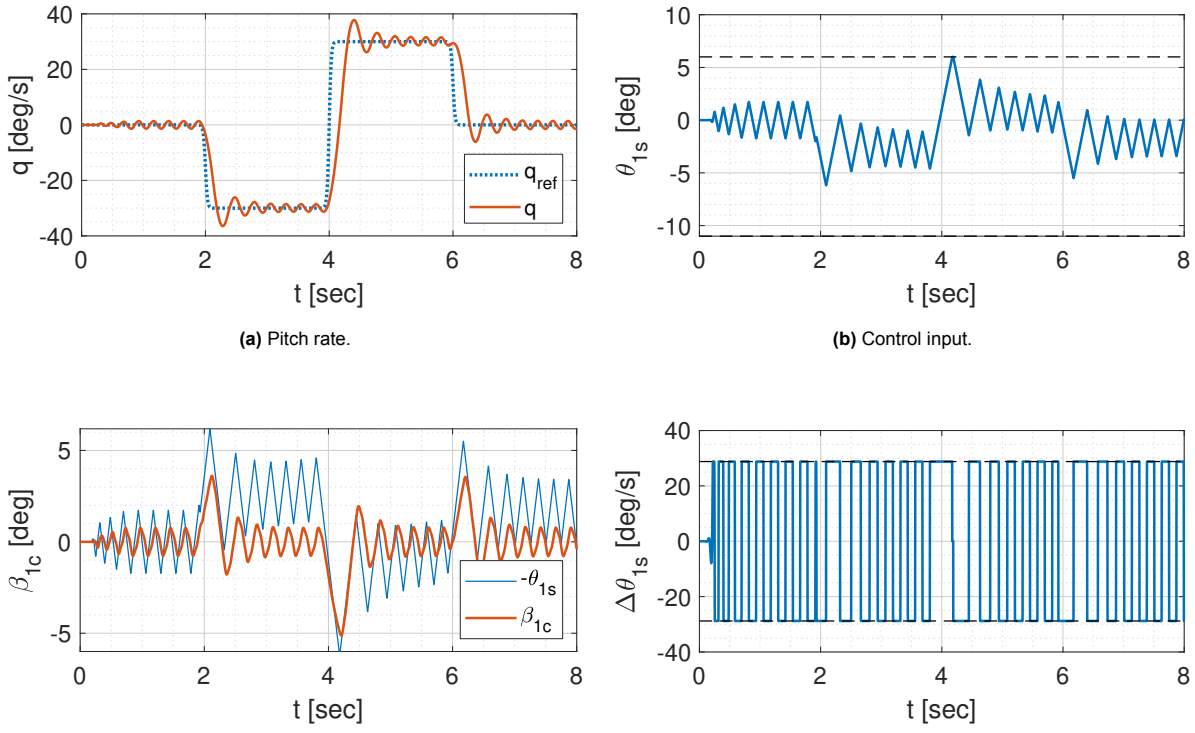

(a) Pitch rate.

(b) Control input.

(c) Longitudinal flap angle.

(d) Control input increment.

Figure 5.2: Tracking task with steady state IBS controller.

Because the controller is unaware of these delays, it keeps increasing its control input and this results in overcorrecting the signal. Due to the applied maximum deflection and rate limits of the actuator the signal is still bounded. If these limits are not applied, the helicopter model diverges.

5.2. 2 DoF model - Adding longitudinal flap

The most important reason why the controller discussed in the previous section did not work properly was the lack of flap dynamics in its controller model. To investigate the influence of these dynamics, a first order approximation of the flap dynamics is added to the previous model. This has been done by means of a flap time constant. The adaption can be seen in Equation (5.8) and essentially incorporates the regressing flap mode into the dynamics.

$$\begin{aligned} \dot{q} &= -K\left(\beta_{1c}\right) \\ \tau_\beta \dot{\beta}_{1c} + \beta_{1c} &= -\theta_{1s} + \frac{16}{\gamma}\frac{q}{\Omega} \end{aligned} \tag{5.8}$$

Calculating the poles of this system, given by Equation (5.9), one can see that two situations are possible depending on the value of K. If $K > \frac{\gamma\Omega}{64\tau_\beta}$ the two modes are separated in a disk tilt mode and a body mode. If the opposite holds, the two modes couple and produce oscillatory poles. This shows that increasing the moment transfer between the rotor blades and the hub, as is the result of a hingeless configuration, speeds up the body motion.

$$\mathbf{s}_{1,2} = -\frac{1}{2\tau_\beta} \pm \sqrt{\frac{1}{4\tau_\beta^2} - \frac{16}{\gamma}\frac{K}{\Omega\tau_\beta}} \tag{5.9}$$

The equations of system 5.8 can be reformulated to a state space system. This system is shown in Equation (5.10). A number of remarks can be made about this system. First, one can see that the control dependency of the pitch acceleration is diminished to zero. This means that time scale separation cannot be applied, thus the current controller is unable to control this system. Furthermore

one can see that the influence of the control input on the flap angle is large. Just removing the flap dynamics by means of residualization will not result in adequate performance. Also synchronization has to be applied here.

$$\begin{bmatrix} \dot{q} \\ \dot{\beta}_{1c} \end{bmatrix} = \begin{bmatrix} 0 & -K \\ \frac{16}{\gamma}\frac{1}{\Omega\tau_\beta} & -\frac{1}{\tau_\beta} \end{bmatrix} \begin{bmatrix} q \\ \beta_{1c} \end{bmatrix} + \begin{bmatrix} 0 \\ -\frac{1}{\tau_\beta} \end{bmatrix} \theta_{1s} \tag{5.10}$$

A normal procedure would then be to control the $\dot{q}$ by means of controlling flap angle β_{1c} with θ_{1s}. However, this is not possible with current helicopters since there is no measurement of the flap angle of the rotor blades. This is needed for the incremental control law. Therefore it is necessary to remove the flap angle from the state vector and increase the control dependency of q on the control input. This is done by residualization by means of Equation (4.27). Applying Equation (4.27) to model (5.10) with $\underline{x}_{res} = q$, the following system remains:

$$\dot{q} = -\frac{16}{\gamma}\frac{K}{\Omega}q + K\theta_{1s} \tag{5.11}$$

$$G_R = G_{R_q} = K \tag{5.12}$$

The residualization procedure solves the time scale separation problem by increasing the control dependency of q. Practically, it returns the model to the system description in Section 5.1. However, the residualization procedure neglects the time delay that the flap time constant is introducing into the system. In order to compensate for the effect of the flap time constant a synchronization filter has to be applied.

$$\begin{bmatrix} \dot{\beta}_{1c,sync} \\ \theta_{1s,sync} \end{bmatrix} = \begin{bmatrix} F_{\beta,\beta} \\ G_R^{-1}F_{q,\beta} \end{bmatrix} \beta_{1c,sync} + \begin{bmatrix} G_\beta \\ G_R^{-1}G_q \end{bmatrix} \theta_{1s,meas} \tag{5.13}$$

Combining the results from the synchronization filter and the residualized dynamics, the final IBS control law is shown in Equation (5.14):

$$\theta_{1s} = \theta_{1s,sync,0} + G_{R_q}^{-1}\left(-\dot{q}_0 + \dot{q}_{ref} - c_q z_q\right) \cdot dt \tag{5.14}$$

The resulting tracking performance can be seen in Figure 5.3. Looking at the figure it is obvious that this controller performs much better than the steady state controller, close to optimal tracking. Only some oscillations are visible in the control input increment signal, but they die out as the signal stabilizes. The difference between this simulation and the previous one shows the importance of including flap dynamics in controller design for helicopters.

In the quasi-steady controller model, the flap dynamics is modeled as a quasi-steady approximation of the second order flap model of Equation (2.4) using the variable τ_β. By applying the correct simplifications and assumptions to the second order flap model the value of τ_β can accurately be determined to be $\frac{16}{\gamma\Omega}$. For the MBB Bo-105 helicopter this results in a time constant of 0.07 seconds. The formula is also used in the synchronization filter. To see the influence of the estimation of τ_β on the tracking performance, three simulations are done with different time constant values. The result of these simulations is shown in Figure 5.4, for τ_β = [0.00711 0.0711 0.711]. The figure shows that for large τ_β the synchronization filter is overestimating the impact of control input, thereby delaying the control signal more than necessary. This leads to stable but sub-optimal tracking. For small values of τ_β the pitch and control response show oscillatory behavior. In fact, the oscillations are bounded because of actuator rate limits. This can be explained by comparing the simulation with a small tau to the simulation with the steady state controller in place (Figure 5.2). Because τ_β is very small, the synchronization filter assumes that the flap dynamics are almost instant. Therefore the calculated control inputs are too rigorous for the helicopter model and the divergent behavior explained for the steady state controller happens here as well. In general it can be said that it is important to use an accurate estimate of τ_β when using the quasi-steady controller, with overestimation leading to sub-optimal control and underestimation leading to (bounded) instability.

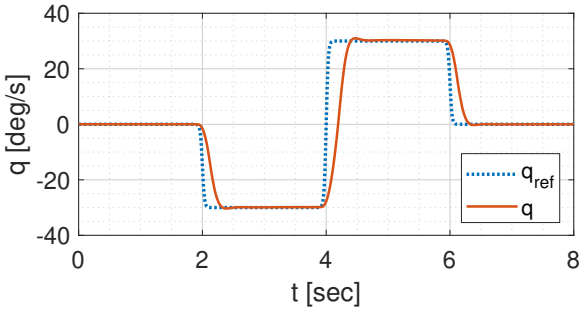

(a) Pitch rate.

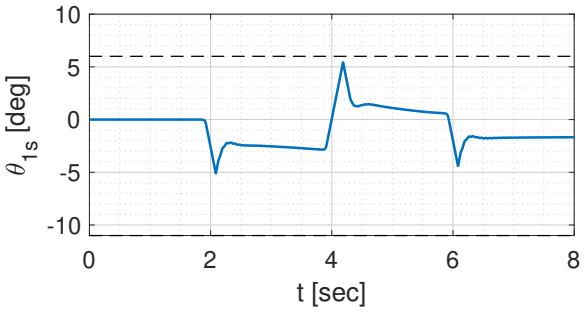

(b) Control input.

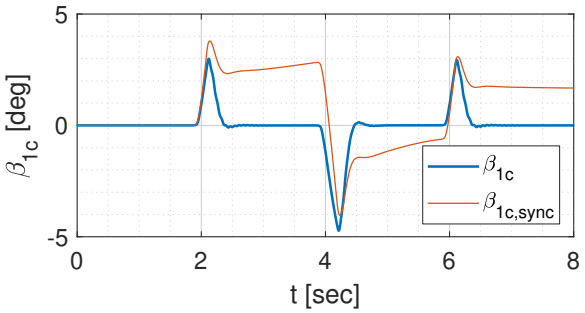

(c) Longitudinal flap angle.

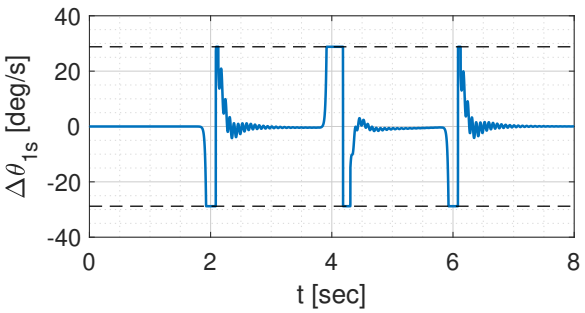

(d) Control input increment.

Figure 5.3: Tracking task with quasi-steady IBS controller.

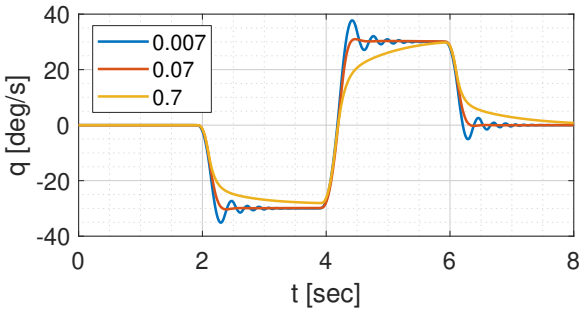

(a) Pitch rate for varying τ_β.

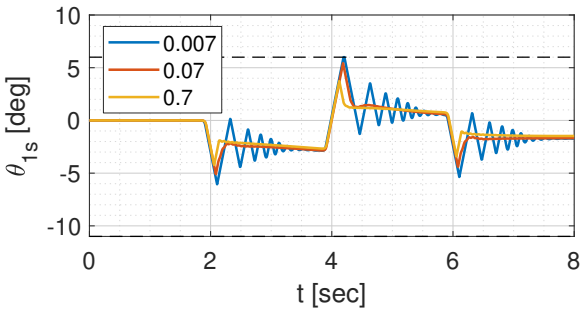

(b) Control input for varying τ_β.

Figure 5.4: Influence of τ_β on pitch rate and control input.

5.3. 5 DoF model - Adding uniform inflow and forward velocity

Compared to the 2 controller models above, the difference between the model that simulates the helicopter and the controller model is still substantial. For instance no forward velocity is included, a parameter that has a large influence on helicopter behavior in general. Therefore a third IBS controller is constructed using first order flap dynamics, derived from Equation (2.5) and retaining the influence of flight velocities. The systems of equations for this controller model are:

$$\begin{aligned} \dot{q} &= -K\beta_{1c} \\ \dot{\theta}_f &= q \\ \dot{u} &= \frac{X}{m} - g\sin(\theta_f) - qw \\ \dot{w} &= \frac{Z}{m} + g\cos(\theta_f) + qu \\ \dot{\beta}_M &= -\Omega \mathsf{C}_{M0}^{-1}\mathsf{D}_{M0}\beta_M + \Omega \mathsf{C}_{M0}^{-1}\mathsf{H}_{M0} \\ \tau_{\lambda_i}\dot{\lambda}_i &= C_T^{elem} - C_T^{glauert} \end{aligned} \tag{5.15}$$

As can be seen a uniform inflow component is taken into account by using a time constant. The equations for both thrust coefficients can be found in Chapter 3. Since the controller model now includes the β_{1c} derivative by means of the flap equation, this controller model now encompasses the regressive flap mode. The next step is to residualize the flap and inflow states. System (5.16) is constructed in such a way that the remaining states and states that need to be residualized are grouped in $\underline{x}_1 (= \underline{x}_{res})$ and $\underline{x}_2$ respectively. Equation (4.27) is applied to this system to arrive at the residualized system to be used for the controller. Since the IBS controller only uses the residualized control matrix G_R its formulation is repeated in Equation (5.17).

$$\left[\begin{array}{c} \dot{q} \\ \dot{u} \\ \dot{w} \\ \hline \dot{\beta}_{1c} \\ \dot{\lambda}_i \end{array}\right] = \left[\begin{array}{ccc|cc} 0 & F_{q,u} & F_{q,w} & F_{q,\beta 1c} & F_{q,\lambda_i} \\ -w & F_{u,u} & F_{u,w} & F_{u,\beta_{1c}} & F_{u,\lambda_i} \\ u & F_{w,u} & F_{w,w} & F_{w,\beta_{1c}} & F_{w,\lambda_i} \\ \hline F_{\beta_{1c},q} & F_{\beta_{1c},u} & F_{\beta_{1c},w} & F_{\beta_{1c},\beta_{1c}} & F_{\beta_{1c},\lambda_i} \\ 0 & F_{\lambda_i,u} & F_{\lambda_i,w} & F_{\lambda_i,\beta_{1c}} & F_{\lambda_i,\lambda_i} \end{array}\right] \left[\begin{array}{c} q \\ u \\ w \\ \hline \beta_{1c} \\ \lambda_i \end{array}\right] + \left[\begin{array}{c} G_q \\ G_u \\ G_w \\ \hline G_{\beta_{1c}} \\ G_{\lambda_i} \end{array}\right] \theta_{1s} \tag{5.16}$$

$$G_R = G_{x_1} - F_{x_1,x_2}F_{x_2,x_2}^{-1}G_{x_2} \tag{5.17}$$

Because this controller requires more states to be residualized, also the synchronization filter is more extensive than for the quasi-steady controller. The extended synchronization filter is shown in Equation (5.18). G_{R_q} is the first entry of the residualized control effectiveness matrix of Equation (5.17), representing the residualized control effectiveness of θ_{1s} with respect to q. The final control law for the first order IBS controller is equal to the control law for the quasi-steady control law, given in Equation (5.14). The only difference is in the values for G_{R_q} and $\theta_{1s,sync}$.

$$\begin{bmatrix} \dot{\beta}_{1c,sync} \\ \dot{\lambda}_{i,sync} \\ \theta_{1s,sync} \end{bmatrix} = \begin{bmatrix} F_{\beta_{1c},\beta_{1c}} \\ 0 \\ G_{R_q}^{-1}F_{q,\beta_{1c}} \end{bmatrix} \beta_{1c,sync} + \begin{bmatrix} 0 \\ F_{\lambda_i,\lambda_i} \\ G_{R_q}^{-1}F_{q,\lambda_i} \end{bmatrix} \lambda_{i,sync} + \begin{bmatrix} G_{\beta_{1c}} \\ G_{\lambda_i} \\ G_{R_q}^{-1}G_q \end{bmatrix} \theta_{1s,meas} \tag{5.18}$$

To make a preliminary investigation whether taking into account inflow dynamics in the controller design is improving tracking performance, the controller model for the first order controller included the regressing flap model and inflow dynamics. Therefore it is able to take into account more aspects of the helicopter dynamics and, in theory, improves the tracking of the reference signal. As the simulation results in Figure 5.5 show, tracking did not improve significantly. It seems that the correction for the regressing flap, as was done in the previous example, has much more impact than accounting for inflow dynamics. Only the oscillations in the increments of the control signal have disappeared.

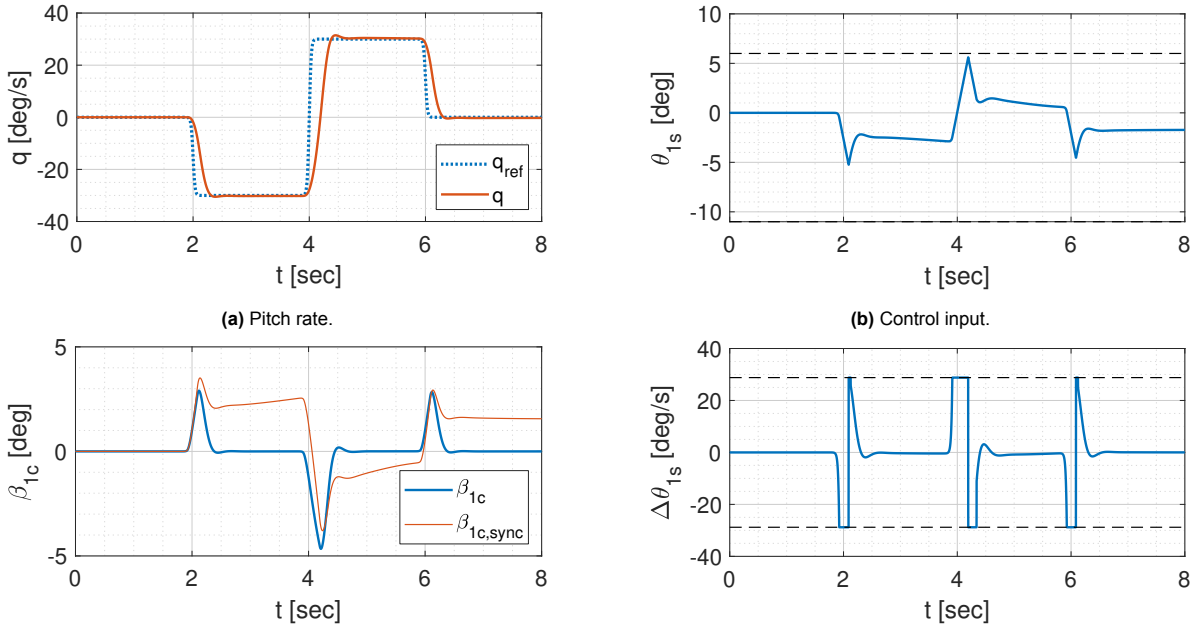

(a) Pitch rate.

(b) Control input.

(c) Longitudinal flap angle.

(d) Control input increment.

Figure 5.5: Tracking task with first order IBS controller.

This makes clear that the oscillations are coming from a mismatch in time delay of the flap dynamics modeling between the helicopter model and the controller model, comparable with the statements made when discussing the steady state controller. The controller model in the previous example has a tau based time delay, while the helicopter model and the controller model in this example has the more accurate regressing flap modeled time delay. This causes the latter model to be closer to the original model, obtaining better performance. Including inflow dynamics in the controller model, and subsequently using it for residualization and synchronization, does not seem to solve this problem.

5.3.1. Influence of τ_{λ_i}

The goal for this report is, among others, to investigate the effect of inflow dynamics on the performance of IBS controllers. In the previous section it was stated that including inflow dynamics in the controller model and thereby taking it into account in the synchronization filter did not make any significant improvement in tracking performance. During this investigation the inflow was modeled with the last equation of system 5.15. Until now, time constant τ_{λ_i} was set at a value of 0.1 seconds (Pavel 2001). By varying the time constant to a value of 0.01 and 1 seconds, the influence of changing inflow behavior can be investigated.

Figure 5.6 summarizes the findings of the simulations. In Figure 5.6(a) on can see that increasing the time constant indeed changes the behavior of the inflow dynamics. To see if the inflow also affects the controller, the synchronized inflow that is used in the synchronization filter is displayed in Figure 5.6(c). Here one can see that the inflow with lowest time constant not only reacts the quickest, it also reaches the largest amplitudes. Since the inflow has no direct relation to the control law itself, the influence of the synchronized inflow is examined in the synchronization filter. As can be deducted from Equation (5.18) the 2 states that can influence the synchronized control input $\theta_{1s,sync}$ are the synchronized inflow and flap angle. Their influence on $\theta_{1s,sync}$ is plotted in Figure 5.6(b), with the signal of λ_i being the one for $\tau_{\lambda_i} = 0.01$ as this one reaches the largest amplitudes. It is shown that the synchronized inflow has very little effect on the control input compared to the flap angle. Therefore the effect of changing τ_{λ_i} on the control input is very limited, as can be seen in Figure 5.6(d). Only minor differences in the control signal are visible at the end of the simulation.

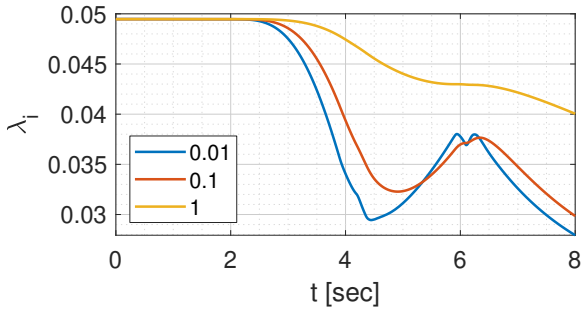

(a) Inflow for varying τ_{λ_i}.

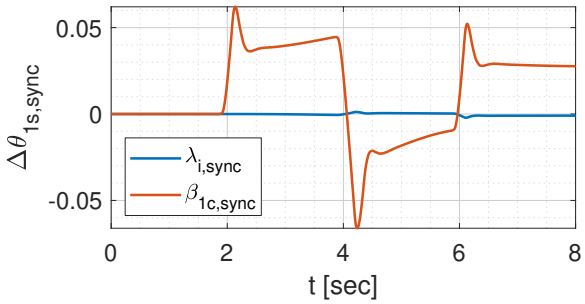

(b) Influence of synchronized $\lambda_i(\tau_{\lambda_i} = 0.01)$ and β_{1c}.

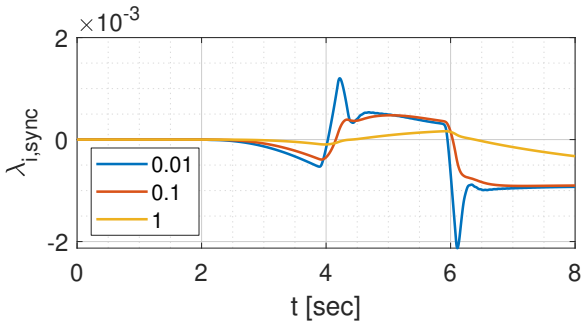

(c) Synchronized inflow for varying τ_{λ_i}.

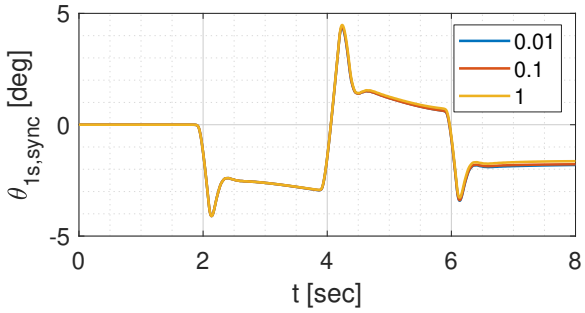

(d) Influence of inflow on θ_{1s}.

Figure 5.6: Influence of τ_{λ_i} on inflow and control parameters.

5.3.2. Influence of forward flight speed u

As stated in the introduction of this chapter, all simulation results shown in this report are performed without any initial horizontal velocity. To show the influence flight speed has on tracking performance, three simulation runs at initial speeds of 0, 30 and 60 meters per second are displayed in Figure 5.7. As one can see from Figure 5.7(b) the sustained required longitudinal control increases with increasing airspeed. This is because the rotor wants to blow-back due to the dissymmetry in lift between the advancing side and the retreating side of the blades. From Figure 5.7(a) it is clear that flight speed has no large effect on tracking the reference signal, other than a small steady state error. This will of course be different if due to the larger required control inputs the actuation limits of the control system are reached. In real life this will not happen often has helicopters have a certain never-exceed airspeed.

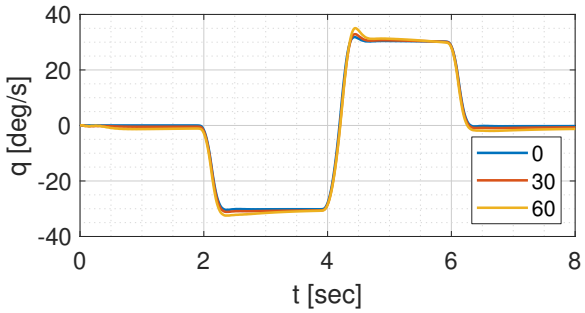

(a) Pitch rate for varying u.

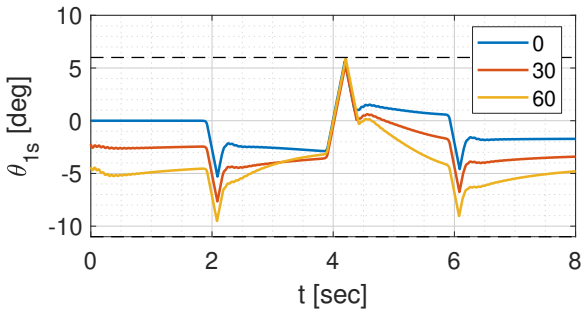

(b) Control input for varying u.

Figure 5.7: Influence of u on pitch rate and control input.

5.4. 13 DoF model - Adding inflow states and lateral states

After performing a preliminary investigation on simplified longitudinal models in the previous sections, all evaluations made in this section are based on the higher fidelity model from Van der Goot (2017). The most important dynamics of this simulation model are covered in Chapters 2 to 4. The effects of changing the inflow model from a Pitt-Peters model to the Keller model is discussed in Section 5.4.1. The analysis is based on pole-zero locations and simulations of the free response to control input, without any interference of the control system. The results of adapting the residualized dynamic model and synchronization for accounting for inflow dynamics is given in Section 5.4.2.

5.4.1. Applying Keller inflow model

Before the inflow model correction described by Equation (3.4) from Keller and Curtiss (1998) could be implemented in the simulation, it had to be converted to a form that is easier to implement in the current set up of the inflow calculations. As a basis the Pitt-Peters inflow model that is currently implemented is used. This is possible since it is known that when K_R is set to zero the two models are equal. The new inflow model including the correction proposed by Keller is shown in Equation (5.19), with the matrices unchanged from their original description given in Equation (3.3).

$$\begin{bmatrix} \dot{\lambda}_0 \\ \dot{\lambda}_{1s} \\ \dot{\lambda}_{1c} \end{bmatrix} = M^{-1} \left(\begin{bmatrix} C_T \\ C_L \\ C_M \end{bmatrix} - VL^{-1} \begin{bmatrix} \lambda_0 \\ \lambda_{1s} \\ \lambda_{1c} \end{bmatrix} + VL^{-1} K_R \begin{bmatrix} 0 \\ \bar{p} - \frac{\dot{\beta}_{1s}}{R} \\ \bar{q} - \frac{\dot{\beta}_{1c}}{R} \end{bmatrix} \right) \tag{5.19}$$

Before the rotational rates and flap velocities can be used in the model, they have to be transformed to another reference frame. Namely, the inflow model is defined in the disk plane-wind reference frame, which is the disk plane axis system rotated by the side slip angle. This causes the velocity vector to only have forward and downward components. Both the angular rates and the flap velocities are defined in the hub plane. Therefore two transformations are needed, the first from the hub plane to the disk plane and the second to the disk plane-wind frame. The value for K_R is set to 3.0, as this is the recommended value based on curve fitting to experimental data (Keller and Curtiss 1998). However, as the authors of (Arnold et al. 1998) also suggest, the identified value differs depending on the identification method of the parameter. Values for K_R are ranging from 0.75 to 3.5 in literature.

One way to see if the modified inflow dynamics have influence on the helicopter dynamics as a whole, one can look at the complex plane representation of the linearized systems. With this method one can see if the inflow modes cause the body modes or flap modes to change position with respect to the nominal model. Figure 5.8 shows the complex plane representation of the nominal model and a zoomed-in figure for the poles near the origin. Note that only the positive side of the imaginary axis is displayed, as the locations of oscillatory poles is mirrored across the real axis. In order to compare both models, the complex plane representation of the linearized helicopter model with the Keller inflow model is given in Figure 5.9.

Comparing the complex plane representations Figure 5.8 (a) and Figure 5.9 (a), one can conclude that they look very similar. For both hover and forward flight no shifting of the poles is visible due to the change in inflow dynamics. In Figure 5.8 (a) some typical modes are identified. Two of the three flap modes, namely the advancing flap mode and the coning mode, are located at the same position as if the flap dynamics would be treated separately. This is to be expected since they are of relatively high frequency compared to the body modes. Leaving out the second derivative of the flap angles in Equation (2.5) of a helicopter simulation, the origin of this high frequency mode, is therefore justifiable in most cases. The regressing flap mode, normally on the same vertical axis as the other two modes but much closer to the real axis, has coupled with the pitch subsidence and roll subsidence. If only the body states would be treated, these would be non-oscillatory modes in case of the MBB Bo-105. This shows that for the MBB Bo-105 there is coupling between the regressing flap mode and the body modes, speeding up the body motion.

The poles close to the origin are visualized in Figure 5.8 and Figure 5.9. Also in this view the location of the poles have not changed significantly. One can identify the Dutch roll and phugoid modes in the figure, with the heave and spiral subsidence remaining on the real axis near the origin. The

only observable difference are two non-oscillatory poles close to coordinate -0.5. As the flight speed increases they move from the real axis and become lightly oscillatory. However, no major coupling with other modes can be seen in this view. All three inflow modes start on the real axis, with one mode becoming oscillatory as flight speed increases.

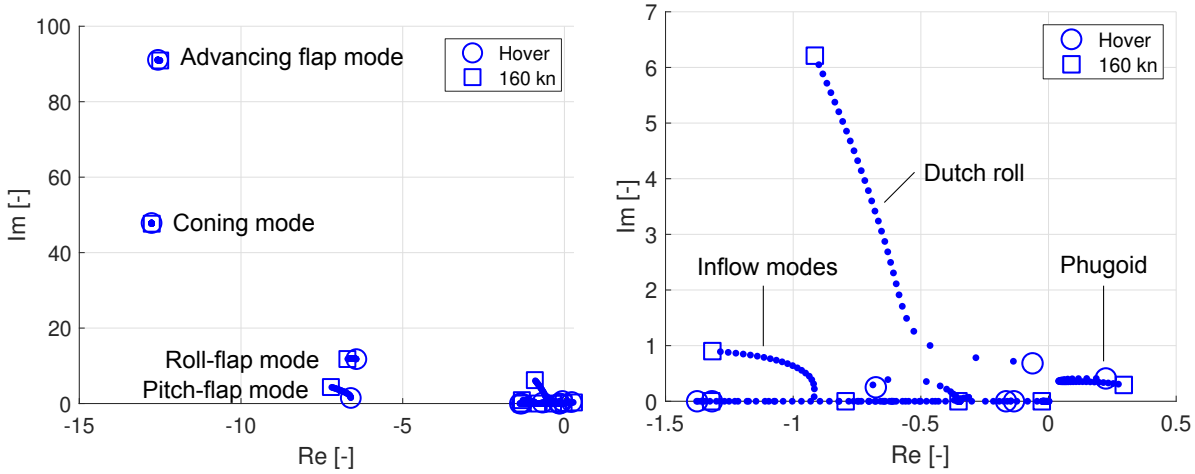

(a) Nominal model.

(b) Nominal model, zoomed-in around origin.

Figure 5.8: Complex plane representation of linearized nominal helicopter model.

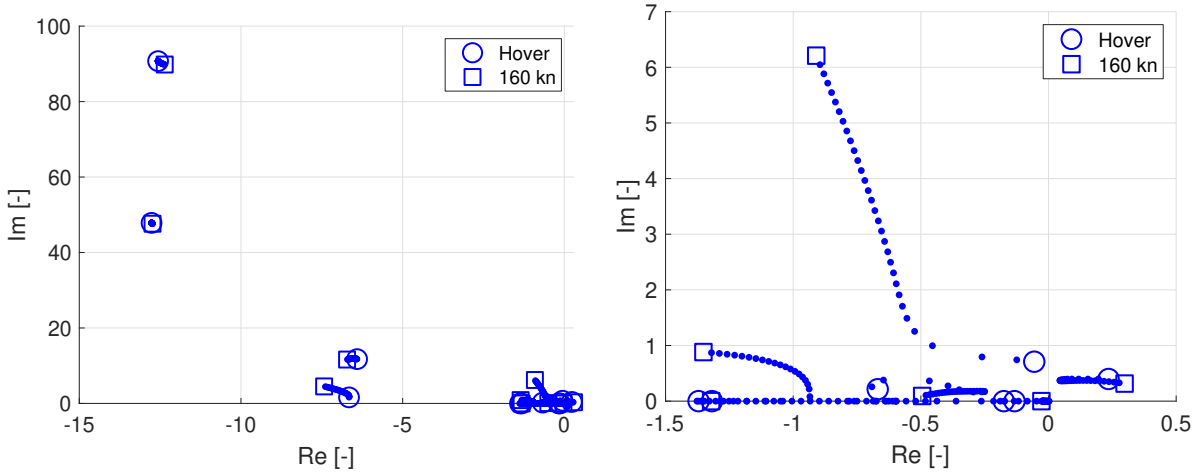

(a) Modified model with K_R=3.

(b) Modified model with K_R=3, zoomed-in around origin.

Figure 5.9: Complex plane representation of linearized helicopter model with Keller correction.

Another way to see the possible influence of the changed inflow model is by looking at the free response of the helicopter model subjected to a step in control input without interference of the controller. The four inflow states of the helicopter model are presented in Figure 5.10 together with the angular rated of the helicopter. These are the responses to a doublet consisting of a negative step input of 1 second on the longitudinal cyclic of -3 degrees at 1 seconds follow by an opposite command at 2 seconds. For the remainder of simulation time and for the other control inputs there is no action. The simulation is performed from a hovering initial position.

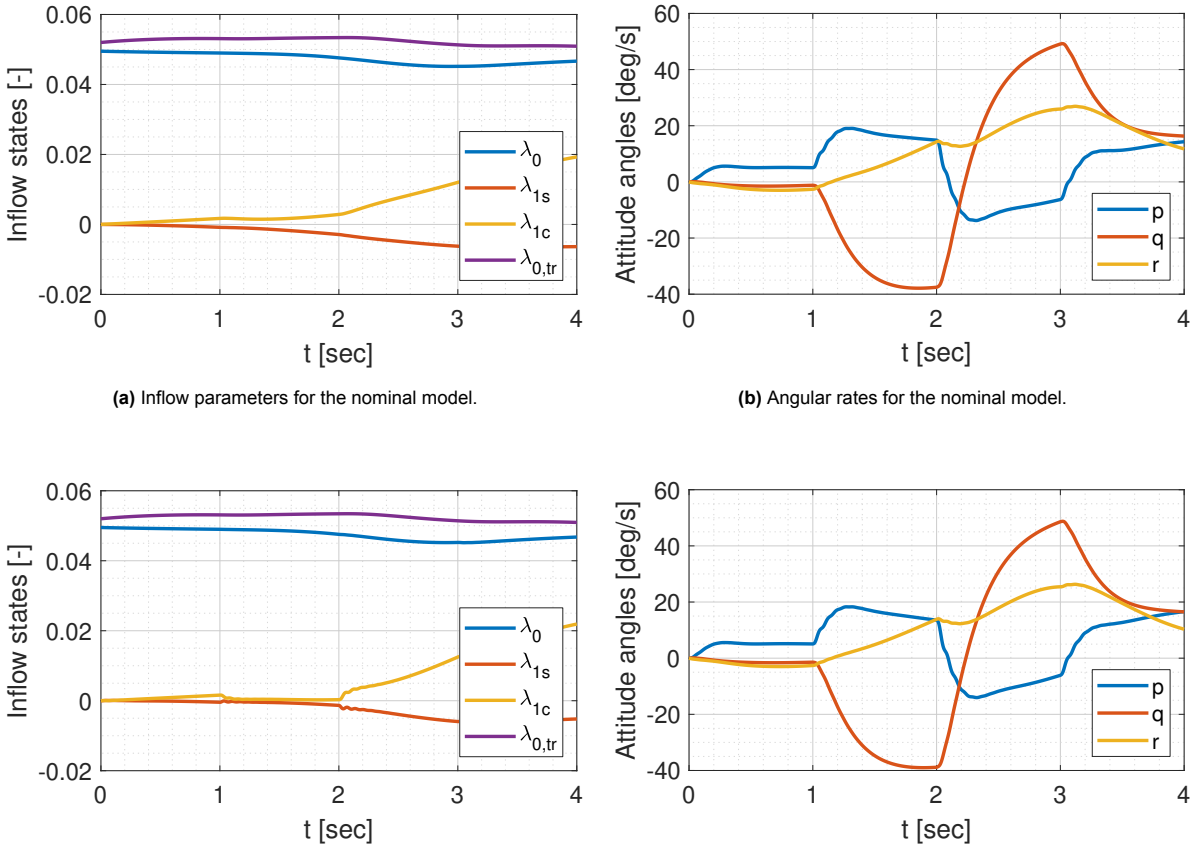

(a) Inflow parameters for the nominal model.

(b) Angular rates for the nominal model.

(c) Inflow parameters for the modified model.

(d) Angular rates for the modified model.

Figure 5.10: Free helicopter response to step input in longitudinal cyclic in hover.

From Figure (a) and (c) there are small differences visible during the time that longitudinal control input is given. This also translates into slightly different angular rates. However, between the nominal and modified model there should be a notably different reaction in the off-axis angular rates. An example of this difference has been given in Figure 3.2 in Section 3.1.3 (Arnold et al. 1998). Because longitudinal cyclic is applied in this example, there should be a difference between the roll rate of the nominal and modified simulation. The simulation is performed for hover, as in this initial state the Keller correction is most effective. Simulations at other airspeeds were also performed but did not give other results.

Finally, it is investigated whether the control inputs generated by the CFIBS controller have been altered by the change inflow dynamics. To this end a simulation has been performed in which the controller has to track a doublet in the pitch axis and roll axis. The results can be seen in Figure 5.11, which shows the calculated control inputs by the controller, the angular rates of the helicopter together with the reference signals and lastly the resulting inflow coefficients. In this experiment the residualization and synchronization procedure has only been performed for the flap states. Note that in Figure 5.11 (c) and (d) besides the reference input there is also a commanded input. This is the signal that the CFIBS is trying to track and is calculated based on the reference signal itself and the response requirements set in the ADS-33E-PRF handling qualities requirements (Baskett 2000).

As with the other experiments, no large difference is visible between the nominal and modified model. The harmonic inflow coefficients show a sharper change after the doublets are initiated, but the overall effect is insignificant. The largest effect during this simulation should be visible in the control inputs generated by the control system. If a change in off-axis coupling would be present, the lateral control input would change when a longitudinal doublet is performed because the controller tries to keep the other angular rates at zero. This also applied to the longitudinal control input when a roll doublet is performed. But just as for the other simulations in this section, the change inflow model hardly causes any difference in the tracked parameters.

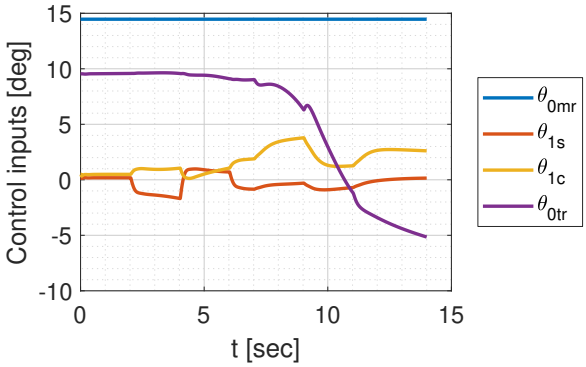

(a) Control inputs for the nominal model.

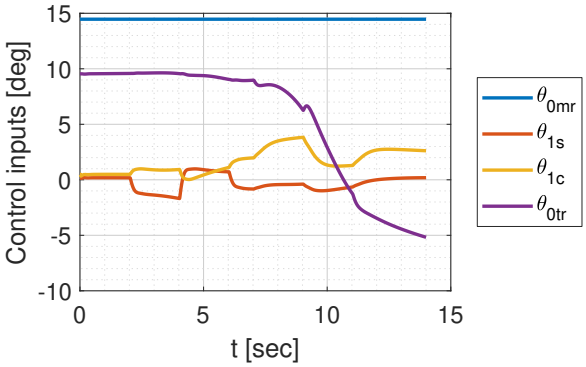

(b) Control inputs for the modified model.

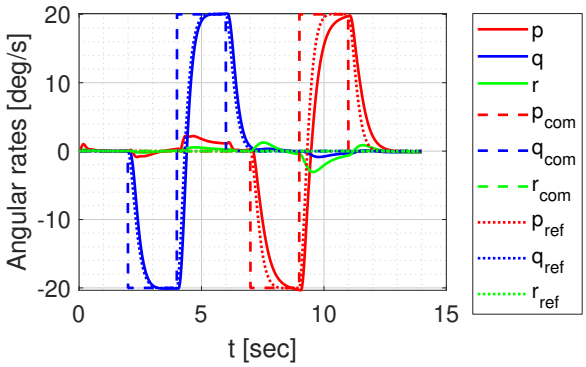

(c) Angular rates for the nominal model.

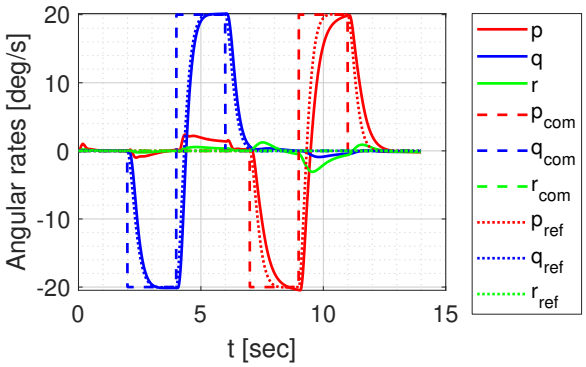

(d) Angular rates for the modified model.

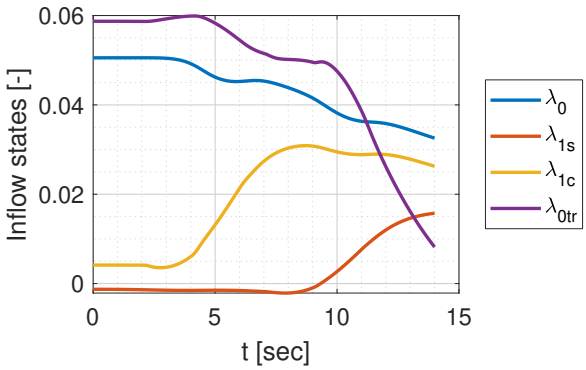

(e) Inflow parameters for the nominal model.

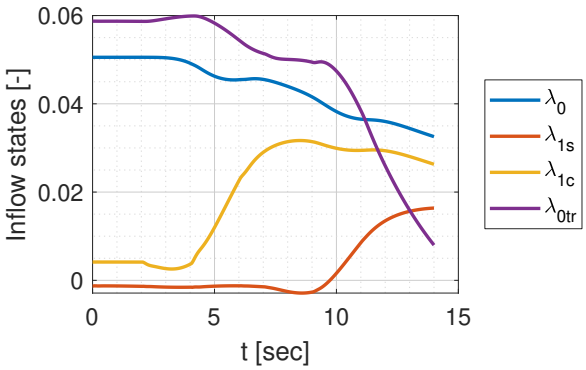

(f) Inflow parameters for the modified model.

Figure 5.11: Helicopter response to angular rate doublets using CFIBS controller in hover.

It can be concluded from the investigations above that the implementation of the Keller correction in the inflow model did not give any major difference in the helicopter characteristics. It is unclear why this is the case, as simulation experiments from Keller and Curtiss (1998) do show differences in the response of the helicopter and changes in the off-axis correction. The simulations shown here are only for hover, as this should be the condition in which the largest effect is visible, but are also carried out for a range of airspeeds. These showed no other behavior than the simulations discussed above. The modified model is implemented correctly and the mathematical model is checked against multiple other sources (Barocela et al. 1997; Zhao 2005). Increasing the value of K_R multiple factors only increases the coupling between the harmonic inflow coefficients and the angular rates in the same axis, but the off-axis couplings remain the unchanged. There is some ambiguity between the references whether some parameters are divided by Ω or not, but multiplying K_R by Ω gives unrealistic results and in turn

do not change the off-axis coupling. Dividing K_R by Ω has no use, as the effect of the correction goes to zero as K_R approaches zero. Then the original Pitt-Peters model remains.

5.4.2. Inflow residualization and synchronization

Besides the investigation into the effect of modifying the inflow model, efforts have also been made to analyze the effect of including the inflow dynamics in the residualization and synchronization procedure. These can be seen as separate parts; for the analysis of these procedures it does not matter whether the original inflow model or the modified inflow model is used in the helicopter model.

Currently only the flap angles are residualized from the controller model. This is a logical choice as the flap angle states cannot be measured and are the most important states relating to controlling the helicopter. Controlling a helicopter while being unable to account for the time delays that the flap dynamics introduce is impossible. However, the inflow states are currently not residualized. An incremental control law based on such a model is not possible in real life as it is impossible to measure the inflow states. Therefore they either have to be removed from the controller model, leaving a model with a lower fidelity, or they have to be residualized and accounted for in the synchronization filter. Removing the inflow states from the controller model seems unwanted, since the rotor inflow has an effect on the flap dynamics according to the literature mentioned in Chapter 3. Therefore this step is not merely to account for time scale separation, but also from an implementation point-of-view.

To analyze if residualizing and synchronizing the inflow dynamics is beneficial for controller performance, the synchronization filter of Equation (4.28) is added to the flap synchronization in the model of Van der Goot (2017). Furthermore, the system and control dependency matrices are adapted so both inflow states and flap dynamics are residualized. The updated model is compared to the original model by means of their tracking performance of attitude angle reference signals. As with other simulations in this chapter, the simulations are initiated in hover condition, as this is the situation wherein the inflow states are supposed to have the most influence on the helicopter dynamics.

Figure 5.12 shows a comparison for a pitch and roll attitude tracking task with and without additional inflow residualization and synchronization using the CFIBS controller. It can be seen that the tracking performance with only flap synchronization is better than the adapted version of the controller. The tracking performance of the respective attitude angles to which a doublet reference signal is given is still somewhat satisfactory. However, large deviations in the other attitude angles are visible. The controller is unable to keep them close to their reference signal. The doublet tracking shows both overshoot of the reference value and time delay, with roll angle tracking worse than pitch angle tracking. This is unexpected, since the moment of inertia of the helicopter around the roll axis is less than around the pitch axis.

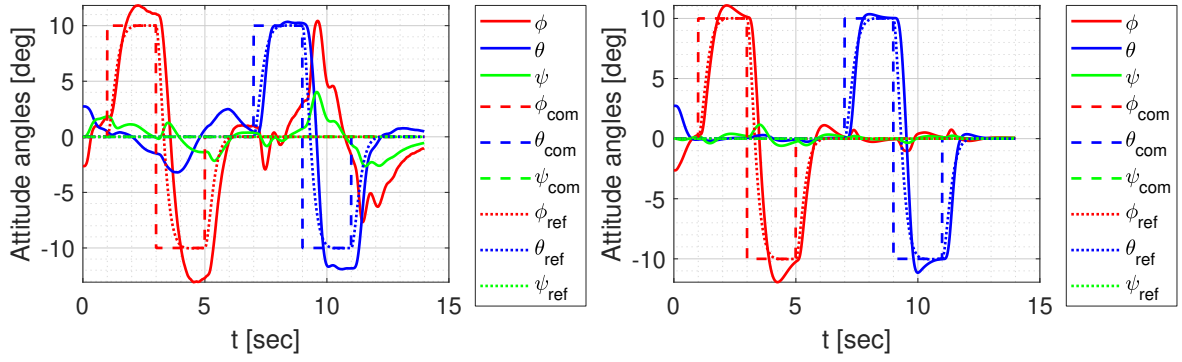

(a) Flap and inflow synchronization.

(b) Only flap synchronization.

Figure 5.12: Tracking of attitude reference signals with CFIBS controller in hover.

The comparison between inflow synchronization of the nominal model and the model with the off-axis correction can be seen in Figure 5.13. It can be concluded that lack of tracking performance is not due to the added correction itself, but rather due to inflow synchronization as a whole. Moreover, the tracking performance keeps degrading for higher reference angles. If the reference signals reach above 30 degrees for this series of doublets, the simulation model will diverge in attitude control due to reaching actuator magnitude limits.

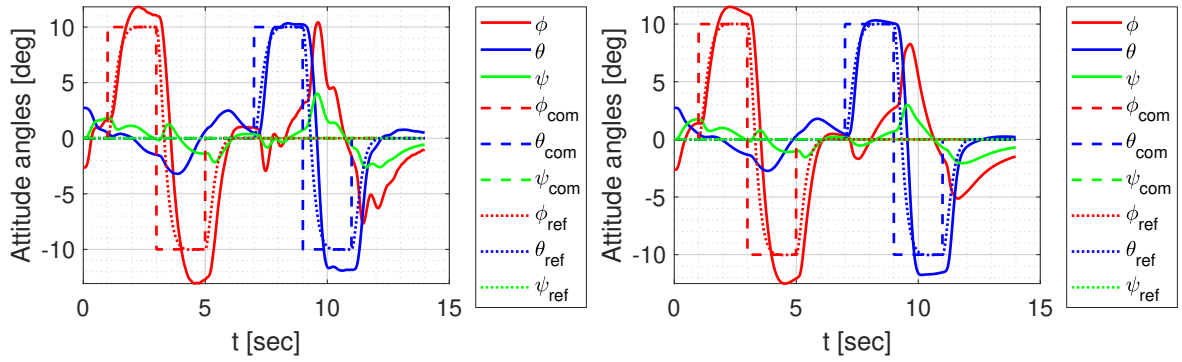

(a) Model with added inflow correction.

(b) Nominal model.

Figure 5.13: Flap and inflow synchronization with CFIBS controller in hover.

The tracking task is also performed with an INDI controller to see whether the lack of tracking performance is specific to the CFIBS controller. Figure 5.14 (a) shows the tracking task for both flap and inflow synchronization, while subfigure (b) only employs flap synchronization. From subfigure (a) it can be concluded that INDI controller performance is also inadequate when using flap and inflow synchronization. This shows that the poor performance is not due to a specific control algorithm, but rather the application of residualization and synchronization of the inflow dynamics.

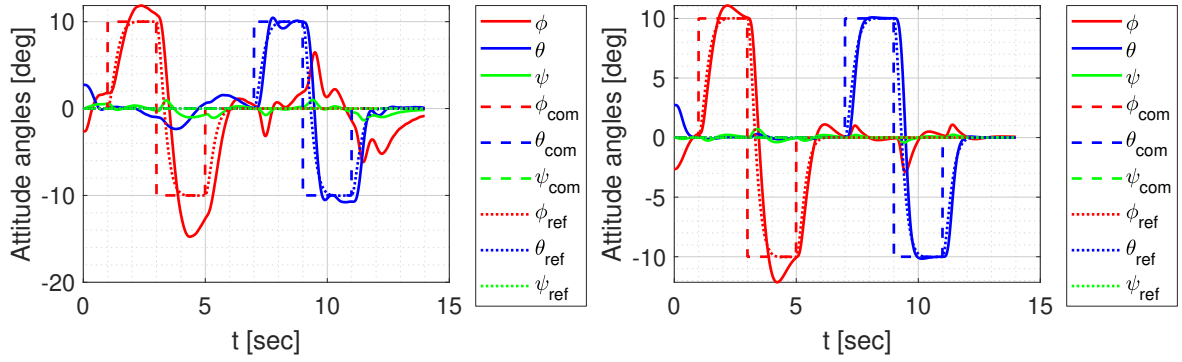

(a) Flap and inflow synchronization.

(b) Only flap synchronization.

Figure 5.14: Tracking of attitude reference signals with INDI controller in hover.

6

Conclusion

This report considers the investigation into the improvement of the off-axis response of an MBB Bo-105 hingeless helicopter due to the improvement of the current Pitt-peters inflow model. It was found in literature that the Keller inflow model improves the off-axis response of the helicopter simulation model due to a change in inflow dynamics. Furthermore, an analysis has been performed on the inclusion of inflow dynamics in the controller model of incremental controllers. Adding the inflow dynamics to the residualization and synchronization of the controller model could increase its performance and make the controller more suited for application in real life, since it is currently impossible to measure the inflow of the rotor.

After applying the Keller inflow model in the helicopter model it was found that the improved model did not have the desired outcome. The off-axis response did not change and the overall effect on the inflow states was very minor. This resulted in no changes in the overall helicopter dynamics, as was proved by analysis of the complex plane representation of the linearized helicopter dynamics and the execution of several angular rate tracking tasks.

The inclusion of the inflow states in the synchronization filter and the residualized system description also did not have the wanted effect. Tracking performance of the command filtered incremental backstepping controller degraded significantly, not being able to track attitude reference signal doublets above 30 degrees magnitude for the tested reference signals. Especially the attitude angles that were supposed to stay at zero showed significant coupling, compared to the simulation with only flap synchronization. However, the inflow residualization and synchronization is necessary because the inflow states cannot be measured in real life. The results did not change whether the simulation was performed with the improved Keller inflow model or the original Pitt-Peters inflow model. The tracking task was also performed with and incremental non-linear dynamic inversion controller, but this did not result in better tracking performance. From this it can be concluded that the degradation of controller performance is due to the process of residualization and synchronization, not from a specific incremental control methodology.

7

Recommendations

This investigation shows that more work is necessary to be able to implement non-linear controllers in real-life and to model helicopter dynamics to a high degree of precision. Future recommendations can be set to continue research on these topics.

Other inflow models with different approaches to the inflow modelling could be applied to arrive at a more realistic dynamic inflow model. Inflow models are available that correct for the off-axis response by means of an aerodynamic phase correction that shifts the phase of the aerodynamic flap moment. Another correction is an aerodynamic lag term, which lags the aerodynamic load of a blade compared to the change in angle of attack of the blade. Other inflow models with correction coefficients that are empirically obtained could give better results, but are helicopter specific. Furthermore, prescribed and free wake models become increasingly computational efficient while computers get more computational power. In the near future it might be possible to apply these methods in real-time for piloted simulation or control related purposes.

To solve the issues with the synchronization filter described in this report, the sensitivity of the synchronization filter needs to be investigated. Furthermore, entirely other control methods could be explored as well, such as adaptive or reinforcement learning. These could circumvent the necessity of the residualization and synchronization procedure that will remain necessary for incremental controllers. One can also look at applying estimators or Kalman filters that estimate the state of the flap angles and inflow coefficients, in combination with a non-incremental non-linear controller.

References

Acquatella, P. J. (2020). “Robust nonlinear attitude control of aerospace vehicles: An incremental nonlinear control approach”. PhD thesis. Delft University of Technology.

Arnold, U. T. P. et al. (1998). “The Effect of Inflow Models on the Predicted Response of Helicopters”. In: *Journal of the American Helicopter Society* 43.1, pp. 25–36. DOI: 10.4050/JAHS.43.25.

Arons, M. D. C. (2020). “Effect of Lead-Lag Dynamics on Command Filtered Incremental Adaptive Backstepping Hingeless Rotorcraft”. Master thesis. Delft University of Technology, p. 163.

Barakos, G. N. et al. (2020). “CFD simulation of helicopter rotor flow based on unsteady actuator disk model”. In: *Chinese Journal of Aeronautics* 33.9, pp. 2313–2328. DOI: 10.1016/j.cja.2020.03.021.

Barocela, E. et al. (1997). “The Effect of Wake Distortion on Rotor Inflow Gradients and Off-Axis Coupling”. In: *22nd Atmospheric Flight Mechanics Conference*, pp. 272–282. DOI: 10.2514/6.1997-3579.

Baskett, B. J. (2000). *ADS-33E-PRF: Aeronautical Design Standard, Performance Specification and Handling Qualities Re- quirements for Military Rotorcraft*. Tech. rep. US Army Aviation and Missile Command, p. 106.

Basset, P. and F. Tchen-Fo (1998). “Study of the Rotor Wake Distortion Effects on the Helicopter Pitch-Roll Cross-Coupling”. In: *24th European Rotorcraft Forum*. September, p. 13.

Bottai, A. et al. (2018). “Fully Coupled Flight Dynamics/CFD Simulations of a Helicopter with Actuator Disk Models for the Main Rotor and Tail Rotor”. In: *Proceedings of the AHS International Technical Meeting on Aeromechanics Design for Transformative Vertical Flight 2018*.

Bramwell, A. R. S., G. Done, and D. Balmford (2001). *Bramwell’s Helicopter Dynamics*. second edi. Butterworth Heinemann, p. 397.

Carpenter, P. J. and B. Fridovich (1953). *Effect of a Rapid Blade-Pitch Increase on the Thrust and Induced-Velocity Response of a Full-Scale Helicopter Rotor*. Tech. rep., pp. 1–26.

Chu, Q. P., M. D. Pavel, and R. R. Van der Goot (2017). “Incremental Adaptive Backstepping Flight Control for Rigid Rotor Helicopters”. In: *American Institute of Aeronautics and Astronautics*, pp. 1–33.

Curtiss, H. C. (1986). “Stability and Control Modelling”. In: *Twelfth European Rotorcraft Forum*. 41. Garmisch-Partenkirchen, pp. 1–17. DOI: 19870056154.

Du Val, R. W. and C. J. He (2018). “Validation of the FLIGHTLAB virtual engineering toolset”. In: *Aeronautical Journal* 122.1250, pp. 519–555. DOI: 10.1017/aer.2018.12.

Filippone, A. and R. Mikkelsen (2009). “Advances in CFD & actuator disk models for helicopter aerodynamics”. In: *35th European Rotorcraft Forum 2009, ERF 2009* 2.January, pp. 661–669.

Garcia-Duffy, C. (2009). “Applying Dynamic Wake Models to Induced Power Calculations for an Optimum Rotor”. PhD thesis. Washington University, p. 192.

Gennaretti, M. et al. (2017). “Identification of rotor wake inflow finite-state models for flight dynamics simulations”. In: *CEAS Aeronautical Journal* 8.1, pp. 209–230. DOI: 10.1007/s13272-016-0235-y.

Güner, F. (2016). “Comparison of Rotor Inflow Models for Flight Simulation Fidelity”. Master thesis. Middle East Technical University, p. 139.

Hidalgo, D. F. (2014). “Assessment of a State-Space free wake model”. Master thesis.

Ho, J. C. and H. Yeo (2021). “Evaluation of Finite-State Dynamic Inflow for Rotors”. In: *Journal of Aircraft* 58.5, pp. 1068–1082. DOI: 10.2514/1.C036208.

Hohenemser, K. H. and S. Yin (1972). “Some Applications of the Method of Multiblade Coordinates”. In: *Journal of the American Helicopter Society* 17.3, pp. 3–12. DOI: 10.4050/JAHS.17.3.3.

Horn, J. F. (2019). “Non-Linear Dynamic Inversion Control Design for Rotorcraft”. In: *Aerospace* 6.3, pp. 1–25. DOI: 10.3390/aerospace6030038.

Huang, J., D. A. Peters, and J. V. R. Prasad (2015). “Converged Velocity Field for Rotors by a Blended Potential Flow Method”. In: *Journal on Aviation Technology* 1.2, pp. 44–54. DOI: 10.5176/2382-5758{_}1.2.8.

Huang, J., Y. Zhang, et al. (Feb. 2022). “Time-Delay Margin and Robustness of Incremental Nonlinear Dynamic Inversion Control”. In: *Journal of Guidance, Control, and Dynamics* 45.2, pp. 394–404. DOI: 10.2514/1.G006024.

Johnson, W. (1994). *Helicopter Theory*. New York: Dover Publications, p. 1120.

Keijzer, T. et al. (2019). “Flight Testing of Incremental Backstepping Based Control Laws with Angular Accelerometer Feedback”. In: *AIAA Scitech 2019 Forum*. January, pp. 1–25. DOI: 10.2514/6.2019-0129.

Keller, J. D. (1996). “An Investigation of Helicopter Dynamic Coupling Using an Analytical Model”. In: *Journal of the American Helicopter Society* 41, pp. 322–330. DOI: 10.4050/JAHS.41.322.

Keller, J. D. and H. C. Curtiss (1996). “Modeling the Induced Velocity of a Maneuvering Helicopter”. In: *Annual Forum Proceedings - American Helicopter Society*. Vol. 1, pp. 841–851.

Keller, J. D. and H. C. Curtiss (1998). “A Critical Examination of the Methods to Improve the Off-Axis Response Prediction of Helicopters”. In: *Annual Forum Proceedings - AHS International*, pp. 1134–1147.

Komerath, N. and M. J. Smith (2009). “Rotorcraft Wake Modeling: Past, Present and Future”. In: *35th European Rotorcraft Forum 2009*. Vol. 1, pp. 1–26.

Koschorke, J. (2012). “Advanced Flight Control Design and Evaluation”. Master thesis. Delft University of Technology, p. 246.

Kumtepe, Y., T. Pollack, and E. Van Kampen (Jan. 2022). “Flight Control Law Design using Hybrid Incremental Nonlinear Dynamic Inversion”. In: *AIAA SCITECH 2022 Forum*. Reston, Virginia: American Institute of Aeronautics and Astronautics, pp. 1–18. DOI: 10.2514/6.2022-1597.

Leza, D. V. (2015). “Development of a Blade Element Method for CFD Simulations of Helicopter Rotors using the Actuator Disk Approach”. Master thesis, p. 118.

Lu, L. et al. (2021). “Rotorcraft Simulation Fidelity Improvements through Augmented Rotor Inflow”. In: *47th European Rotorcraft Forum*. September, p. 8.

Makinen, S. M. and D. A. Peters (2005). “Comparison of Dynamic Wake Models with Closed-Form Optimum Propeller Solutions”. In: *30th European Rotorcraft Forum*, pp. 93–106.

Martini, L. (2019). “Identification of simulation-based rotor dynamic wake inflow models suited for helicopter flight dynamics”. Master thesis. Rome: Roma Tre Univeristy, p. 96.

Padfield, G. D. (2007). *Helicopter Flight Dynamics : The Theory and Application of Flying Qualities and Simulation Modelling*. John Wiley & Sons, Incorporated, p. 680.

Pavel, M. D. (2001). “On the Necessary Degrees of Freedom for Helicopter and Wind Turbine Low-Frequency Mode Modeling”. PhD thesis. Delft University of Technology, p. 340.

Pavel, M. D., P. Shanthakumaran, Q. P. Chu, et al. (2020). “Incremental nonlinear dynamic inversion for the apache AH-64 helicopter control”. In: *Journal of the American Helicopter Society* 65.2, pp. 1–16. DOI: 10.4050/JAHS.65.022006.

Pavel, M. D., P. Shanthakumaran, O. Stroosma, et al. (2016). “Development of Advanced Flight Control Laws for the AH-64 Apache Helicopter - Sketches from the Work of TU Delft-Boeing Project in SIMONA Simulator”. In: *Annual Forum Proceedings - AHS International*. Vol. 3, pp. 1778–1792.

Peters, D. A. (1974). “Hingeless Rotor Frequency Response with Unsteady Inflow”. In: *AHS/NASA-Ames Specialists’ Meeting on Rotorcraft Dynamics*, pp. 1–12.

Peters, D. A. (2009). “How Dynamic Inflow Survives in the Competitive World of Rotorcraft Aerodynamics”. In: *Journal of the American Helicopter Society* 54.1, pp. 1–15. DOI: 10.4050/JAHS.54.011001.

Peters, D. A., D. D. Boyd, and C. J. He (1989). “Finite-State Induced-Flow Model for Rotors in Hover and Forward Flight”. In: *Journal of the American Helicopter Society* 34.4, pp. 5–17. DOI: 10.4050/JAHS.34.5.

Peters, D. A. and C. J. He (1991). “Correlation of Measured Induced Velocities with a Finite-State Wake Model”. In: *Journal of the American Helicopter Society* 36.3, pp. 59–70. DOI: 10.4050/JAHS.36.59.

Peters, D. A. and C. J. He (1995). “Finite State Induced Flow Models II: Three-Dimensional Rotor Disk”. In: *Journal of Aircraft* 32.2, pp. 323–333. DOI: 10.2514/3.46719.

Peters, D. A., A. Hsieh, and C. Garcia-Duffy (2009). “A Complete Finite-State Inflow Theory from the Potential Flow Equations”. In: *3rd International Basic Research Conference on Rotorcraft Technology*.

Pitt, D. M. and D. A. Peters (1980). “Theoretical Prediction of Dynamic-Inflow Derivatives”. In: *Sixth European Rotorcraft and Powered Lift Aircraft Forum*, p. 19.

Rand, O. and V. Khromov (2018). “Free-Wake-Based Dynamic Inflow Model for Hover, Forward, and Maneuvering Flight”. In: *Journal of the American Helicopter Society* 63.1, pp. 1–16. DOI: 10.4050/JAHS.63.012008.

Rosen, A. and A. Isser (1995). “A New Model of Rotor Dynamics During Pitch and Roll of a Hovering Helicopter”. In: *Journal of the American Helicopter Society* 40.3, pp. 17–28. DOI: 10.4050/JAHS.40.17.

Saberi, H. et al. (2015). “Overview of RCAS Capabilities, Validations, and Rotorcraft Applications”. In: *Proceedings of the American Helicopter Society 71st Annual Forum*, p. 328.

Simplício, P. et al. (2013). “An Acceleration Measurements-Based Approach for Helicopter Nonlinear Flight Control using Incremental Nonlinear Dynamic Inversion”. In: *Control Engineering Practice* 21.8, pp. 1065–1077. DOI: 10.1016/j.conengprac.2013.03.009.

Sissingh, G. J. (1951). *The Effect of Induced Velocity Variation on Helicopter Rotor Damping in Pitch or Roll*. Tech. rep. London, p. 22.

Skogestad, S. and I. Postlethwaite (2001). *Multivariable Feedback Control - Analysis and Design*. Second edi. John Wiley & Sons, p. 585. DOI: 10.11406/rinketsu.20.1191.

Stiles, R. L. et al. (2004). “”Impossible to Resist” The Development of Rotorcraft Fly-By-Wire Technology”. In: *Annual Forum Proceedings - AHS International*, pp. 1–18.

Su, A., K. M. Yoo, and D. A. Peters (May 1992). “Extension and Validation of an Unsteady Wake Model for Rotors”. In: *Journal of Aircraft* 29.3, pp. 374–383. DOI: 10.2514/3.46172.

Van Aalst, R. and M. D. Pavel (2002). “On the question of adequate modelling of steady-state rotor disc-tilt for helicopter manoeuvring flight”. In: *29th European Rotorcraft Forum 2002, ERF 2002*, pp. 1–20.

Van der Goot, R. R. (2017). “Helicopter Control using Incremental Adaptive Backstepping”. Master thesis. Delft University of Technology, p. 198.

Van Hoydonck, W. R. M., H. Haverdings, and M. D. Pavel (2009). “A Review of Rotorcraft Wake Modeling Methods for Flight Dynamics Applications”. In: *35th European Rotorcraft Forum*. Vol. 1, pp. 27–53.

Wilke, G. (2019). “Variable-Fidelity Methodology for the Aerodynamic Optimization of Helicopter Rotors”. In: *AIAA Journal* 57.8, pp. 3145–3158. DOI: 10.2514/1.J056486.

Zawawi, M. H. et al. (2018). “A review: Fundamentals of computational fluid dynamics (CFD)”. In: *AIP Conference Proceedings*. Vol. 2030. November, pp. 1–8. DOI: 10.1063/1.5066893.

Zhao, J. (2005). “Dynamic Wake Distortion Model for Helicopter Maneuvering Flight”. PhD thesis. Georgia Institute of Technology, p. 177.

Zhao, J., J. V. R. Prasad, and D. A. Peters (2004). “Rotor Dynamic Wake Distortion Model for Helicopter Maneuvering Flight”. In: *Journal of the American Helicopter Society* 49.4, pp. 414–424. DOI: 10.4050/jahs.49.414.

A

Helicopter Data MBB Bo-105

Table A.1: Bo-105 main rotor properties.

Parameter	Value	Unit	Description
Ω	44.4	rad/s	Rotational speed
R	4.91	m	Rotor radius
N	4	-	Number of blades
c_e	0.27	m	Equivalent blade chord
C_{l_α}	6.11	rad^{-1}	Blade lift curve slope
θ_{tw}	-8	deg	Linear blade twist
I_β	231.7	kg*m^2	Blade moment of inertia about flapping hinge
γ_s	0.0524	rad	Rotor shaft tilt angle
l	-0.00761	m	Longitudinal position w.r.t. helicopter CG
l_1	0.02995	m	Lateral position w.r.t. helicopter CG
h_{cg}	0.94468	m	Vertical position w.r.t helicopter CG
K_β	113330	Nm/rad	Center-spring rotor stiffness
γ	5.087	rad^{-1}	Rotor Lock number
σ	0.007	-	Rotor solidity
λ_β	1.12	-	Normalized flapping frequency

Table A.2: Bo-105 tail rotor properties.

Parameter	Value	Unit	Description
Ω_{tr}	233.1	rad/s	Rotational speed
R_{tr}	0.95	m	Rotor radius
N_{tr}	2	-	Number of blades
$c_{e,tr}$	0.18	m	Equivalent blade chord
$C_{L_\alpha,tr}$	5.7	rad^{-1}	Blade lift curve slope
K_{tr}	1	-	Main rotor downwash factor
l_{tr}	6.01	m	Longitudinal position w.r.t. helicopter CG
h_{tr}	1.05	m	Vertical position w.r.t. helicopter CG
σ_{tr}	0.1206	-	Rotor Solidity

Table A.3: Bo-105 fuselage properties.

Parameter	Value	Unit	Description
F_0	1.3	m^2	Parasite drag area
$V_{fus,M}$	6.13	m^3	Equivalent volume in the horizontal plane
$V_{fus,N}$	25.5	m^3	Equivalent volume in the lateral plane
$\alpha_{fus,M}$	0	rad	Incidence angle for zero pitch moment
K_{fus}	0.83	-	Correction coefficient in pitch moment

Table A.4: Bo-105 horizontal tail properties.

Parameter	Value	Unit	Description
S_{ht}	0.803	m^2	Surface area
$C_{L_\alpha,ht}$	4.0	rad^{-1}	Lift curve slope
$\alpha_{ht,0}$	0.0698	rad	Built-in surface incidence
K_{ht}	1.5	-	Correction coefficient in pitch moment
l_{ht}	4.548	m	Longitudinal position w.r.t helicopter CG

Table A.5: Bo-105 vertical tail properties.

Parameter	Value	Unit	Description
S_{vt}	0.805	m^2	Surface area
$C_{L_\alpha,vt}$	4.0	rad^{-1}	Lift curve slope
$\beta_{vt,0}$	-0.0812	rad	Built-in surface incidence
l_{vt}	5.416	m	Longitudinal position w.r.t helicopter CG
h_{vt}	0.97	m	Vertical position w.r.t helicopter CG

Table A.6: Bo-105 mass properties.

Parameter	Value	Unit	Description
m	2200	kg	Helicopter mass
I_{xx}	1433	kg*m^2	Moment of inertia about roll-axis
I_{yy}	497	kg*m^2	Moment of inertia about pitch-axis
I_{zz}	4099	kg*m^2	Moment of inertia about yaw-axis
I_{xz}	660	kg*m^2	Moment of inertia about nonsymmetry-axis

Table A.7: Bo-105 actuator limits.

Parameter	Min. saturation limit [deg]	Max. saturation limit [deg]	Rate rate [deg/s]	Description
θ_0	-0.2	20.0	16.0	Collective pitch
θ_{1s}	-6.0	11.0	28.8	Rotor radius
θ_{1c}	-5.7	4.2	16.0	Number of rotor blades
$\theta_{0,tr}$	-8.0	20.0	32.0	Equivalent blade chord

B

Control Plane versus Disk Plane for Control

During the research on flap dynamics some ambiguity arose with respect to which angle the simplified flap dynamics apply. The final tilting of the rotor disk plane because of the flap angle can be described by three angles, shown in Figure B.1 for the longitudinal case. The longitudinal situation will also be the example in this appendix. All reasoning also applies to the lateral case. When assuming steady state flapping angles one can quantify the relation through Equation (B.1).

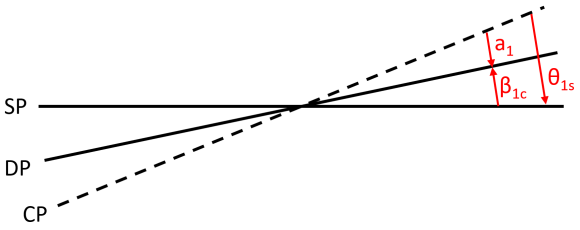

$$\begin{aligned} \beta_{1c} &= -\theta_{1s} - a_1 \\ a_1 &= -\frac{16}{\gamma}\frac{q}{\Omega} \end{aligned} \tag{B.1}$$

Figure B.1: Reference planes of rotor including a_1.

Until now the terminology for angle a_1, and b_1 for the lateral case, has not been used in this report and is not visible in Figure 2.4 to avoid confusion. In the book of Padfield (2007) the flap angle is denoted by β_{1c} and is described as the angle between the shaft plane and the disk plane. The second order flap dynamics, Equation (2.5), used for the helicopter model is also from this book. In some other earlier books, such as Bramwell, Done, and Balmford (2001) and Johnson (1994), the flap angle is denoted by a_1. This originates from describing the flapping motion as a Fourier series, instead of multi-blade coordinates. However, it is unclear whether they just use a_1 as a replacement of the term β_{1c} from Padfield or that their flap dynamics equations apply to the a_1 term of Equation (B.1) and consequently Equation (B.1) is needed to calculate the final flap angle from SP to DP. If the last statement is true, this is a fundamentally different modeling approach as the first one. Namely, by using the flap dynamics equations to calculate a_1 and then using Equation (B.1) to calculate the final flap angle leaves a direct link between pitch rate q and control input θ_{1s}. This requires a very different control approach then the approach taken in this report, where θ_{1s} is indirectly influencing q through the flap angle β_{1c}. To explain the difference, a state-space system is created with the quasi-steady flap equation in hover.

Approach A (β_{1c} / DP)

$$\dot{q} = -K\left(\beta_{1c}\right)$$

$$\tau\dot{\beta}_{1c} + \beta_{1c} = -\theta_{1s} + \frac{16}{\gamma}\frac{q}{\Omega}$$

$$\begin{bmatrix} \dot{q} \\ \dot{\beta}_{1c} \end{bmatrix} = \begin{bmatrix} 0 & -K \\ \frac{16}{\gamma}\frac{1}{\Omega\tau} & -\frac{1}{\tau} \end{bmatrix} \begin{bmatrix} q \\ \beta_{1c} \end{bmatrix} + \begin{bmatrix} 0 \\ -\frac{1}{\tau} \end{bmatrix} \theta_{1s}$$

Approach B (a_1 / CP)

$$\dot{q} = -K\left(-\theta_{1s} - a_1\right)$$

$$\tau\dot{a}_1 + a_1 = -\frac{16}{\gamma}\frac{q}{\Omega}$$

$$\begin{bmatrix} \dot{q} \\ \dot{a}_1 \end{bmatrix} = \begin{bmatrix} 0 & K \\ -\frac{16}{\gamma}\frac{1}{\Omega\tau} & -\frac{1}{\tau} \end{bmatrix} \begin{bmatrix} q \\ a_1 \end{bmatrix} + \begin{bmatrix} K \\ 0 \end{bmatrix} \theta_{1s}$$

The differences between the 2 approaches originate from the β_{1c} and a_1 equations. Approach A assumes that both θ_{1s} and the $\frac{16}{\gamma}\frac{q}{\Omega}$ term experience the same dynamics (modeled by adding a τ term), while approach B only assumes dynamics in a_1. An argument against approach A would be that it is incorrect to model the contribution of θ_{1s} to q, which happens in the control plane, and the contribution of $\frac{16}{\gamma}\frac{q}{\Omega}$, which happens in the shaft plane, by means of a single time constant τ. On the other hand, approach B assumes an instantaneous relation between $\dot{q}$ and θ_{1s}. This is physically counter-intuitive since some time must pass before a changed pitch angle of the blade results in a change in flap angle 90 degrees later. Furthermore, controlling this system would also be very convenient. Since there is a direct relation between $\dot{q}$ and θ_{1s}, the influence of a_1 on $\dot{q}$ is just treated as some unknown system dynamics by the controller. As the incremental control law of the IBS controller is neglecting system depended dynamics and the control effectiveness of θ_{1s} with respect to $\dot{q}$ is very good due to its direct relation, tracking is not at all influenced by the flap angle dynamics in a_1. Finally, when looking at the second order flap models of Bramwell and Johnson, and simplifying the equations to hover condition, neglecting flap derivatives, inflow and lateral motion, the equation that remains is Equation (B.2).

$$a_1 = -\theta_{1s} + \frac{16}{\gamma}\frac{q}{\Omega} \tag{B.2}$$

This confirms that approach A is used in all three sources, as it is the same equation as Equation (B.1) only with β_{1c} switched to a_1. A cause for the confusion might be that Bramwell and Johnson switched from describing an individual blade motion, where they use a_1 correctly as the angle between control plane and disk plane, to a Fourier series representation without clear separation. Furthermore, one can see that the system A matrix of both state-space models are equivalent. Therefore eigenvalues and eigenmotions of both systems would be equal, the only difference is in the control matrix B. Therefore the system dynamics of both approach A and B would be similar.